University of Louisville

ThinkIR: The University of Louisville's Institutional Repository

Electronic Theses and Dissertations

6-2009

Development of an integrated solar heat pipe system for improving building energy efficiency.

Michael Vincent Albanese
University of Louisville

Recommended Citation

Albanese, Michael Vincent, "Development of an integrated solar heat pipe system for improving building energy efficiency." (2009). *Electronic Theses and Dissertations.* Paper 26.
https://doi.org/10.18297/etd/26

DEVELOPMENT OF AN INTEGRATED SOLAR HEAT PIPE SYSTEM FOR
IMPROVING BUILDING ENERGY EFFICIENCY

By

Michael Vincent Albanese

B.S. in Mechanical Engineering, University of Louisville, 2005

A Thesis
Submitted to the Faculty of the
University of Louisville
J.B. Speed School of Engineering
As Partial Fulfillment of the Requirements
for the Professional Degree

MASTER OF ENGINEERING

Department of Mechanical Engineering

June 2009

TABLE OF CONTENTS

DEVELOPMENT OF AN INTEGRATED SOLAR HEAT PIPE SYSTEM FOR
IMPROVING BUILDING ENERGY EFFICIENCY

Submitted by:_____
Michael Vincent Albanese

A Thesis Approved on

_____
(Date)

by the following Reading and Examination Committee

_____
M. Keith Sharp, Thesis Director

_____
Ellen Brehob

_____
R. Eric Berson

ACKNOWLEDGMENTS

ABSTRACT

The one dimensional heat transfer, thermal diode effect of heat pipes makes

them ideal for passive solar applications. Gains in a heat pipe passive solar wall are not

lost during cloud cover or periods of low irradiation. An experimental model was built to

test the performance of a heat pipe passive solar wall in a laboratory setting.

Experimental variations included varying fluid fill levels and the addition of insulation

along the adiabatic section of the heat pipe. Filling the heat pipe to 120% volume of the

evaporator section and insulating the adiabatic section achieved efficiencies of 85%. The

average rate of water tank temperature change for 80%, 100%, 120%, and 140% fill

levels was 1.153°C/hr, 1.195°C/hr, 1.227°C/hr, and 1.203°C/hr, respectively.   The

addition of fins along the condenser of the heat pipe did not significantly enhance the

overall performance.

A computer model was constructed to simulate the performance of direct gain,

indirect gain, and integrated heat pipe passive solar systems in different climates. The

locations selected include: Louisville, Kentucky; Albuquerque, New Mexico; Madison,

Wisconsin; and Rock Springs, Wyoming. Integrated heat pipe systems performed better

than their direct and indirect gain counterparts in all climates. The water wall indirect

gain system outperformed concrete wall systems in all climates. The lowest solar

fractions were achieved by the direct gain system in all climates except Albuquerque, New Mexico (sunny and cool). The mild temperatures and cloudiness of Louisville, Kentucky provided an excellent climate for passive solar systems. Passive solar systems in Louisville (cloudy and cool) performed better than Madison, Wisconsin (cloudy and cold) and Rock Springs Wyoming (sunny and cold).

Integrated heat pipe wall design variations were analyzed to achieve the best overall performance. These variations included: glazing thickness, extinction coefficient, absorber plate and heat pipe material, selective surface, insulation thickness, and water tank size. Decreasing the thickness of the glazing by 7.15 mm improved the solar fraction by 2.69%. Changing from a greenish cast glass to a low iron glass reduces the extinction coefficient and improves solar fraction by 8.82%. Switching absorber plate and heat pipe material from copper to aluminum reduces cost and decrease the solar fraction by 2.23%. Having the absorber plate electroplated with a black chrome surface opposed to painting the collector with flat black paint increase the solar fraction from 19.28% to 48.36%. Changing the insulation thickness around the collector improves the overall losses of the collector. Raising the R-value by a factor of 5 improved the solar fraction by 0.12%. Increased water tank size improves solar fraction but increases the units weight.

Validation of the computer model was made by simulating the laboratory experiments and comparing the data. Temperatures across the system were matched by adjusting the calculated conductances. The computer simulation was able to graphically match the measured temperatures of the experiment. Conduction between the evaporator and condenser sections of the heat pipe was only 6% of the calculated value.

An economic assessment was then performed to analyze the overall cost of the unit, deliver design recommendations, optimize cost, complete life cycle costing and calculate payback period. The most cost effective design would incorporate an aluminum absorber plate with four heat pipes. The solar glazing would have one cover and be made with low iron glass (3/32nd inch thick). For the city of Louisville with a load to collector ratio of 10 W/m^{2}K the total cost of the unit would be \$1825.46 for a collector area of 2.43 m^2 (26.12 ft^2). The solar fraction provided by this optimized unit would be 42.67% of the heating load.

LIST OF TABLES

LIST OF FIGURES

I. INTRODUCTION

A. Current and Future Energy Needs

Currently, energy concerns and consumption are at an all time high. The United

States Department of Energy states worldwide consumption is 123.3 quadrillion Watt-

hours (420.7 quadrillion Btu's) a year, with the nation's own demand at 29.2 quadrillion

Watt-hours (99.8 quadrillion Btu's). By the year 2030 these figures are projected to rise

to 211.5 and 39.2 quadrillion Watt-hours (721.6 and 133.9 quadrillion Btu's)

respectively. These staggering figures are complemented by equally disturbing analysis

of the United States' energy imports and exports. Petroleum imports account for 34.5%

of the nation's energy consumption while coal exports are a mere 6.3% of the nation's

production. The net energy imports for the United States in 2006 amounts to 252.86

billion dollars [Energy Information Administration 2006].

Many scientists have forecasted a peak in fossil fuel production in upcoming years.

In a report to the Energy Watch Group in 2007, North American oil production is

expected to decline by 80% by the year 2030 [Zittel and Schindler 2007]. This decrease

in fossil fuel production will increase the need for energy imports and accelerate the

rising cost of fuel. Coupled with increasing global populations, worldwide

industrialization and geopolitical concerns, the stress on global energy demand will only

become greater. Renewable energies account for only 6.8% of the nation's consumable

energy [Energy Information Administration 2006]. To alleviate some of the pressure

caused by increasing energy demand, renewable energy needs to take a greater

percentage of consumable energy.

Political and public attention has increased with respect to energy concerns over the

past years due to rising energy cost. However, the environmental impacts of current

energy consumption has also risen to the forefront of current energy debates. Climate

change and global warming are now common terms and the environmental consequences

of fossil fuel combustion is spreading world wide. The rate of temperature change of the

last 50 years, 0.13 °C, is almost double that of the last one hundred years, 0.07 °C. And

the average temperature of the last 50 year period has been warmer than any other 50

year period of the last 1,300 years [Hegerl and Zweirs 2007]. While many factors can

contribute to rising global temperatures, many scientists are attributing this increase to

carbon dioxide levels. Changes in carbon dioxide levels are among the dominant

mechanisms driving long term climate change [Rothman 2002]. The National Oceanic

and Atmospheric Administration states that carbon dioxide levels prior to the industrial

revolution were at 280 parts per million per volume (ppmv). In the last 650,000 years

carbon dioxide levels ranged between 100 and 300 ppmv [NOAA 2007]. Levels in the

year 2000 were at 380 ppmv and increasing at a rate of 1.9 ppmv per year. The effects of

burning fossil fuels and increasing carbon dioxide emissions could have potentially

catastrophic effects. Polar ice melt, rising sea levels, regional extremes of drought and

precipitation all bring damaging consequences.

Passive solar systems for space heating are an advantageous way to combat energy and environmental concerns. Residential energy use accounts for 21% of the nation's energy use, and 46% of that total is used solely for space heating. For new buildings, savings of 25% can be expected with no increase in building cost by following energy conscious passive solar design. These design strategies include building orientation, window placement and distribution, and interior space configuration. Small investments can bring even greater savings (typically 10% greater building cost can provide up to 50% energy savings in favorable climates).

B. Passive Solar Systems

Passive solar systems can be used for day lighting, ventilation, and space heating. By developing a passive solar system for space heating a large portion of energy consumption in the residential sector can be alleviated. Traditional passive solar systems experience net gains during sunny weather conditions, however, system losses occur during nighttime and cloudy periods. To offset these losses, solar systems have to be supplemented with conventional heating sources. Climate variations such as temperature and cloudiness affect the net gains of passive solar systems and design considerations can be made to limit thermal losses.

When designing passive solar systems for space conditioning there are two different designs - direct gain and indirect gain. Direct gain systems use south facing windows to allow solar radiation into the living space (Fig. 1.1). Many times, buildings with large window apertures and small living space can incorporate the use of a thermal mass. Traditionally this is a concrete floor, and the thermal mass storage helps provide a more constant energy source throughout nighttime and cloudy periods. The advantage of direct

gain systems is the fast response time; however, the thermal losses through the window are its greatest disadvantage.
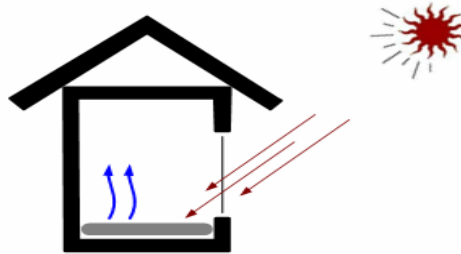
FIGURE 1.1 - Direct Gain Passive Solar System. The thermal storage device is placed in the living space and solar radiation passes through the glazing.

The indirect gain system places the thermal storage device between the window glazing and the living space (Fig. 1.2). This design still has limitations similar to the direct gain system. High thermal losses are experienced during nighttime and cloudy conditions; however, indirect gain systems have losses lower than the direct gain system. One example of indirect gain systems is the Trombe wall, which was popularized in the 1960's by Felix Trombe. These walls are constructed with concrete as the thermal storage material. Concrete Trombe walls have a slow response time due to their high thermal resistance. This is compensated by the steady amount of heat it supplies throughout the day. Water walls have a lower thermal resistance when compared to concrete walls due to the natural convection inside the water tanks. The large mass still allows for relatively steady heat distribution, and low thermal resistance decreases response time.
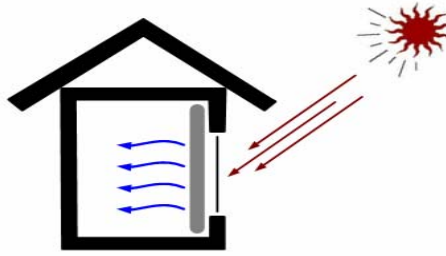
FIGURE 1.2 - Indirect Gain Passive Solar System. The thermal storage device is placed directly between the living space and glazing.

Greenhouse and isolated gain systems are similar to the indirect gain systems in that the thermal storage devices are placed between the living space and solar collection areas (Fig. 1.3). Greenhouse passive solar systems can have the same performances of traditional indirect gains systems. By orienting the slope of the greenhouse to be more parallel to the suns rays, greenhouse systems can have even greater gains. Isolated gain systems use solar collectors placed below the storage mass, which is below the living space, to transfer heat by natural convection. These systems remain passive by using a thermosyphoning effect and usually incorporate air as their working fluid. The thermosyphon of the isolated gain system limits losses during nighttime and cloudy conditions. When the temperature of the solar collector falls below the temperature of the mass storage device, then air circulation doesn't occur.

FIGURE 1.3 - Greenhouse and Isolated Gain Passive Solar Systems.

5

In 1942 heat pipes were introduced by R.S. Gaugler of the General Motors

Corporation, and the unique thermal properties of the devices began to offer solutions to

engineering problems [Peterson 1994]. Isolated gain passive solar system with integrated

heat pipes was first studied by Corliss [1979] (Fig. 1.4). This system places an insulated

wall between the solar collector and mass storage. These two parts are connected by heat

pipes. Heat pipes can only transfer heat in one direction, similar to thermosyphons. This

greatly reduces the heat losses compared to traditional direct and indirect gain systems.

The use of two-phase fluids allows for greater heat transfer and net gains are greater than

isolated gain systems.
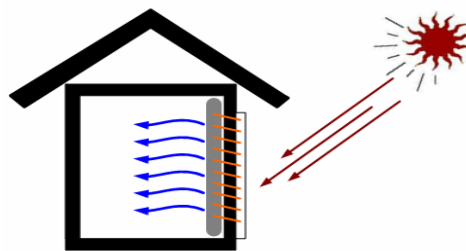
FIGURE 1.4 - Isolated Gain Passive Solar System with Integrated Heat Pipes.

C. Heat Pipe Operation and History

Heat pipes work by absorbing solar radiation in its lower (evaporator) end (Fig.

1.5). Here, liquid is boiled and the vapor rises to the condenser end, where the vapor

condenses, transferring the energy. A vapor or adiabatic section separates the evaporator

and condenser sections. The condensed liquid then travels back to the evaporator end of

the heat pipe by gravity. The driving force in thermosyphons is the density differences in

the fluid created through rising temperatures. These forces are greater in heat pipes due to

greater density differences between fluid phases. Phase change in heat pipes also allows

for better heat transfer, smaller temperature drops, and smaller elevation differences

compared to thermosyphons. Internal wicking structures such as axial grooves and external fins can be used on the heat pipes to further improve heat transfer.
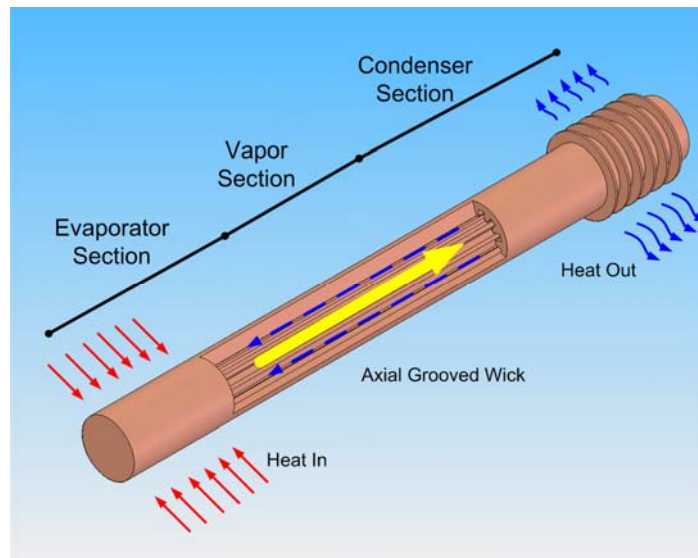
FIGURE 1.5 - Heat Pipe Operation.

Conceptually, the heat pipe was first introduced in 1831 by Angier March Perkins, and Jacob Perkins with mention of the "Perkins" system of heating [Peterson 1994]. This system used a Perkins tube to transfer heat from a furnace to a boiler using a single phase fluid [Peterson 1994]. The Perkins tube would later be classified as a thermosyphon, yet proved to be the ground work for the heat pipe. The United States Atomic Energy Commission coined the term heat pipe in 1963 in a patent filed under the name Grover [Peterson 1994]. Using stainless steel heat pipes and sodium as a working fluid this patent was essentially the same design as the Gaugler patent of 1942 [Peterson 1994]. The theory of heat pipes was researched at Los Alamos Laboratory in the 1960's under Cotter and Cheung [Reay and Kew 2006] for the use of heat pipes in the space program and satellite development. The first heat pipe used in space minimized the temperature

differences between transponders on satellite GEOS-B in 1968 [Reay and Kew 2006].

Consumer electronics saw the first application of heat pipes by the Sony Corporation in

the 1970's. Today the single largest use for heat pipes is for the cooling of central

processing units.

<u>D. Literature Survey</u>

There has been significant research in to the optimization and design of heat pipes

for thermal applications. Wang, Yan, Zing, and Wag [1985] tested flat plate collectors

utilizing gravity assisted heat pipes with various fluid types. Fluids tested included:

water, ammonia, acetone, methanol, pentane, heptane, ethanol, Freon-11, and Freon-12.

Fluid types had varying operating ranges and heat transfer rates, with Freon-12 and

acetone being the most suitable for operation in a gravity assisted heat pipe solar

collector. It was also noted that increasing the outside diameter of the heat pipe improved

the heat transfer rates. Vasilev [1987] fitted a convective solar receiver with heat pipes.

The receivers previously used by Vasilev were not fitted with heat pipes. They

experienced high thermal losses during non-insolation periods and over time deterioration

of the receiver resulted in high maintenance. The application of heat pipes improved

overall gains, lowered maintenance issues, and the thermal diode effect significantly

lowered heat losses. An experimental study was completed by Abo [1996] on working

fluids, heat pipe material, and wick structures. It was concluded that the wicking

structures of a heat pipe notably influence the fluid flow behavior; furthermore, heat pipe

heat transfer rates are dependent on flow behavior. Kempers, Ewing and Ching [2006]

studied copper heat pipe performance, and the effects of mesh layer wicks and fluid fill

levels. It was found that lowering the amount of working fluid reduced the heat transfer

rate. It was also found that increasing the heat flux lowered the thermal resistance of the heat pipe, increasing the overall heat transfer rate.

Passive solar water heater performance has also been advanced through the application of heat pipes. Akyurt [1984] manufactured and filled numerous heat pipes with different design configurations. These designs were tested for a year in a solar hot water system prototype. The heat pipes performed satisfactorily and were 20% more efficient than conventional flat plate solar water heater designs. Azad [1987] built solar hot water heaters with gravity assisted heat pipes filled with methanol. A mathematical model was also created for experimental and theoretical comparison. Azad mounted thermocouples on the back side of the absorber plate and used pyranometers on the outside of the collector house.   The experimental results showed a performance level similar to the mathematical model. Chun [1999] tested various selective surfaces and water storage tank shapes on passive solar hot water heaters using heat pipes and thermosyphons. Throughout the experiment the heat pipe units performed better than the thermosyphons. Regardless of water storage tank design there was not a significant amount of stratification in the tanks.

Development of a passive solar space heating unit utilizing heat pipes was researched initially by John M. Corliss [1979]. Corliss developed separate computer simulations to analyze passive heating and passive cooling systems. These simulations were conducted in four different climates: Phoenix, Arizona; Albuquerque, New Mexico; Columbus, Ohio; and Madison, Wisconsin. The heat pipe system performed better in all climates. Corliss also built a prototype. The evaporator end of the heat pipes were epoxied into the black absorber plates and the condenser end of the heat pipe was placed

9

into plastic water tanks. The entire unit was modular in form to allow the design to easily be incorporated into new buildings and support structural loads. This allowed the design to easily be incorporated into new buildings and support structural loads. The heat pipes were filled with Freon-21 and placed at a 5° angle to gravity assist the condensed fluids return to the evaporator section. Wall insulation was placed between the absorber plate and the water wall with an insulation rating of R-20. Corliss also completed an economic and marketability assessment of the heat pipe system. Small scale new home installations seemed to offer the highest cost effectiveness.

Dijik, Galen and Wit [1984], built a passive solar space heater using heat pipes to achieve higher efficiencies than traditional concrete wall systems. This system used the integrated heat pipe passive solar system with the addition of a vented insulation wall. The insulation wall created an air cavity between the mass storage device and the living space. The air cavity would be heated during insolation periods, and vents at the top and the bottom of the air cavity allowed convective forces to disperse the heat throughout the room. This design was tested in laboratory settings and in real climate conditions. This heat pipe design significantly reduced the overall weight of the space heater and achieved higher gains when compared to the traditional concrete Trombe walls. When compared to active solar space heaters, the cost benefit ratio was extremely competitive. Similar to the work of Corliss, Saman [1985] used heat pipes for space heating and cooling applications. To reduce the heat gains through walls, Saman, placed the evaporator section of heat pipes in the buildings wall structure. The condenser section was left exposed above the roof line. The efficiencies of this heat pipe cooling application showed that the system was not economically feasible. Using a flat plate collector with

heat pipes, Saatci [1989] tested the downward heat transfer of heat pipes in a passive solar space heater. The mass storage device was located nine meters horizontally and five meters vertically away from the collector. Capillary action returned the condensed R-114 refrigerant to the evaporator section, and the water tank was heated to 70 °C. Heat pipe design limited pooling of the working fluid in the condenser section. The effective downward transfer of solar energy in an integrated heat pipe system provides increased design and implementation options.

Analysis of a heat pipe passive solar system was then investigated by Susheela and Sharp [2001]. Computer simulations were performed comparing a heat pipe system to water walls and Trombe walls in varying climates. The climates selected for this analysis included: Albuquerque, New Mexico; Salt Lake City, Utah; and Madison, Wisconsin. Unlike the modular unit developed by Corliss, this analysis used a retrofit design. Using flexible tubes the heat pipes could be connected to water tanks using holes drilled through existing walls. Again analysis showed that the heat pipe system performs better in all climates, and especially well in cold and cloudy climates. A prototype was built and tested in Salt Lake City between February 16th and March 1st, 1994. The heat pipes were filled with SUVA-124 to fluid fill fractions of 0.176 and 0.528. Absorber plate temperatures were lower for the higher fluid fill levels. This suggests increased heat pipe performance with further adjustment of the fluid fill fraction. Collector efficiencies were 40-60% during peak solar periods, and heat pipe efficiencies reached 60-80% during sunny days. Susheela and Sharp recommended that an insulated heat pipe adiabatic section and condenser fins would improve system performance.

E. Research Goals

This research will compare the thermal performance and economic viability of an integrated solar heat pipe wall with that of traditional space heating designs. The specific goals of the project are:

- Build a model passive solar heat pipe wall to test in a laboratory setting.

- With the laboratory experiment, test the effects of fluid fill level, insulating the adiabatic section of the heat pipe, and adding fins to the condenser section of the heat pipe.

- Write a computer program to simulate passive solar systems and their performance in different climate regions.

- Simulate the performance of the solar heat pipe wall and match the performance of the laboratory model.

- Use the computer program to simulate various design changes to the heat pipe wall and study their effects on performance.

- Conduct a complete economic assessment of the unit including, overall unit cost, design change cost, cost optimization, future fuel cost analysis, life cycle costing, and payback period.

- Give recommendations on overall design to aid in the future development of a commercial unit.

Analysis will allow an accurate assessment for implementation of an integrated heat pipe passive solar wall for Louisville, Kentucky, relative to other climates.

II. METHODS

A. Experimental Model

1. Description of an Integrated Heat Pipe Passive Solar System

An experimental model was created to test the overall efficiencies and conductance of the heat pipe passive solar system under controlled conditions (Fig. 2.1). The model was built using one heat pipe attached to an absorber plate. An aluminum frame was constructed to hold a solar glazing material and attach the absorber plate to an insulating wall. Behind the insulating wall a 189 liter (50 gallon) plastic water tank served as a mass storage device. This water tank was insulated to limit thermal losses from the tank.
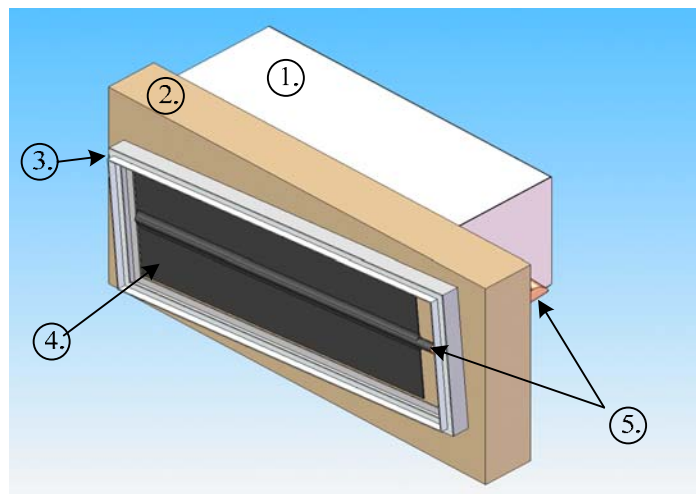
1. Water Tank 2. Insulating Wall 3. Aluminum Frame
4. Absorber Plate 5. Heat Pipe

FIGURE 2.1 - Diagram of Experimental Set Up.

2. Experimental Apparatus Construction

　　Construction materials for the absorber plate included two pieces of copper plate and a copper heat pipe (Fig. 2.2). The heat pipe was constructed of 0.0254 m (1 inch) diameter copper pipe with 0.003175 m (1/8 inch) wall thickness. The evaporator and condenser section was 0.98425 m (38-3/4 inches) long with an adiabatic section that was 0.3683 m (14-1/2 inches) in length. The copper plates measured 0.98425 m x 0.15875 m x 0.003175 m (38-3/4inches x 6-1/4 inches x 1/8 inches) and were soldered onto the evaporator section of the heat pipe (Fig. 2.3).

FIGURE 2.2 - Absorber Plate Construction.

FIGURE 2.3 - Soldered Connection Between Heat Pipe And Absorber Plate.

　　The absorber plate and evaporator section of the heat pipe were than electroplated with a black chrome selective surface. An aluminum frame 1.143 m x 0.3937 m x 0.0762 m (45 inches x 15-1/2 inches x 3 inches) was constructed to fix the absorber plate to the wall (Fig.2.4).

14

FIGURE 2.4 - Left - Entire Frame Construction, Right - Corner Connection Close-Up.

Low iron glass was then inserted into the aluminum frame and a silicone caulking was used to seal the edges. The aluminum frame, glazing and absorber plate were all assembled and attached to a wall construction. The wall was assembled from 0.0127 m (1/2 inches) thick plywood and pieces of 0.0508 m x 0.1524 m (2 inches x 6 inches) wood (Fig. 2.5). R-20 insulation was inserted into the wall cavity. One end of the wall was made removable to allow for the condenser section to be connected.

FIGURE 2.5 - Wall Construction For Experimental Model.

The water tank had a capacity of 189 liters (50 gallons) and the condenser was inserted into the tank via a threaded bulkhead fitting (Fig. 2.6 & Fig. 2.7).

FIGURE 2.6 - Experimental Water Tank For Mass Storage.

FIGURE 2.7 - Water Tank Bulk Head.

Two condensers sections were fabricated for testing. The first was a smooth pipe condenser made of 0.0254 m (1 inch) diameter copper pipe. The other condenser was constructed with copper fins attached (Fig. 2.8). The fins were made of 0.003175 m (1/8 inch) thick washers with an 0.03175 m (1-1/4 inch) O.D. and a 0.028575 m (1-1/8 inch) I.D.. 180 copper fins were than soldered on every 0.00635 m (1/4 inch).

FIGURE 2.8 - Finned Condenser Section.

A pipe pulling apparatus was used to create a hole in the adiabatic section. This hole was then soldered with reducers to a 0.00635 m (1/4 inch) copper refrigerant line (Fig. 2.9). This junction was used for evacuating and filling the heat pipe.
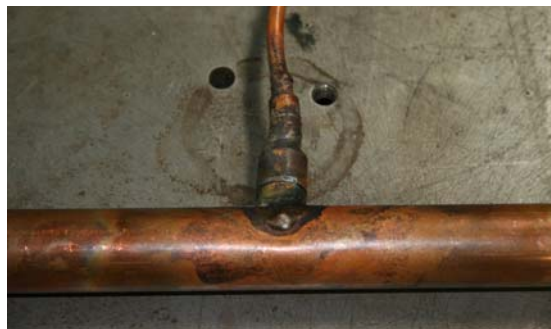
FIGURE 2.9 - Heat Pipe Adiabatic Section Construction.

0.254 meters (10 inches) of R-20 insulation was then placed around the water tank. The aluminum frame, absorber plate and heat pipe were all assembled with an inclination angle of 4.5°.

To simulate solar radiation three 1000 Watt metal halide bulbs were used. These bulbs had standard aluminum reflectors (Fig. 2.10).

FIGURE 2.10 - Metal Halide 1000 Watt Solar Lights.

To evenly distribute light across the absorber plate, larger reflectors created from aluminum foil and insulation board were placed around all four sides of the array of lights (Fig. 2.11). The lights were placed 0.51435 m (20-1/4 inches) apart and fitted with aluminum foil blinders 0.0762 m (3 inches) in width, which also helped distribute the light evenly. From the absorber plate, the lights were placed 1.143 m (45 inches) away.
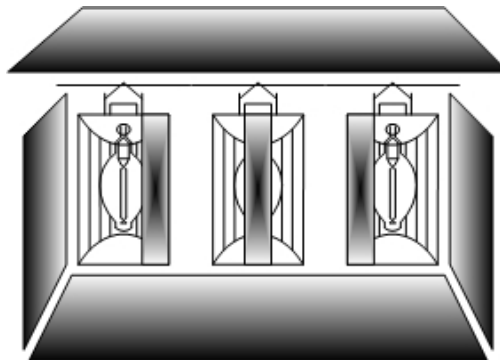
FIGURE 2.11 - Diagram Of Solar Lights And Aluminum Reflectors.

3. Heat Pipe Charging

The two phase fluid selected to charge the heat pipe for the experiment was DuPont SUVA-124. SUVA-124 is a retrofit HCFC refrigerant for applications requiring R-114 and R-124. This refrigerant was selected due to its improved environmental properties.

18

Prior to filling, the heat pipe was washed and connected to a ball valve. The entire

charging apparatus included the refrigerant tank, vacuum pump, vacuum gauge, ball

valves and heat pipe (Fig. 2.12).
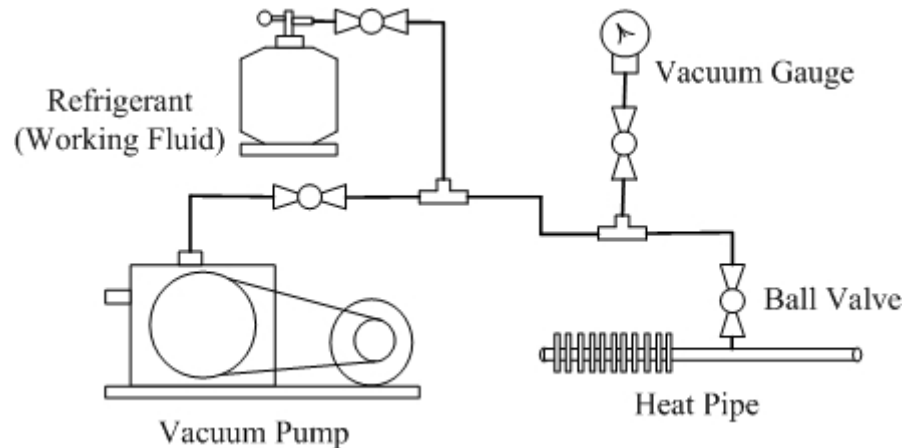
FIGURE 2.12 - Heat Pipe Charging Apparatus.

The first step in charging the heat pipe was to apply a vacuum on the entire system.

Using a Speedivac high vacuum pump, a vacuum of 724 mm (28.5 inches) of mercury

was achieved (Fig. 2.13).

FIGURE 2.13 - Speedivac Vacuum Used To Charge The Heat Pipe.

After evacuating the system, the ball valves were manipulated to charge the heat

pipe. A scale was placed under the refrigerant tank to measure the amount of working

fluid used. The amount of fluid used during charging was based on percentages of

evaporator volume.

4. Data Measurements

  T type thermocouples were selected to measure temperature changes during testing. T type thermocouples are made of copper and constantan and have a useful temperature range of -200 to 300 °C. Thermocouple junctions were welded and then soldered to copper surfaces when applicable.

  To measure the amount of radiation throughout the testing four Kipp and Zonen CM3 pyranometers were used. The CM3 pyranometers are ideal for outdoor and indoor use with natural light. They can also be used with artificial light, including metal halide lamps. The pyranometer consists of a thermopile sensor, housing, glass dome, and cable. There were a total of four pyranometers and 28 thermocouples (Fig. 2.14). The absorber plate had a total of eight thermocouples, four on the top and four on the bottom. There were four thermocouples placed on the evaporator and condenser section. The adiabatic section contained three thermocouples and there was one thermocouple used to measure the ambient temperature. There were a total of eight thermocouples inside the water tank. The pyranometers were mounted to the wall with two above and two below the aluminum frame.
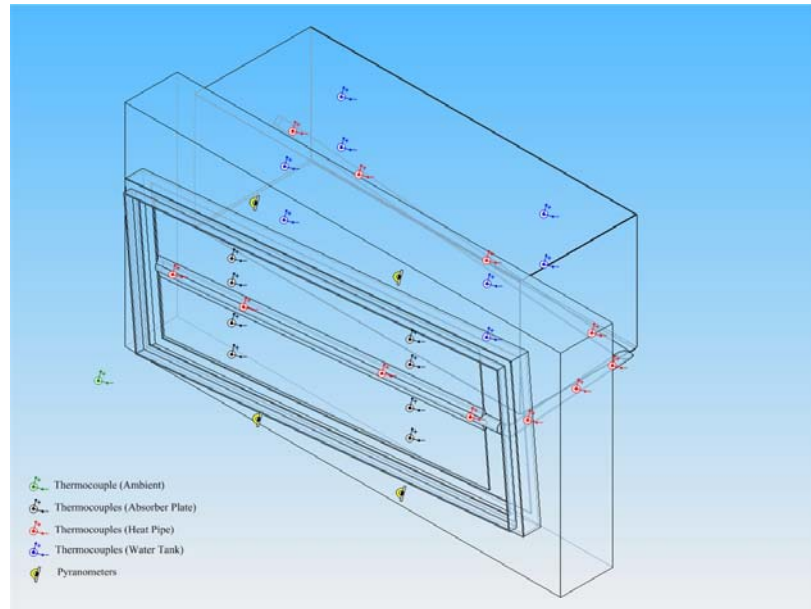
FIGURE 2.14 - Experimental Placement Of Thermocouples And Pyranometers.

The National Instruments SCXI chassis was used in conjunction with the SCXI-1600, 16 bit digitizer module, and the SCXI-1102/B/C module (Fig. 2.15).

FIGURE 2.15 - SCXI Chassis With Digitizer And Module.

The SCXI-1102/B/C module was used for signal conditioning of thermocouples, and low-bandwidth volt and millivolt sources. A Labview program was written for all data acquisition used in the experiment.

B. Computer Simulation

1. Heat Pipe Passive Solar Simulator

Corliss originally developed a system network analysis for passive systems (SNAPS) during his original investigation. Susheela and Sharp [2001] used a modified version of SNAPS to simulate hourly performance of an integrated solar heat pipe system. Using MatLab software a new computer simulation was created to simulate hourly performance of the system and analyze design variables. Similar to SNAPS, a thermal network was created with each node having a mass and specific heat (Fig. 2.16).
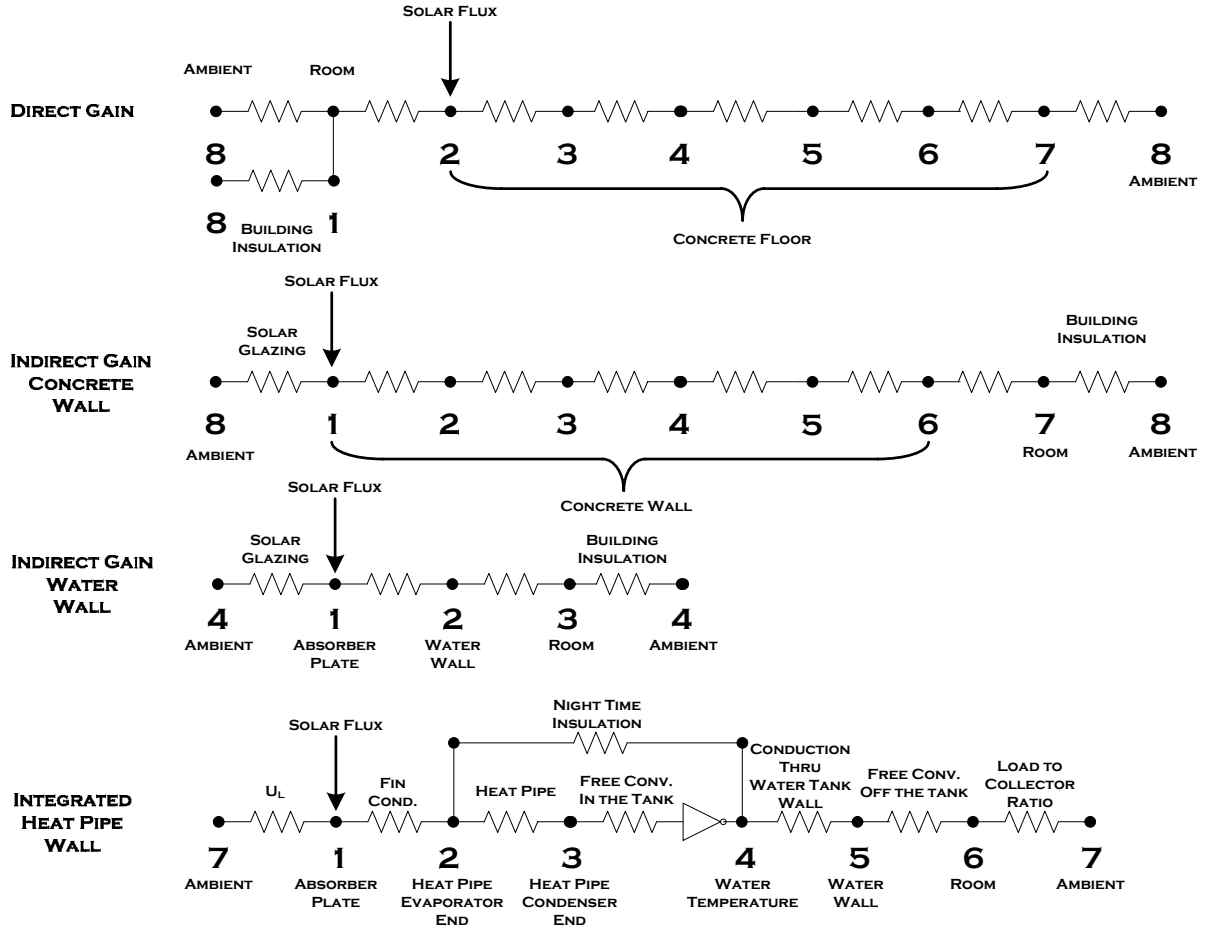
FIGURE 2.16 - Thermal Networks For Passive Solar Computer Simulations.

It was assumed that a heat transfer coefficient linearly related the temperature difference between nodes and the energy flow between them.

$$Q_{ij} = K_{ij}\left(T_j - T_i\right) \tag{1}$$

The heat transfer coefficient, K_{ij} (W/m^2-°C), can vary with time and is a function of temperature. Therefore an iterative process was used to linearly relate the heat transfer coefficient, to the nodal temperatures. For the ith node the energy balance equation is

$$M_i\left(\frac{dT_i}{dt}\right) = \sum_j \left(K_{ij}\left(T_j - T_i\right) + E_i\right) \tag{2}$$

23

where M_i (kJ/m^2-°C) is the product of the mass of the ith node and specific heat, E_i (W/m^2) is the solar energy gain of the ith node, and T is the nodal temperature (°C). Given initial nodal temperatures at time, t, a set of equations can be written for all nodes that can be simultaneously solved for nodal temperatures as a function of time. Using a relatively small time step, Δt, of one minute, equation 3 can be integrated from t to $t+\Delta t$. This integration yields the nodal temperatures of the next time step.

$$\left(\frac{2M_i}{\Delta t}+\left(\sum_j K_{ij}\right)\right)T_i -\left(\sum_j K_{ij}T_j\right)=\frac{2M_iT_{i\circ}}{\Delta t}+\left(\sum_j K_{ij}\left(T_{j\circ}-T_{i\circ}\right)\right)+\left(E_i+E_\circ\right) \qquad (3)$$

A zero subscript denotes the previous time step. Matrix algebra was used to solve the set of equations for all nodes. Repeated iterations were used to calculate heat transfer coefficients when dependent on nodal temperatures. Nodal temperatures for the living space, T_6, were restricted to simulate auxiliary heating and venting, keeping room temperatures at appropriate levels.

$$19°C \prec T_6 \prec 24°C \qquad (4)$$

Typical Meteorological Year data (TMY2) was used to model ambient temperatures, wind speeds and radiation levels. TMY2 data provides hourly meteorological data and is derived from the National Solar Radiation Database from 1961-1990. TMY2 data used during the experiment for Julian Hours 300 to 700 is shown in Appendix I. A copy of the Matlab code for the computer simulation is shown in Appendix II.

2. Calculating Heat Transfer Coefficients and Solar Flux

a. Solar Flux. There are two methods for modeling diffuse solar radiation, isotropic and anisotropic. The isotropic diffuse model is conservative in nature as all diffuse radiation is assumed to be isotropic. This model is easily understood and calculated,

however, the anisotropic model provides more accurate results. The anisotropic model [Duffie and Beckman 1991] which includes three components of diffuse radiation – uniform, circumsolar and horizon brightening - was used for these simulations. The model is described below in equation 5.

$$S_{anisotropic} = \left(I_b + I_d A_i\right)R_b\left(\tau\alpha\right)_b + I_d\left(1 - A_i\right)\left(\tau\alpha\right)_d\left(\frac{1}{2} + \frac{1}{2}\cos\beta\right)\left(1 + f\sin\left(\frac{\beta}{2}\right)^3\right)$$
$$+I\rho_g\left(\tau\alpha\right)_g\left(\frac{1}{2} - \frac{1}{2}\cos\beta\right)$$

(5)

where S is the absorbed solar radiation (W/m^2), and the subscripts b, d, and g, are for the beam, diffuse, and ground reflected radiation respectively. I is the hourly component of radiation, given in the TMY2 data files. The factor f is the square root of I_b/I. R_b is the ratio of beam radiation on a tilted surface to that on a horizontal surface. β is the slope of the collector, ρ_g is the factor for ground reflectance, and $\tau\alpha$ is the transmittance absorptance product. A_i is the anisotropy index.

b. Overall Loss Coefficient. Using the seven node thermal network, the ambient temperature is connected to the absorber plate fin temperature through conductance k_{71}. This heat transfer coefficient accounts for thermal energy loss around the solar collector, including convection, conduction, and radiation. For this reason k_{71} is referred to as the overall loss coefficient. The overall loss coefficient is a summation of the top, and edge losses. Bottom losses are treated as additional heat to the system since this energy is transferred into the heat pipe wall. The overall loss coefficient is defined in equation 6 [Duffie and Beckman 1991].

$$U_L = U_t + U_e$$

(6)

U_t, the losses out of the top of the collector is shown in equation 7 [Duffie and Beckman 1991].

$$U_t = \left\{ \frac{N}{\dfrac{C}{T_{pm}}\left[\dfrac{\left(T_{pm}-T_a\right)}{N+f}\right]^e} + \frac{1}{h_w} \right\}^{-1} + \frac{\sigma\left(T_{pm}+T_a\right)\left(T_{pm}^2+T_a^2\right)}{\left(\varepsilon_p+0.00591\cdot Nh_w\right)^{-1} + \dfrac{2N+f-1+0.133\varepsilon_p}{\varepsilon_g} - N} \qquad (7)$$

σ is the Steffan-Boltzman constant, T_{pm} is the mean plate temperature, T_a is the ambient temperature, N is the number of glass covers on the collector, ε_g is the emittance of the glass cover, and ε_p is the emittance of the absorber plate. The variables f, C, and e, and are defined below in equations 8, 9, and 10 respectively [Duffie and Beckman 1991].

$$f = \left(1+0.089h_w - 0.1166h_w\varepsilon_p\right)\left(1+0.07866N\right) \qquad (8)$$

$$C = 520\left(1-0.000051\beta^2\right) \qquad (9)$$

$$e = 0.430\left(1-\frac{100}{T_{pm}}\right) \qquad (10)$$

The collector slope is β, and for angles over 70° a value of 70° should be used. The wind heat transfer coefficient [Duffie and Beckman 1991], h_w, is defined below in equation 11

$$h_w = \max\left(5, \frac{8.6V^{0.6}}{L^{0.4}}\right) \qquad (11)$$

where V is the wind speed, and L is the cubed root of the house volume. The wind speed is found from the TMY2 data. The edge losses [Duffie and Beckman 1991] are defined as

$$U_e = \frac{UA}{A} \qquad (12)$$

where UA [Duffie and Beckman 1991] is defined as

$$UA = \frac{kPt_c}{t_i} \tag{13}$$

where k is the conductivity of the insulation, P is the perimeter of the collector, $t_{collector}$ and $t_{insulation}$ are the thickness of the collector and insulation respectively. The overall loss coefficient has units of (W/m^2K) and the heat transfer coefficient between nodes 7 and 1 is shown in equation 14.

$$k_{71} = U_L \tag{14}$$

c. Absorber Plate Fin Conduction. The heat transfer coefficient between the absorber plate and the evaporator end of the heat pipe is conductance k_{12}. This resistance is derived from the conduction of the fin to the heat pipe. The effective heat transfer coefficient is defined in equation 15.

$$h = \frac{3kt}{\left(\dfrac{W}{2} - \dfrac{OD}{2}\right)^2} \tag{15}$$

where k is the conductance of the plate material, t is the thickness of the plate, W is the distance between separate heat pipes, and OD is the outside diameter of the heat pipe. This equation is developed from Susheela and Sharp (2001), and accounts for the differences in absorber plate design. This value is normalized for the system by multiplying by the overall fin area to collector area shown in equation 16

$$k_{12} = \frac{hN_f(W - OD)L}{2A} \tag{16}$$

where L is the length of the absorber plate.

d. Heat Pipe Conductance. The conductance from outside the evaporator end of the heat pipe to the adiabatic section is defined by k_{23}. This heat transfer coefficient accounts for conduction through the wall of the heat pipe and is shown in equation 17 [Incropera and Dewitt 2002].

$$k_{23} = \frac{N_p}{\dfrac{\ln\left(\dfrac{OD}{ID}\right)}{2\pi L_e k_p} + \dfrac{\ln\left(\dfrac{OD}{ID}\right)}{2\pi L_c k_p}} \tag{17}$$

OD and ID are the outer and inner diameters of the heat pipe respectfully. L_e and L_c are the lengths of the evaporator and condenser sections. N_p is the number of heat pipes attached to the absorber plate and k_p is the thermal conductivity of the heat pipe.

e. Tank Free Convection. The heat transfer from the condenser section of the heat pipe to the water wall mass storage unit is calculated by first finding the Rayleigh number [Incropera and Dewitt 2002].

$$Ra_D = \frac{g\beta(T_s - T)OD^3}{v\alpha} \tag{18}$$

where g is the acceleration due to gravity, β is the inverse of the film temperature, OD is the outer diameter of the heat pipe, T_s is the temperature of the condenser section, T is the temperature of the water in the tank, v is the kinematic viscosity, and α is the thermal diffusivity. The Nusselt number for a long horizontal cylinder [Incropera and Dewitt 2002] can then be found by equation 19

$$Nu_D = \left\{ 0.6 + \frac{0.387 Ra_D^{\frac{1}{6}}}{\left[1 + 0.720973234 \left(\frac{1}{Pr} \right)^{\frac{9}{16}} \right]^{\frac{8}{27}}} \right\}^2 \qquad (19)$$

where Pr is the Prandlt number. Using the Nusselt number k_{34} can be found by equation 20 [Incropera and Dewitt 2002]

$$k_{34} = \frac{N_p k Nu_D A_t}{OD \cdot A} \qquad (20)$$

where k is the thermal conductivity of water. Multiplying by the surface area of the condenser and the area of the collector normalizes the value. To incorporate finning on the condenser end of the heat pipe equation 21 needs to be modified [Incropera and Dewitt 2002].

$$k_{34} = \frac{\eta_o N_p k Nu_D A_t}{OD \cdot A} \qquad (21)$$

A_{total} is the area of the condenser plus the area of the fins. η_o is the overall fin efficiency and is defined in equation 22 [Incropera and Dewitt 2002].

$$\eta_o = 1 - \frac{N_f A_f \left(1 - \eta_f \right)}{A_t} \qquad (22)$$

N_f is the number of fins, A_f is the area of one fin, η_f is the fin efficiency.

f. Tank Wall Conduction. Conduction through the plastic wall of the water tank, k_{45}, is defined in equation 23 [Incropera and Dewitt 2002]

$$k_{45} = \frac{k_T}{A \cdot L_T} \qquad (23)$$

where k_T is the thermal conductivity of the plastic wall, and L_T is the wall thickness.

g. Water Tank Free Convection. k_{56} is the heat transfer coefficient between the water wall thermal storage unit and the room temperature. A heat transfer coefficient is found for the free convection of air around each side of the tank. The characteristic length for any side of the tank is defined in equation 24 [Incropera and Dewitt 2002]

$$l_c = \frac{A_t}{P} \tag{24}$$

where A_t is the area of the side of the tank and P is its perimeter. The Rayleigh number is then defined by equation 25 [Incropera and Dewitt 2002].

$$Ra = \frac{g\beta(T_t - T_r)l_c^3}{v\alpha} \tag{25}$$

The Nusselt number for a vertical face of the water tank is found by equation 26 [Incropera and Dewitt 2002].

$$Nu_L = \left\{ 0.825 + \frac{0.387Ra^{\frac{1}{6}}}{\left[1 + 0.6710121288\left(\frac{1}{Pr}\right)^{\frac{9}{16}} \right]^{\frac{8}{27}}} \right\}^2 \tag{26}$$

The Nusselt numbers for the bottom and top faces of the tank are found by equation 27, 28, and 29 [Incropera and Dewitt 2002].

$$Nu_{bottom} = 0.27Ra^{0.25} \tag{27}$$

$$Nu_{top} = 0.54Ra^{0.25} \qquad 10^4 < Ra < 10^7 \tag{28}$$

$$Nu_{top} = 0.15Ra^{0.333} \qquad 10^7 < Ra < 10^{11} \tag{29}$$

The heat transfer coefficient for each side is then found by equation 30 [Incropera and Dewitt 2002].

$$h = \frac{Nu \cdot k}{l_c} \tag{30}$$

The overall thermal conductivity between nodes 5 and 6 is

$$k_{56} = \frac{2 \cdot h_{vertical,side} \cdot A_{\tan k,side}}{A} + \frac{2 \cdot h_{vertical,front} \cdot A_{\tan k,front}}{A} + \frac{h_{top} \cdot A_{\tan k,top}}{A} + \frac{h_{bottom} \cdot A_{\tan k,bottom}}{A} \tag{31}$$

the sum of the heat transfer coefficients for each side of the water tank. Each coefficient is normalized by multiplying by the respective surface area of the tank face and dividing by the overall collector area.

h. Heating Load To Collector Ratio. k_{67} completes the network thermally connecting the room temperature and the ambient temperature. This conductance value is equal to the reciprocal of the collector area to load ratio. The UA value [Duffie and Beckman 1991] needs to be calculated for every building element and is shown in equation 32. This generally includes: roof, floor, north wall, south wall, east wall, west wall, doors, and windows.

$$UA = \frac{NA}{I_v} \tag{32}$$

where NA is the net area of the building element, and I_v is the insulation value. Infiltration losses are calculated with equation 33 [Duffie and Beckman 1991]

$$I = 0.018 \cdot V \cdot ACH \cdot ADR \tag{33}$$

where V is the room volume (m^3), ACH is the air changes per hour, and ADR is the air density ratio. The UA$_{total}$ is a summation of each building elements UA value and the infiltration losses and is shown in equation 34 [Duffie and Beckman 1991].

$$UA_{total} = UA_{roof} + UA_{floor} + UA_{N,S,E,Wwalls} + I \tag{34}$$

31

The heat transfer coefficient between nodes 6 and 7 is equal to the reciprocal of the collector area to load ratio and is shown in equation 35 [Duffie and Beckman 1991].

$$k_{67} = \frac{UA_{total}}{A} \tag{35}$$

i. Night Time Insulation. When the temperature at node 4, the water temperature in the mass storage wall, is greater than node 2, the evaporator end of the heat pipe, heat is transferred through the night time insulation because of the thermal diode effect. The heat transfer between nodes 2 and 4 represents the heat losses during cloud cover and night time conditions and is defined in equation 36 [Duffie and Beckman 1991].

$$k_{24} = \frac{1}{A\left(\dfrac{L_{Brick}}{k_{Brick}} + \dfrac{L_{Plywood}}{k_{Plywood}} + \dfrac{L_{Insulation}}{k_{Insulation}} + \dfrac{L_{Drywall}}{k_{Drywall}}\right)} \tag{36}$$

The nighttime insulation value is calculated by using heat transfer coefficients for each building material in the wall. Here a simple construction of brick, plywood, insulation, and drywall is used.

3. Comparisons of Passive Solar Systems in Different Climates

Four cities were selected to evaluate the effect of climate on the relative performance of passive solar systems (Fig. 2.17). Louisville, Kentucky has a cool and cloudy climate. Madison, Wisconsin has a distinctly colder climate when compared to Louisville but receives almost the same amount of radiation. Albuquerque, New Mexico receives twice the amount of radiation compared to Louisville; however, January temperatures are still decidedly cool. Rock Springs, Wyoming has a cold and sunny climate during the month of January.
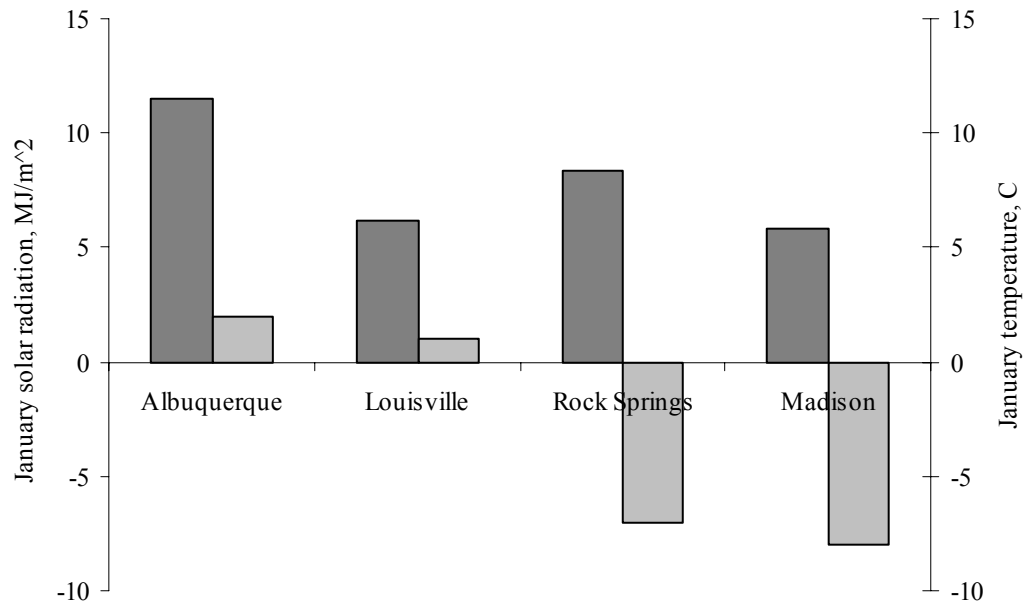
FIGURE 2.17 - Average Daily Radiation (dark bars) And Ambient Temperature (light

bars) For January.

III. PROCEDURE

A. Experimental Procedure

1. Radiation Distribution Analysis

Prior to running the experiments, the distribution of radiation across the absorber

plate was analyzed. The solar lamps were first allowed to warm up for approximately one

hour while their output radiation became constant. Then a pyranometer was used to

measure radiation at fifteen locations across the glazing of the solar collector, and the

four corners of the aluminum frame. These four corners are the locations of the

pyranometers throughout the experiments. The correction factor was determined from

dividing the average radiation value of the fifteen locations across the absorber plate by

the average radiation value of the four measurements taken from the corners of the

aluminum frame.   This correction factor allowed pyranometer measurements made at the

four corners of the frame to be used to accurately predict the amount of radiation striking

the absorber plate throughout the experiments.

2. Testing

The rate of temperature change for each experimental run was analyzed between

water tank temperatures of 23°C and 26.5°C with a constant radiation value. Before each

experiment was run the water tank temperature was tested using Labview. For each test

the water temperature had to be below 23°C at each thermocouple. The temperature

difference between thermocouples did not exceed 0.125°C, this insured there was no

stratification in the water tank. Providing a lower temperature limit insured that each

test's performance could be analyzed and compared. If water tank temperatures

exceeded the lower limit then a mixture of ice and water was added until a steady

temperature below the given limit was achieved. Adequate time was also required to

ensure the absorber plate and heat pipe temperatures reached the ambient temperature.

Prior to starting the data acquisition program, Labview, and beginning the test, the

correction factor and sampling rate were setup. Throughout the experiment a sampling

rate of 0.2 Hz was used. Once the data collection had begun the lights were turned on

and left until the tank temperature reached 26.5 °C. The lamps were then turned off and

the Labview program was stopped. For the test to be accepted the lights had to warm up

and reach a constant radiation value before the water tank temperatures reached 23°C.

The rate of temperature increase was only analyzed when the radiation level was

constant. Thermocouple, pyranometer, and time data were exported from Labview to

Excel for further analysis.

This testing procedure was then repeated using both an un-insulated and insulated

adiabatic section. Styrofoam pipe insulation was used to cover all sections of the

adiabatic section and this was then further insulated with wall insulation. The amount of

fluid used in the heat pipe was tested to find the optimum charging level. Four levels of

80%, 100%, 120% and 140% of the evaporator section volume were tested. Once the

optimum fluid fill level was discovered the non-finned condenser section was replaced

with a finned condenser section. Repeatability was analyzed by conducting three tests for

each experimental setup for a total of 27 tests. Each experimental test run is shown in

Table I.

TABLE I

EXPERIMENTAL TESTS

Test	Fill Level	Number	Adiabatic Insulation	Condenser Finning
1	80%	3	NO	NO
2	80%	3	YES	NO
3	100%	3	NO	NO
4	100%	3	YES	NO
5	120%	3	NO	NO
6	120%	3	YES	NO
7	140%	3	NO	NO
8	140%	3	YES	NO
9	120%	3	YES	YES

3. Experimental Calculations

a. Temperature Rate Of Change. Each thermocouple in the water tank

represented one eighth of the water tank. The mean water tank temperature was than

calculated and plotted.   Using a linear curve fit, the rate of temperature change for each

experimental run was found.

b. Overall System Efficiency. The overall system efficiency was calculated with the

following equation

$$Eff = \frac{m \cdot c_p \cdot \dfrac{(T_2 - T_1)}{t}}{R \cdot A} \qquad (37)$$

where R is the measured level of radiation (W/m^2), A is the area of the absorber

plate (m^2), m is the mass of the water storage tank (kg), c_p is the specific heat (J/kg), T is

the temperature of the water tank (°C), and t is time (s).

36

c. Error Propagation. The procedure for calculating the overall accuracy of the data acquisition system was given by National Instruments online accuracy advisor (National Instruments Corporation 2009). The National Instruments modules account for temperature drift errors when the ambient temperature is between 15°C and 35°C. If the ambient temperature is outside of this range than the temperature drift needs to be calculated as

$$T_D = \pm \left(V_i \cdot \frac{\% R_m}{°C} + \frac{O}{°C} \right) \cdot \Delta T \qquad \left(15°C \succ T_{\text{Ambient}} \succ 35°C \right) \quad (38)$$

where V_i is the input voltage, $\% R_m$ is the percentage of the reading, O is the offset value, and ΔT is the temperature change. The absolute accuracy for each component of the data acquisition system is calculated as

$$AA = \pm \left(\left(V_i \cdot \% R_m \right) + O + N + T_D \right) \qquad (39)$$

where V_i is the input voltage, $\% R_m$ is the percentage of the reading, O is the offset value, N is the system noise, and T_D is the temperature drift. The data acquisition system accuracy is calculated as

$$SA = \sqrt{\sum_{i=1}^{N} AA_i^2} \qquad (40)$$

where AA is the absolute accuracy of each component of the data acquisition system. The system accuracy with respect to voltage input is calculated as

$$SA_{RTI} = \frac{SA}{V_{i,\max}} \qquad (41)$$

where SA is the system accuracy and $V_{i,\max}$ is the maximum voltage input from the SCXI data modules. The uncertainty of the measurements taken by the data acquisition system is calculated as

37

$$w = \sqrt{SA_{RTI}^2 + w_{ins}^2} \tag{42}$$

where SA_{RTI} is the system accuracy relative to input voltage, and w_{ins} is the instruments uncertainty. The total uncertainty for the overall efficiency of the heat pipe system is calculated as

$$w_T = \sqrt{\left(\frac{\partial Eff}{\partial m} w_m\right)^2 + \left(\frac{\partial Eff}{\partial T} w_T\right)^2 + \left(\frac{\partial Eff}{\partial R} w_R\right)^2} \tag{43}$$

where Eff is the overall system efficiency, m is the mass of the water tank, T is the temperature (°C), R is the radiation (W/m^2), w_m is the uncertainty of the mass of the water tank, w_T is the uncertainty of the temperature, w_R is the uncertainty of the radiation level.

B. Computer Simulation Procedure

1. Computer Simulation Variables

a. Climate Comparisons. Meteorological data was used to analyze the differences in performance associated with climate variables. TMY2 data was analyzed to find cities with winter temperatures, cloud cover, and radiation values different than that of Louisville, Kentucky. Computer simulations compared the effects of these climate variations. The imported data for each citiy included temperature, wind speed, and solar radiation. The baseline solar system and load requirement for the comparison was constant between climates tested. A load to collector ratio was chosen to produce a solar fraction of approximately 50% for the heat pipe system in Louisville. The load to collector ratio chosen was 10 W/m^{2}K, and achieved a solar fraction of 48.36%. This load to collector ratio and its solar fraction was expected to be close to a practical and economic maximum.

      b. System Design Comparisons. Variables in design, for a heat pipe passive solar

wall, were individually simulated. Results were compared based on the solar fraction of

each trial. Solar fraction is the percentage of the space heating load that is supplied by

the passive solar system. The variables that will be investigated using the computer

simulation are tabulated in Table II.

TABLE II

PASSIVE SOLAR SIMULATION DESIGN VARIABLES

Parameter	Variable
Cover (Number)	N_c
Cover (Thickness)	t_c
Cover (Emittance)	ε_g
Cover (Extinction Coefficient)	α_g
Absorber Plate (Material Conductivity)	k_a
Absorber Plate (Selective Surface)	N/A
Absorber Plate (Thickness)	t_a
Absorber Plate (Insulation Thickness)	t_i
Absorber Plate (Insulation Conductivity)	k_i
Absorber Plate (Height)	H_a
Absorber Plate (Width)	W_a
Heat Pipe (Number, Spacing)	N_p, W
Heat Pipe (Material Conductivity)	k_p
Heat Pipe (Inclination Angle)	N/A
Heat Pipe (Wick Structure)	N/A
Condenser Fin (Number)	N_{cf}
Water Tank (Number)	N
Water Tank (Height)	H_t
Water Tank (Length)	L_t
Water Tank (Width)	W_t
Water Tank (Wall Thickness)	t_t
Water Tank (Material Conductivity)	k_t
Night Time Insulation Conductivity	k_{24}
Ground Reflectance Factor	ρ_g
Load to Collector Ratio (LCR)	k_{71}

The baseline parameters for the trials were representative of the original integrated heat
pipe wall investigated by Corliss. The baseline glazing used one low iron glass cover,
3.175 mm (1/8 inch) thick. The absorber plate was constructed of 3.175 mm (1/8 inch)

thick copper and was 2.0828 m (6'-10") tall and 1.165225 m (3 foot- 9-7/8 inches) in width. The baseline selective surface was electroplated black chrome. There were five heat pipes used and they were constructed of 0.0254 m (1 inch) OD copper pipe with 3.175 m (1/8 inch) wall thickness. The base line condenser section was smooth pipe without fins. The water tank was 0.2032 m (8 inches) wide and had 3.175 mm (1/8 inch) wall thickness. The baseline values can be found in Appendix IV.

2. Experimental And Computer Simulation Comparison

The computer simulation was also run to replicate the experiments. Using calculated conductances, overall efficiencies, and heat flux values, the performance of the experiments was compared to that of the simulation. This process provided validation of the computer model.

IV. RESULTS

A. Experiments

1. Radiation Distribution

The average radiation value measured at the fifteen spots across the absorber plate was 709.4 W/m^2 (Fig. 4.1). The maximum and minimum values were 757.27 W/m^2 and 645.8 W/m^2 respectively. The average radiation value measured at the four corners of the aluminum frame were 576.74 W/m^2, thus the correction factor to estimate the average radiation on the absorber from the average at the four corners was calculated as 1.23. Please refer to Appendix V for the measured values for all fifteen locations.
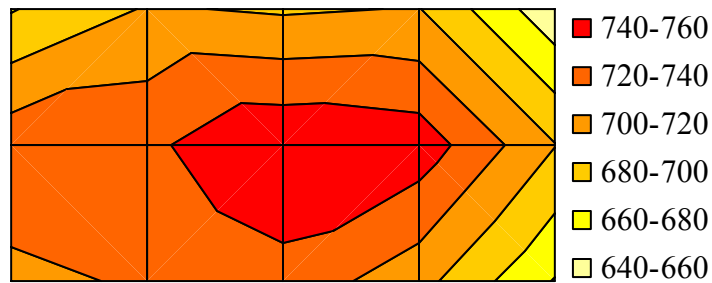
FIGURE 4.1-Absorber Plate Contour Plot (W/m^2).

2, Fill Level, Adiabatic Section Insulation and Condenser Fins Results

This section describes the performance of the heat pipe under various charging levels with both an insulated and un-insulated adiabatic section. Each fill level test was

conducted using a smooth un-finned condenser section. The optimum fill level was then tested using a finned condenser. For each experiment the measured radiation values were compared. The experimental procedure was designed to keep the input power as constant as possible. However, differences in radiation levels did exist. Variations between runs during startup occurred based on differences in the ambient temperature and the starting temperature of the bulb. Differences could also be attributed to small changes in reflector positioning.

a. 80% Fill Level. An example of the raw data for tank temperature with respect to time, for the case with an un-insulated adiabatic section and a charge level of 80% of the volume of the heat pipe evaporator section, is plotted in Fig. 4.2.
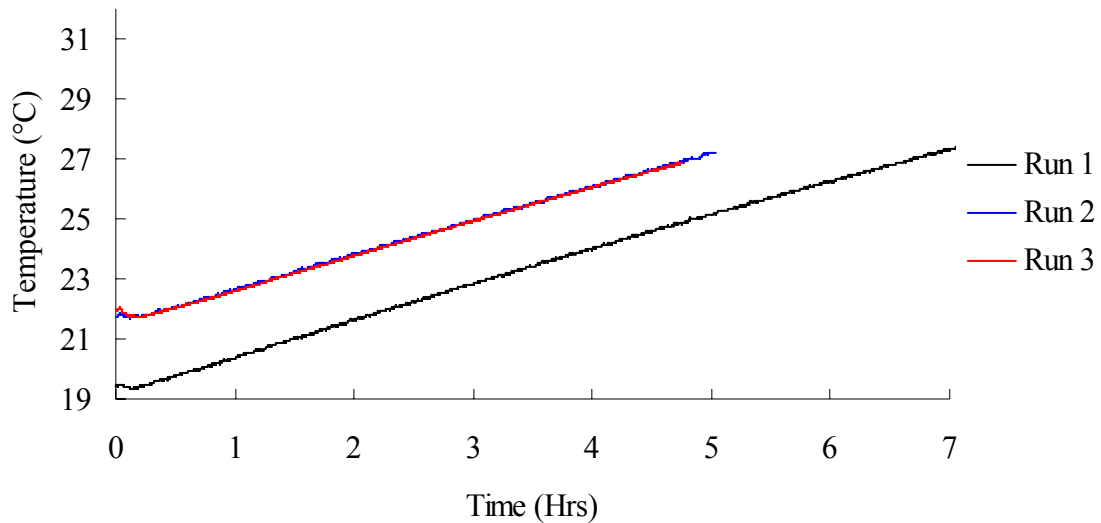
FIGURE 4.2 – Raw Data for Water Tank Temperature (Un-insulated / 80% Fill).

As explained in the methods section, system performance depends on temperature. Therefore, system performance was compared among the cases for temperatures between the same two limits, 23°C and 26.5°C. The selected temperature data for this case are shown in Fig. 4.3. Subsequent plots for the other cases will show only the temperature

rise from 23°C to 26.5°C. (For each experimental trial the complete run data is plotted and shown in Appendix VI.) The average rate of temperature change was 1.136°C/hr, and the standard deviation normalized by the mean was 0.5%.

The figure contains the following equations:

$$y_1 = 1.1321x + 23.013$$
$$R_1^2 = 0.9995$$
$$y_2 = 1.1339x + 23.011$$
$$R_2^2 = 0.9994$$
$$y_3 = 1.1426x + 23.019$$
$$R_3^2 = 0.9998$$

Legend: Run 1, Run 2, Run 3, Linear (Run 1), Linear (Run 2), Linear (Run 3)

Axis labels: Temperature (°C), Time (Hrs)
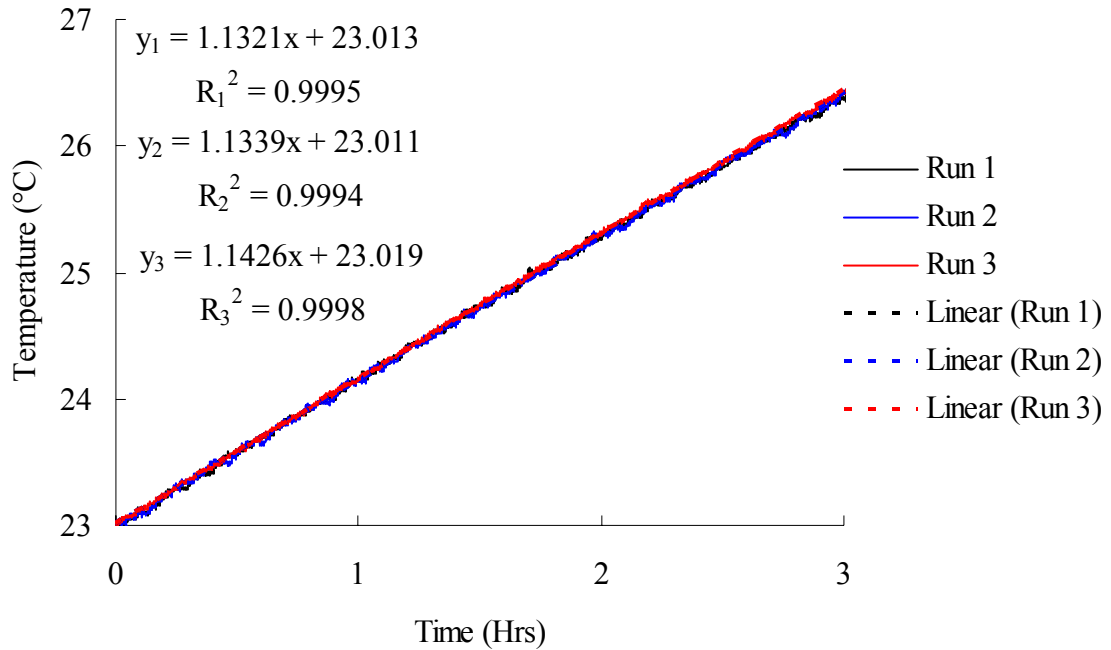
FIGURE 4.3 - Water Tank Temperature Change Between 23°C and 26.5°C (Un-insulated / 80% Fill).

Using the measured data from the four pyranometers and applying the correction factor, the radiation across the absorber plate was determined. The raw data for radiation level is shown in Fig. 4.4.
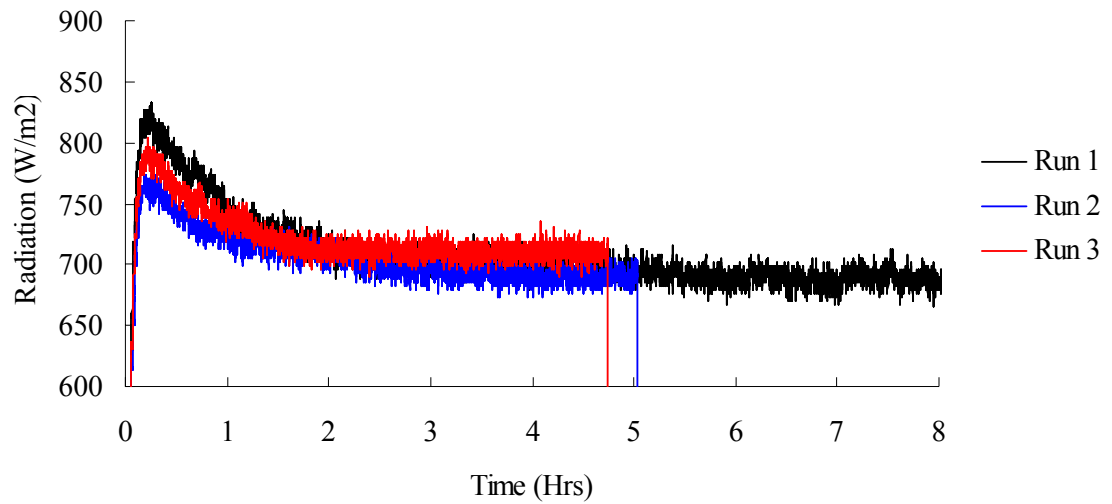
FIGURE 4.4 – Raw Data for Average Radiation Level (Un-insulated / 80% Fill).

The warm up period for the solar lamp is evident in Fig. 4.4. Because of the variability

of the radiation, it was important to select the radiation data that corresponded exactly

with the selected tank temperature interval. Radiation as a function of tank temperature

from 23°C to 26.5°C is shown in Fig. 4.5. Subsequent plots of radiation for the rest of

the cases will show only the selected data. (The complete radiation data is available for

each trial in Appendix VII.)
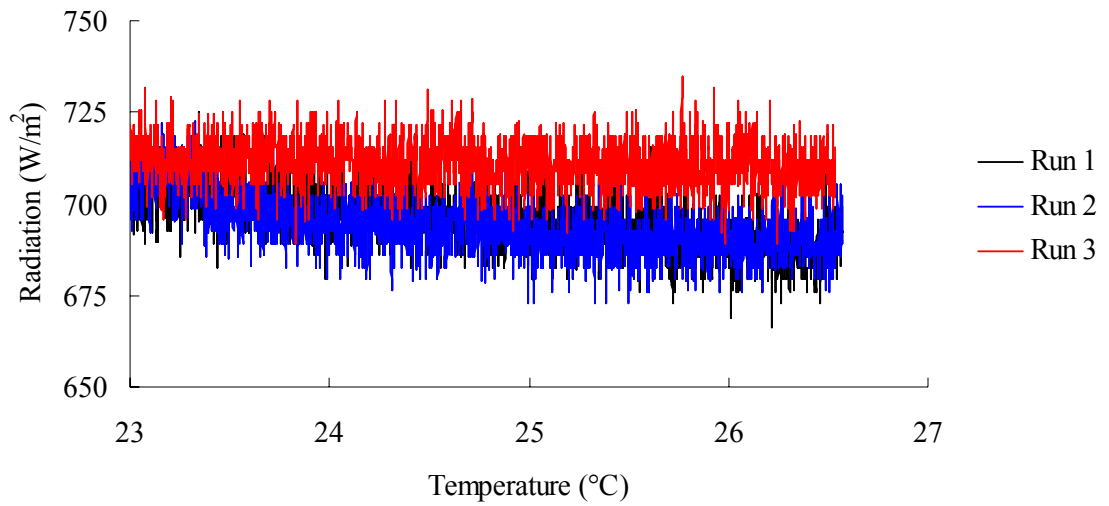
FIGURE 4.5 –Average Radiation Level Between Tank Temperature of 23°C and 26.5°C

(Un-insulated / 80% Fill).

The minimum, mean, maximum, standard deviation and standard deviation normalized

by the mean are shown in Table III.

TABLE III

RADIATION DATA FOR 80% FILL AND UN-INSULATED ADIABATIC SECTION

Minimum	666.50	W/m^2
Mean	700.45	W/m^2
Maximum	734.88	W/m^2
Standard Deviation	10.66	
StDev / Mean	1.52%	

The plot below shows the water tank temperature change for an insulated adiabatic

section with 80% volume fill level (Fig. 4.6).

$$y_1 = 1.1611x + 23.025$$
$$R_1^2 = 0.9998$$
$$y_2 = 1.1483x + 23.024$$
$$R_2^2 = 0.9997$$
$$y_3 = 1.1487x + 23.002$$
$$R_3^2 = 0.9998$$
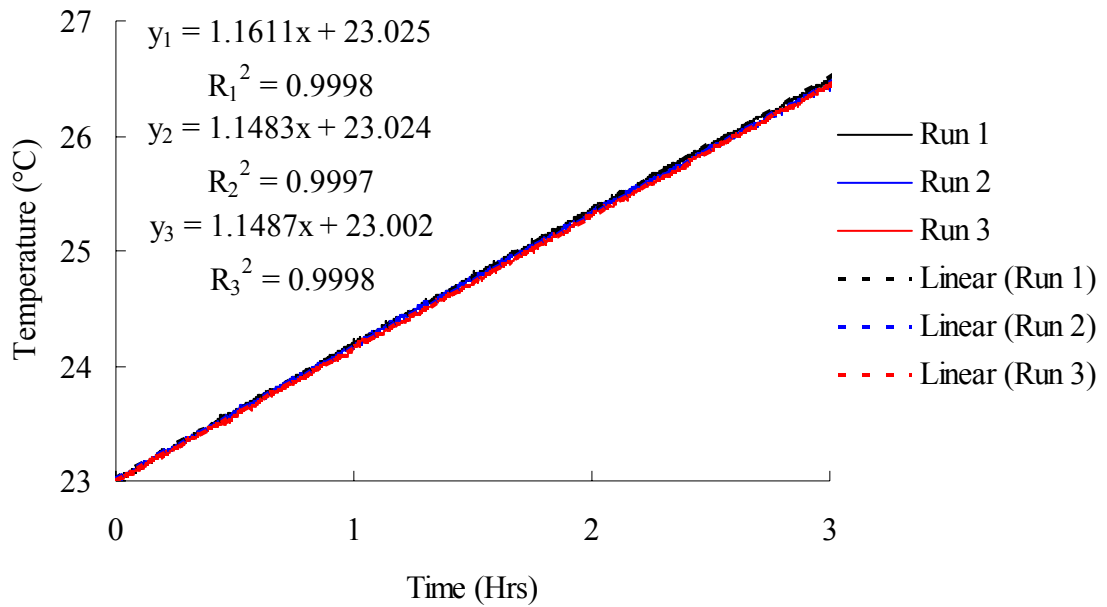
FIGURE 4.6 - Water Tank Temperature Change (Insulated / 80% Fill).

The average rate of temperature change was 1.153°C/hr, and the normalized standard deviation was 0.6%. The plot below shows the radiation level during the test (Fig. 4.7).
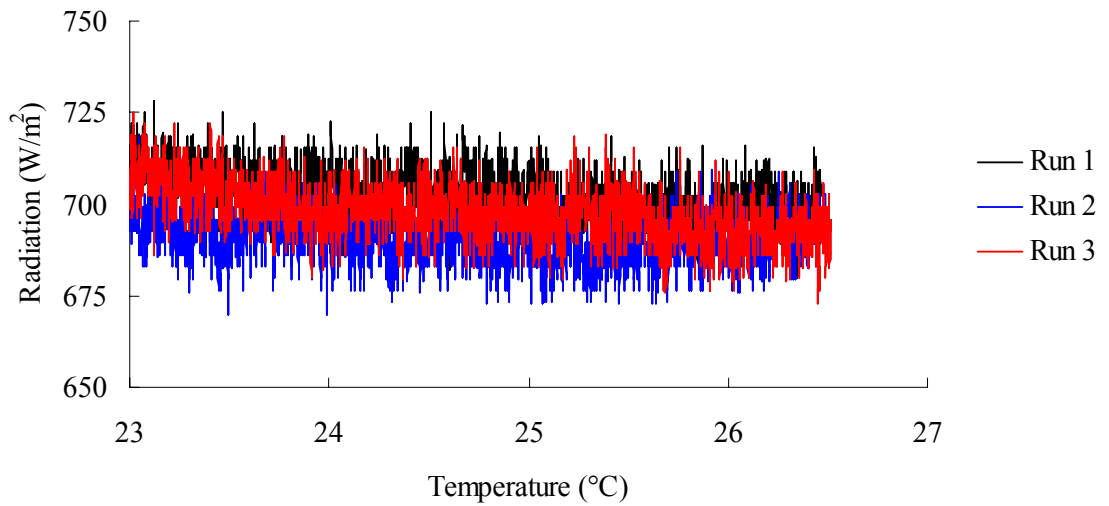
FIGURE 4.7 – Sampled Average Radiation Level (Insulated / 80% Fill).

The statistical results are shown in Table IV.

TABLE IV

RADIATION DATA FOR 80% FILL AND INSULATED ADIABATIC SECTION

Minimum	669.94	W/m^2
Mean	696.95	W/m^2
Maximum	728.32	W/m^2
Standard Deviation	8.87	
StDev / Mean	1.27%	

b. 100 % Fill Level. The water tank temperature change is shown in the plot below (Fig. 4.8). The heat pipe was charged to 100% volume of the evaporator section and an un-insulated adiabatic section was used.

$$y_1 = 1.1401x + 23.031$$
$$R_1^2 = 0.9997$$
$$y_2 = 1.1555x + 23.007$$
$$R_2^2 = 0.9998$$
$$y_3 = 1.1845x + 23.006$$
$$R_3^2 = 0.9998$$

Run 1
Run 2
Run 3
Linear (Run 1)
Linear (Run 2)
Linear (Run 3)
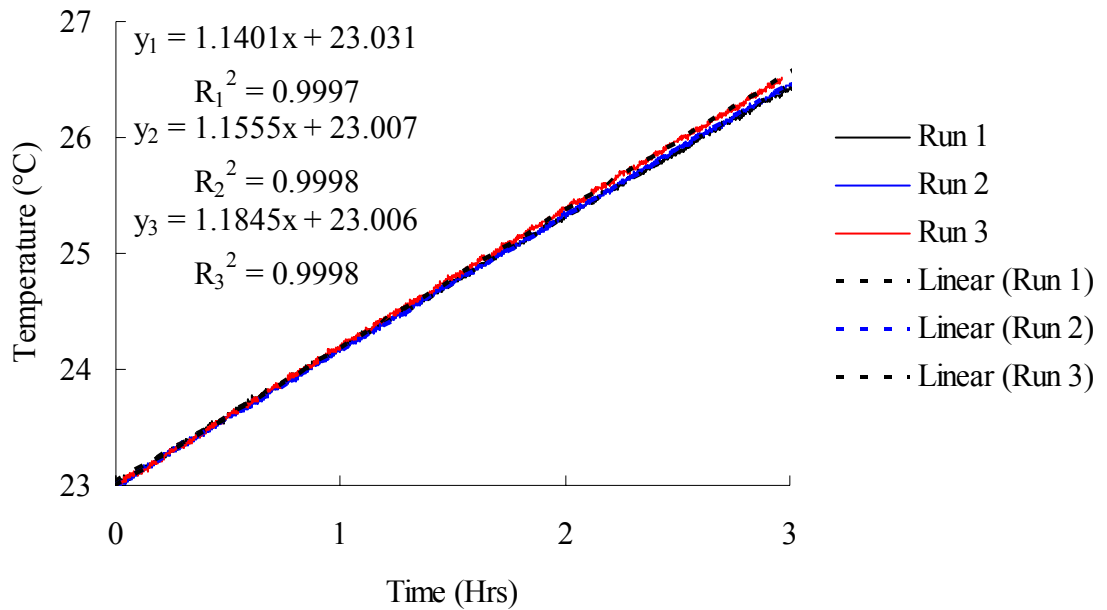
FIGURE 4.8 - Water Tank Temperature Change (Un-insulated / 100% Fill).

The average rate of temperature change was 1.160°C/hr, and the normalized standard deviation was 1.9%. The tested radiation levels are shown in the plot below (Fig 4.9).

48
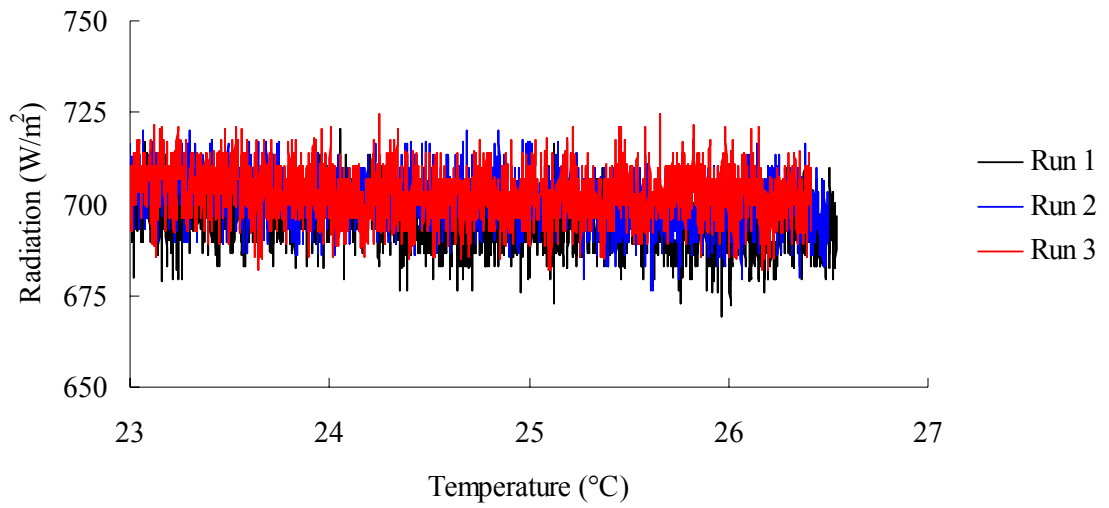
FIGURE 4.9 - Sampled Average Radiation Level (Un-insulated / 100% Fill).

The statistical results for the radiation level are shown in Table V.

TABLE V

RADIATION DATA FOR 100% FILL AND UN-INSULATED ADIABATIC

Minimum	669.35	W/m^2
Mean	699.37	W/m^2
Maximum	724.73	W/m^2
Standard Deviation	7.62	
StDev / Mean	1.09%	

The water tank temperature change using an insulated adiabatic section is shown in the plot below (Fig. 4.10).
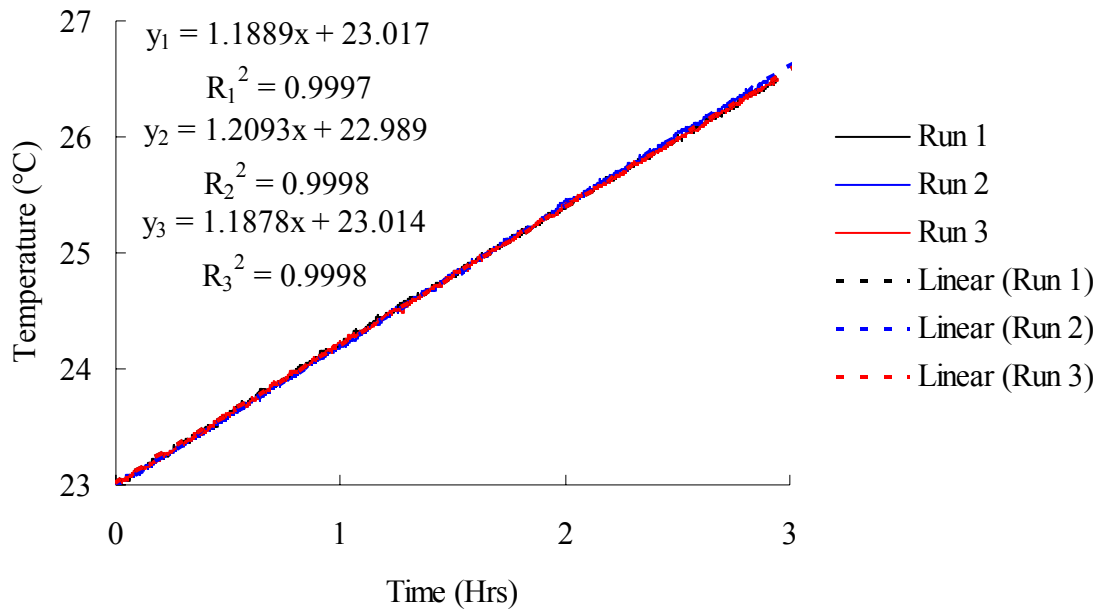
FIGURE 4.10 - Water Tank Temperature Change (Insulated / 100% Fill).

The average rate of temperature change was 1.195°C/hr, and the normalized standard deviation was 1.0%. The measured radiation values for the trail are plotted below (Fig. 4.11).
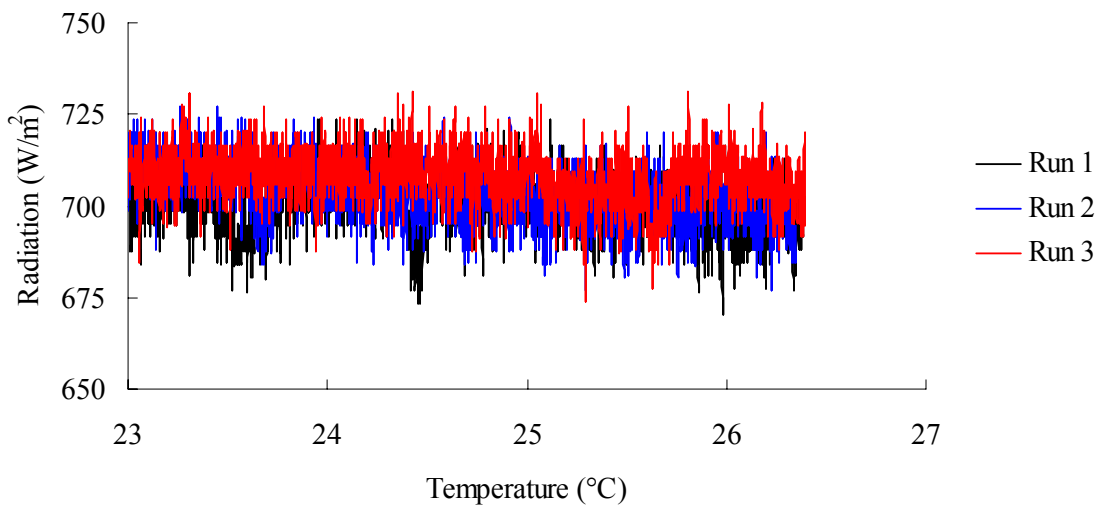
FIGURE 4.11 – Sampled Average Radiation Level (Insulated / 100% Fill).

The statistics of the radiation measurements are shown in Table VI.

TABLE VI

RADIATION DATA FOR 100% FILL AND INSULATED ADIABATIC SECTION

Minimum	670.08	W/m^2
Mean	701.98	W/m^2
Maximum	727.14	W/m^2
Standard Deviation	7.97	
StDev / Mean	1.13%	

c. 120 % Fill Level. Using an un-insulated adiabatic section and charging the heat pipe evaporator section to 120% volume, the change in tank temperature with respect to time is plotted (Fig. 4.12).

$y_1 = 1.175x + 23.042$
$R_1^2 = 0.9994$
$y_2 = 1.1988x + 22.993$
$R_2^2 = 0.9998$
$y_3 = 1.1948x + 23.017$
$R_3^2 = 0.9997$

Run 1
Run 2
Run 3
Linear (Run 1)
Linear (Run 2)
Linear (Run 3)
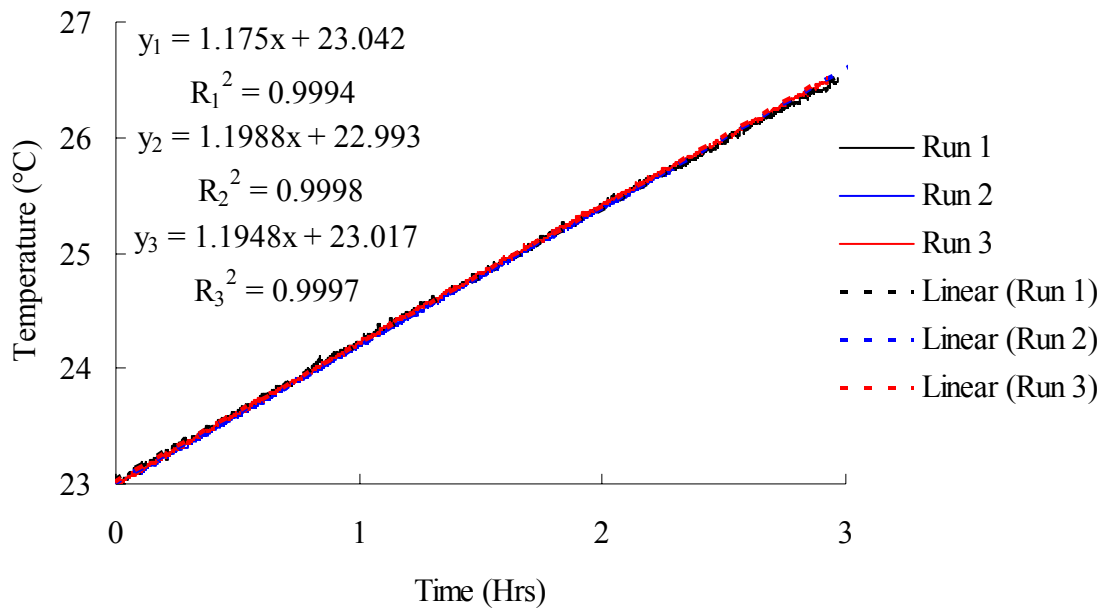
FIGURE 4.12 - Water Tank Temperature Change (Un-insulated / 120% Fill).

The average rate of temperature change was 1.190°C/hr, and the normalized standard deviation was 1.1%. The measured radiation values for the trial are plotted below (Fig. 4.13).
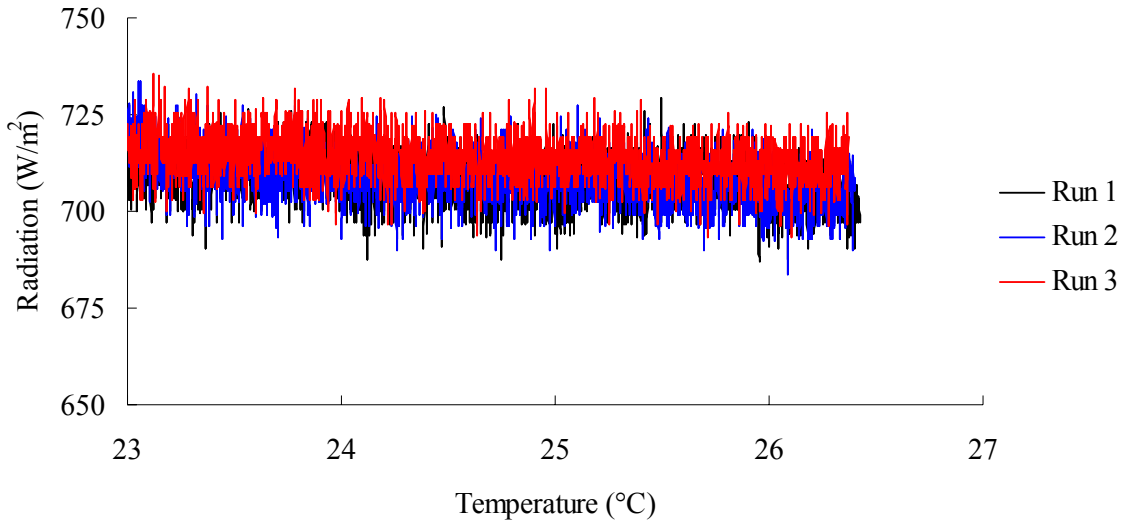
FIGURE 4.13 - Sampled Average Radiation Level (Un-insulated / 120% Fill).

The radiation results are tabulated in Table VII.

TABLE VII

RADIATION DATA FOR 120% FILL AND UN-INSULATED ADIABATIC SECTION

Minimum	683.55	W/m^2
Mean	710.09	W/m^2
Maximum	735.17	W/m^2
Standard Deviation	7.08	
StDev / Mean	1.00%	

Fig. 4.14 shows the water tank temperature change with an insulated adiabatic section.

$y_1 = 1.2122x + 23.001$

$R_1{}^2 = 0.9998$

$y_2 = 1.2301x + 23.016$

$R_2{}^2 = 0.9998$

$y_3 = 1.2259x + 23.004$

$R_3{}^2 = 0.9998$
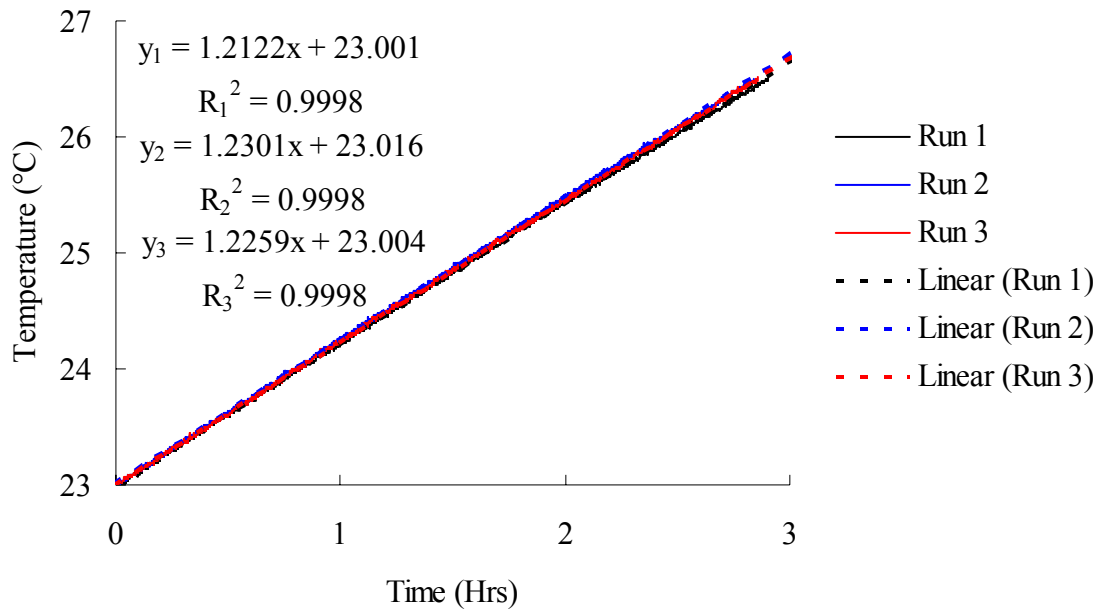
FIGURE 4.14 - Water Tank Temperature Change (Insulated / 120% Fill).

The average rate of temperature change was 1.223°C/hr, and the normalized standard deviation was 0.8%. Fig. 4.15 shows the measured radiation levels during the trial.
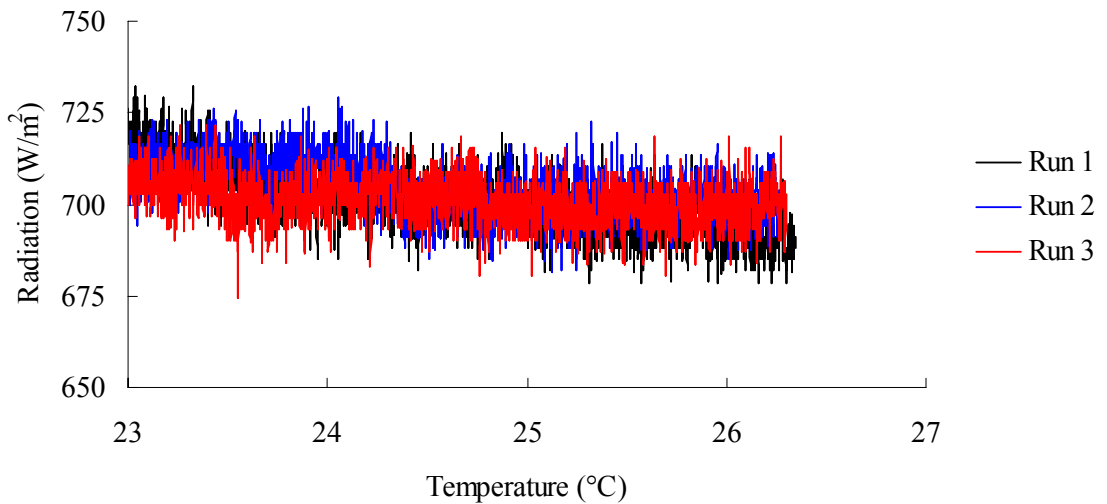
FIGURE 4.15 - Sampled Average Radiation Level (Insulated / 120% Fill).

The measured results are shown in Table VIII.

TABLE VIII

RADIATION DATA FOR 120% FILL AND INSULATED ADIABATIC SECTION

Minimum	674.53	W/m^2
Mean	702.32	W/m^2
Maximum	732.26	W/m^2
Standard Deviation	8.13	
StDev / Mean	1.16%	

d. 140 % Fill Level. Fig. 4.16 shows the temperature change for the un-insulated adiabatic section with 140 % fill level.
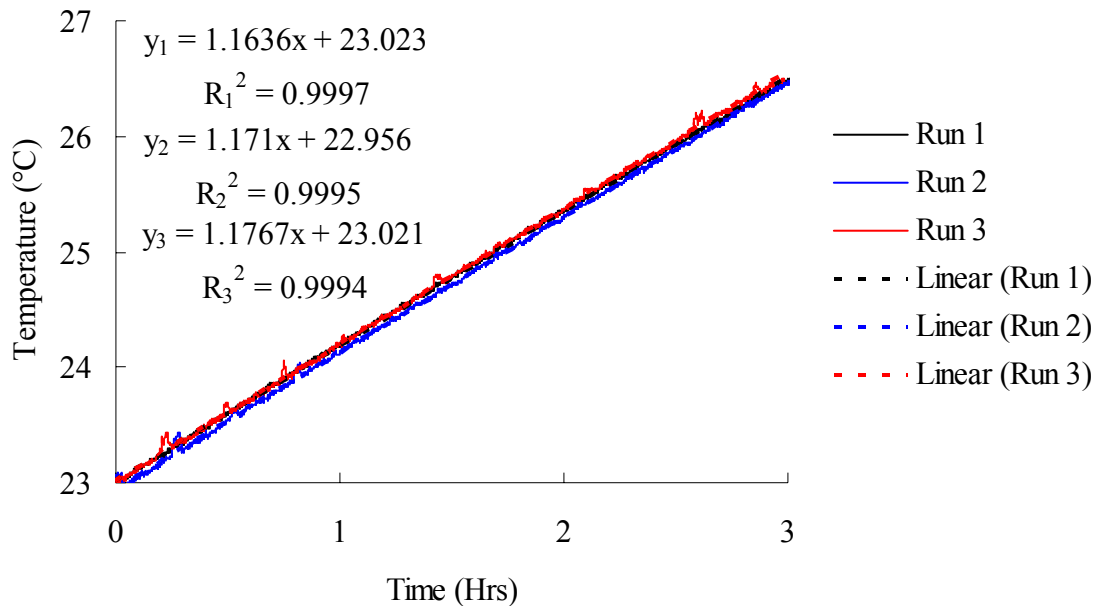
FIGURE 4.16 - Water Tank Temperature Change (Un-insulated / 140% Fill).

The average rate of temperature change was 1.170°C/hr, and the normalized standard deviation was 0.6%. The measured radiation levels are shown in Fig. 4.17.
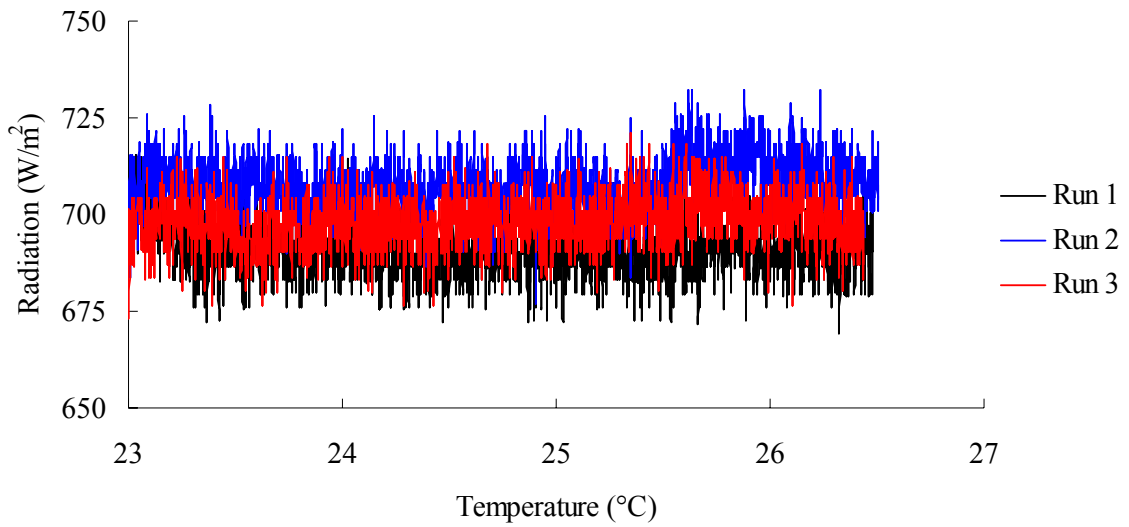
FIGURE 4.17 - Sampled Average Radiation Level (Un-insulated / 140% Fill).

Table IX shows the statistical radiation results.

TABLE IX

RADIATION DATA FOR 140% FILL AND UN-INSULATED ADIABATIC SECTION

Minimum	669.06	W/m^2
Mean	699.12	W/m^2
Maximum	732.36	W/m^2
Standard Deviation	9.95	
StDev / Mean	1.42%	

Fig. 4.18 shows the water tank temperature change with an insulated adiabatic section.

$y_1 = 1.2073x + 23.02$
$R_1^2 = 0.9998$
$y_2 = 1.2186x + 23.012$
$R_2^2 = 0.9998$
$y_3 = 1.1786x + 23.016$
$R_3^2 = 0.9998$
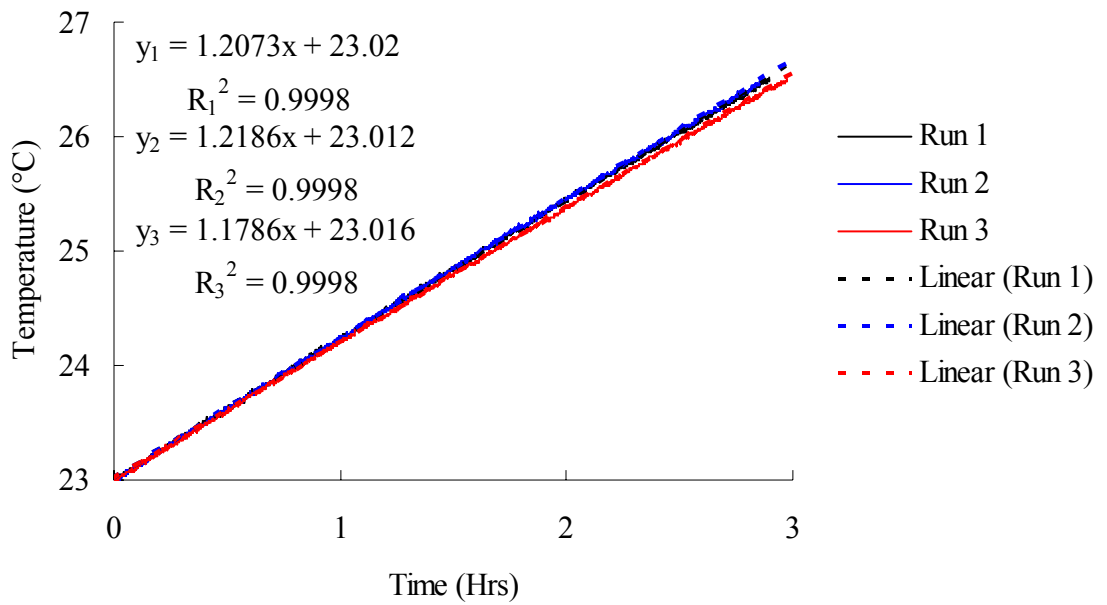
FIGURE 4.18 – Water Tank Temperature Change (Insulated / 140% Fill).

The average rate of temperature change was 1.202°C/hr, and the normalized standard deviation was 1.7%. The measured radiation levels are plotted below (Fig. 4.19).
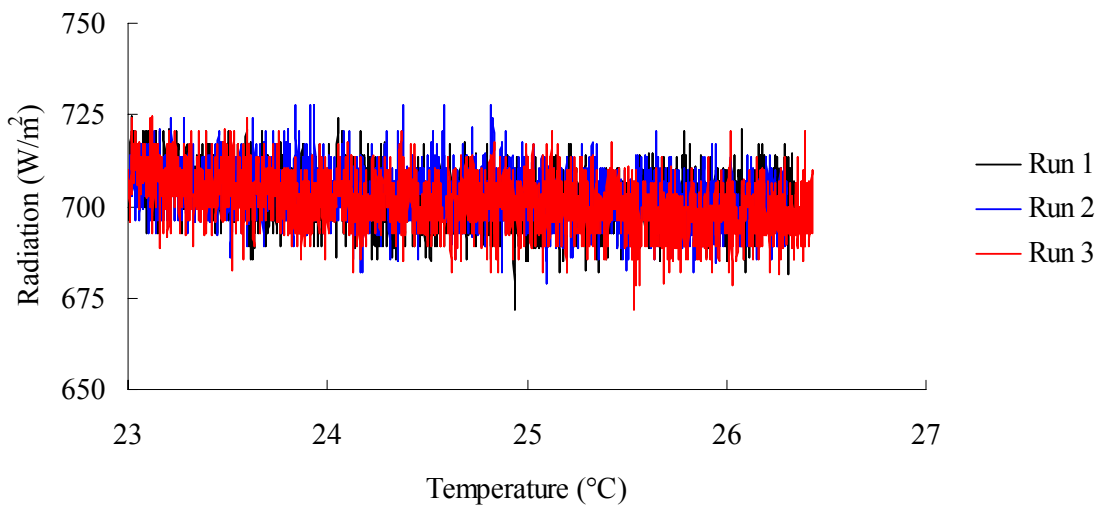
FIGURE 4.19 - Sampled Average Radiation Level (Insulated / 140% Fill).

The radiation results are shown in Table X.

TABLE X

RADIATION DATA FOR 140% AND INSULATED ADIABATIC SECTION

Minimum	671.73	W/m^2
Mean	702.21	W/m^2
Maximum	727.63	W/m^2
Standard Deviation	7.34	
StDev / Mean	1.04%	

e. Finned Condenser Section. The highest average temperature change per hour was achieved with a charge of 120% volume of the evaporator section. The insulated adiabatic section performed better in all cases. A finned condenser was then tested on the heat pipe using an insulated adiabatic section and 120% fill level. Fig. 4.20 shows the performance of the finned condenser section.
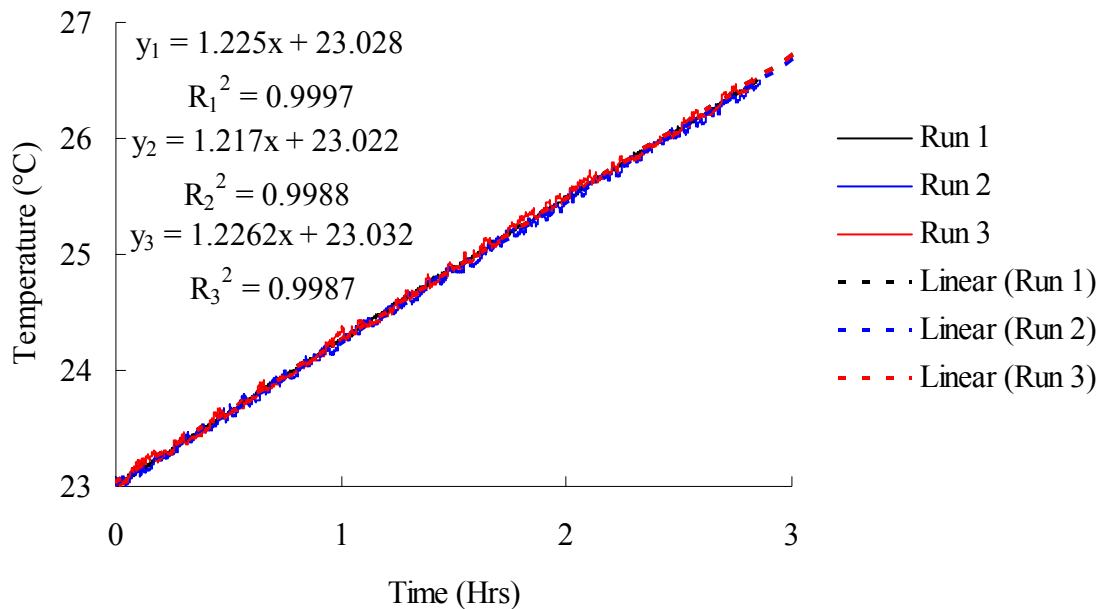
FIGURE 4.20 - Water Tank Temperature Change (Insulated / 120% Fill / Finned).

The average rate of temperature change was 1.223°C/hr, and the normalized standard deviation was 0.4%. After increasing the surface area of the condenser the rate of temperature change was expected to increase. The lack of improvement in this design change suggest that heat transfer between the condenser and the radial fins is limited and performing incorrectly. The measure radiation levels are shown in Fig. 4.21.
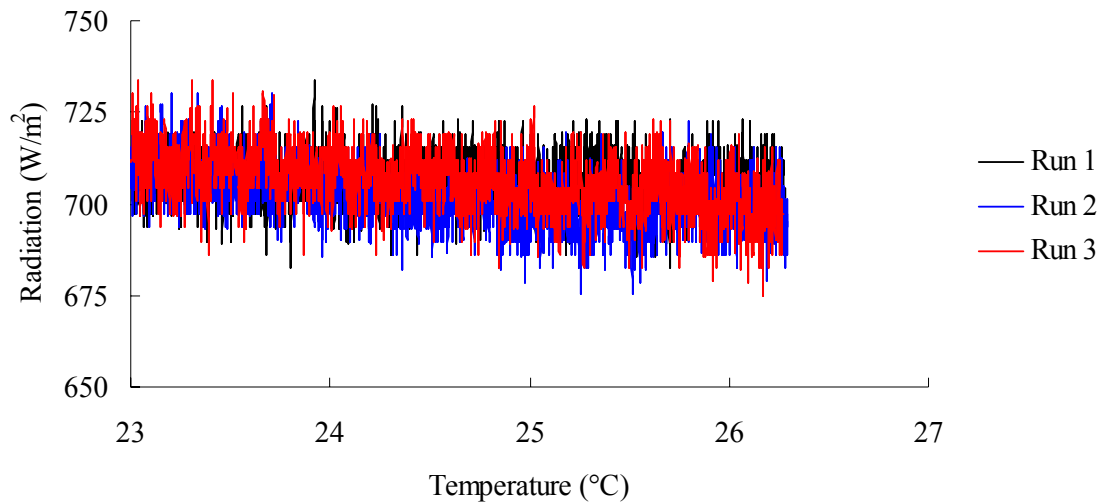
FIGURE 4.21 - Sampled Average Radiation Level (Insulated / 120% Fill / Finned).

The results are shown in Table XI.

TABLE XI

RADIATION DATA FOR 120% FINNED CONDENSER AND INSULATED

Minimum	675.19	W/m^2
Mean	704.86	W/m^2
Maximum	733.93	W/m^2
Standard Deviation	8.23	
StDev / Mean	1.17%	

3. Overall System Efficiency

For each experimental setup the overall system efficiency was averaged and are shown below (Fig. 4.22).
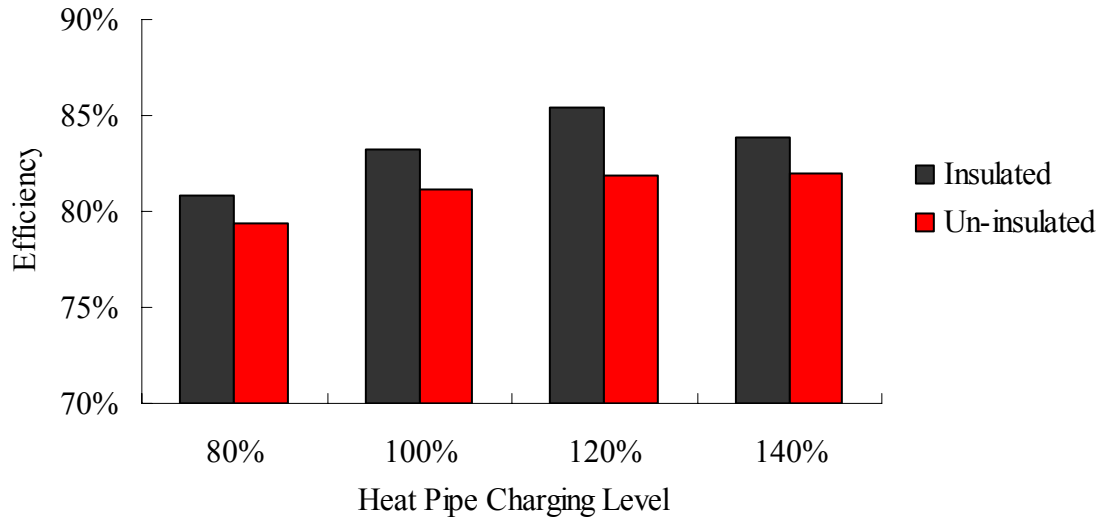
FIGURE 4.22 – Experimental Overall System Efficiency.

System efficiency for the different fill levels were compared using analysis of variance. The one-way ANOVA results with a 95% confidence interval for fill level percentage are shown in Table XII.

TABLE XII

ONE-WAY ANOVA: SYSTEM EFFICIENCY VS. FILL LEVEL PERCENTAGE

Level	N	Mean	Std. Dev.		
80%	6	0.80107	0.00945		
100%	6	0.82197	0.01636		
120%	6	0.83679	0.02089		
140%	6	0.82927	0.01315		
Source	Degrees of Freedom	Sum of Squares	Mean Squares	F	p
Fill Level Percentage	3	0.004257	0.001419	5.87	0.005
Error	20	0.004832	0.000242		
Total	23	0.009089			

The boxplot of system efficiency versus fill level percentage is shown below (Fig. 4.22). The whisker lines on the boxplot show the maximum and minimum data values. 25% of the data is less than the lower fence of the boxplot. 25% of the data is greater than the upper fence of the boxplot. The line in the box represents the median of the data. The statistical mean of the data is represented by a circle and the means for each data set are connected.
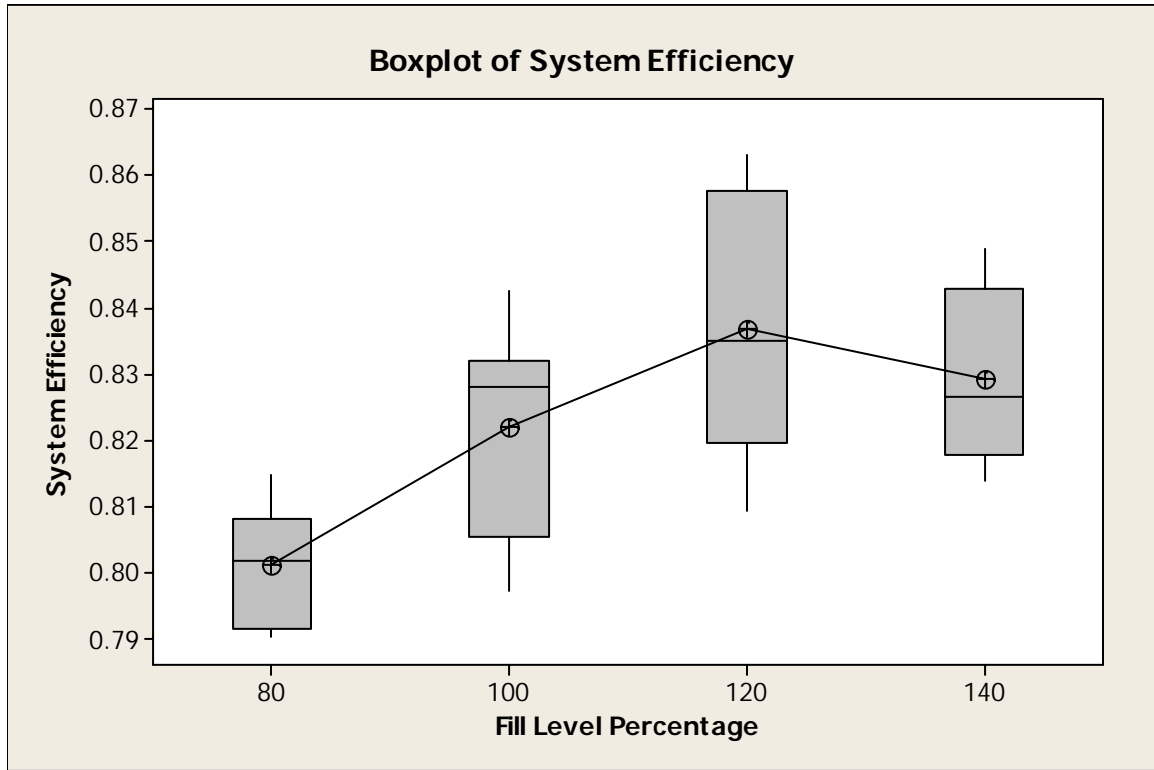
FIGURE 4.23 - System Efficiency Vs. Fill Level Percentage Boxplot.

The one-way ANOVA results with a 95% confidence interval for insulated

adiabatic section are shown in Table XIII.

TABLE XIII

ONE-WAY ANOVA: SYSTEM EFFICIENCY VS. INSULATED ADIABATIC

Level	N	Mean	Std. Dev.		
Un-Insulated	12	0.81081	0.01386		
Insulated	12	0.83374	0.01864		

Source	Degrees of Freedom	Sum of Squares	Mean Squares	F	p
Insulated Adiabatic	1	0.003154	0.003154	11.69	0.002
Error	22	0.005935	0.00027		
Total	23	0.009089			

The boxplot of system efficiency versus fill level percentage is shown below (Fig. 4.24).

61

Boxplot of System Efficiency

System Efficiency

0.87
0.86
0.85
0.84
0.83
0.82
0.81
0.80
0.79

No   Yes
Insulated Adiabatic Section
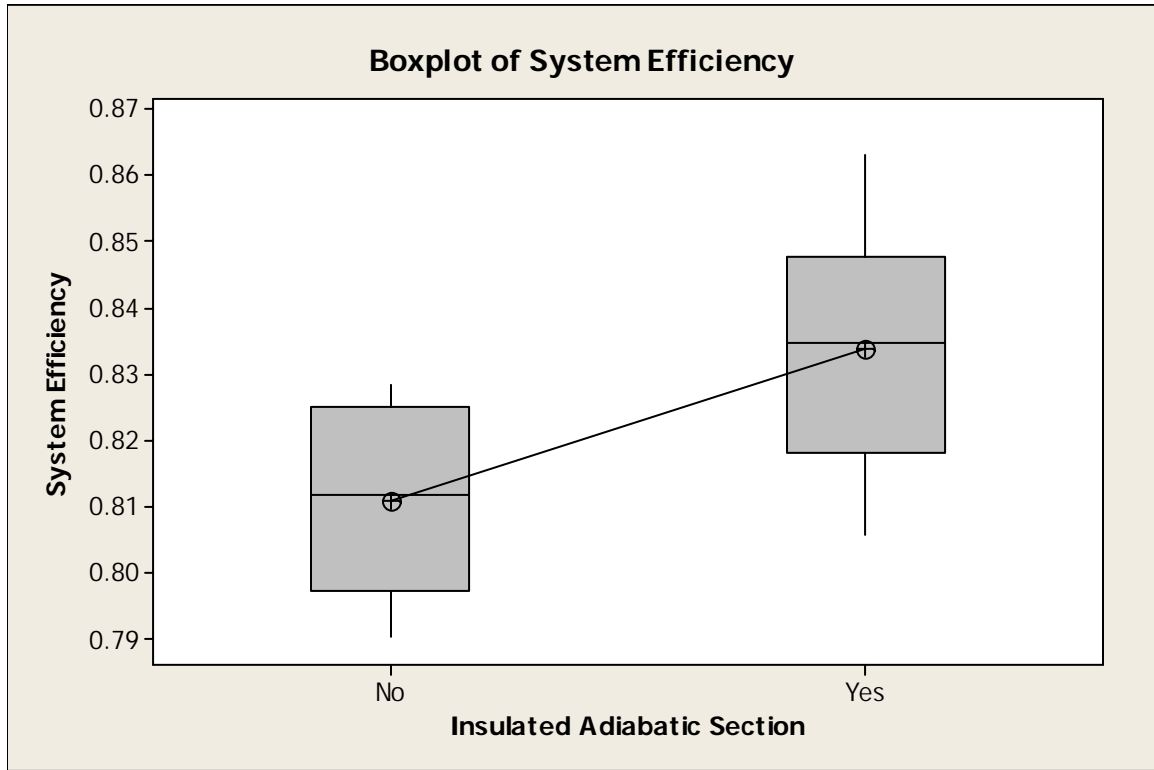
FIGURE 4.24 - System Efficiency Vs. Insulated Adiabatic Section.

The one-way ANOVA results with a 95% confidence interval for finned

condenser section are shown in Table XIV.

TABLE XIV

ONE-WAY ANOVA: SYSTEM EFFICIENCY VS. FINNED CONDENSER

Level	N	Mean	Std. Dev.		
No	3	0.85434	0.00954		
Yes	3	0.8519	0.00867		

Source	Degrees of Freedom	Sum of Squares	Mean Squares	F	p
Finned Condenser	1	0.0000089	0.0000089	0.11	0.76
Error	4	0.0003322	0.000083		
Total	5	0.0003411			

4. Error Propagation

Input Voltage, % of reading, offset, and noise for each data acquisition system module are shown in Table XV.

TABLE XV

DATA ACQUISITION ABSOLUTE ACCURACY INPUTS

D.A.Q. Module	V_i	% of Reading	Offset	Noise
SCXI-1102	100 mV	0.0200	15 μV	5 μV
SCXI-1600	500 mV	0.0588	29 μV	3 μV

After calibration the absolute accuracy of the SCXI-1102 module was ± 2 mV, and the SCXI-1600 module was ± 3 mV. The system accuracy of the entire data acquisition system was ± 3.6 mV, and the system accuracy with respect to input was 0.72%. The pyranometers had an overall error of $\pm 2\%$ as stated by the manufacturer Kipp and Zonnen. The T type thermocouples had an error of ± 0.1 °C. The uncertainty of the water tank mass, radiation, and temperature measurement was $\pm 0.27\%$, $\pm 2.13\%$, and $\pm 0.79\%$ respectively. The uncertainty in the calculated system efficiency is 0.72%.

B. Computer Simulation

1. Climate Comparison

The computer simulation was used to compare four types of passive solar systems including: direct gain, indirect gain concrete wall, indirect gain water wall, and the heat pipe wall. The climates selected for performance comparison were: Albuquerque, New Mexico (cool and sunny); Louisville, Kentucky (cool and cloudy); Rock Springs,

Wyoming (cold and sunny); Madison, Wisconsin (cold and cloudy). Below, (Fig. 4.25),

the solar fraction achieved by each passive solar system in the separate climates is shown.
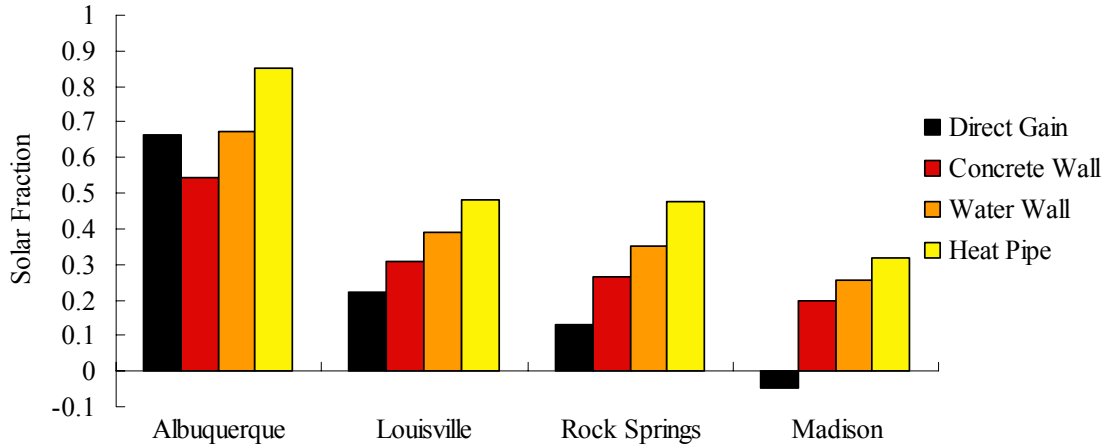
FIGURE 4.25 - Climate Comparison Of Passive Solar Systems.

The direct gain and water wall system in Albuquerque had solar fractions of 0.6639 and

0.6715 respectfully. The direct gain system in Madison had a solar fraction of -0.0451.

The concrete wall system in Louisville, Rock Springs and Madison had solar fractions of

0.3077, 0.2663, and 0.1988 respectfully. Albuquerque had the highest overall solar

fraction with 0.8512 for the heat pipe system. The water wall system in Madison had a

solar fraction of 0.2576 compared to the heat pipe system which had a solar fraction of

0.3189. Comparing the water wall system, Louisville had a solar fraction of 0.3884 and

Rock Springs had a solar fraction of 0.3517. The heat pipe system in Rock Springs had a

solar fraction of 0.4785 and in Louisville the heat pipe system had a solar fraction of

0.4836.

2. Heat Pipe Performance

The computer simulation was first run for a baseline scenario (Table XVI) for

Julian hours 300 to 700 (January 13th –January 30th). This baseline design was used to

compare all design parameters and is similar to the design used by Susheela and Sharp [2001].

<div align="center">TABLE XVI</div>

<div align="center">COMPUTER SIMULATION BASE CASE PARAMETERS</div>

Parameter	Variable	Value
Cover (Number)	N_c	1
Cover (Thickness)	t_c	0.003175 (m)
Cover (Emittance)	ε_g	0.88
Cover (Extinction Coefficient)	α_g	4 (m-1)
Absorber Plate (Material Conductivity)	k_a	Copper
Absorber Plate (Selective Surface)	N/A	Black Chrome
Absorber Plate (Thickness)	t_a	0.003175 (m)
Absorber Plate (Insulation Thickness)	t_i	0.025 (m)
Absorber Plate (Insulation Conductivity)	k_i	0.05 (W/mK)
Absorber Plate (Height)	H_a	2.0828 (m)
Absorber Plate (Width)	W_a	1.165225 (m)
Heat Pipe (Number, Spacing)	N_p,W	5 , 0.3471342 (m)
Heat Pipe (Material Conductivity)	k_p	Copper
Heat Pipe (Inclination Angle)	N/A	(No Vapor Column Conductance)
Heat Pipe (Wick Structure)	N/A	(None)
Condenser Fin (Number)	N_{cf}	(None)
Water Tank (Number)	N	1
Water Tank (Height)	H_t	1.9558 (m)
Water Tank (Length)	L_t	1.190625 (m)
Water Tank (Width)	W_t	0.2032 (m)
Water Tank (Wall Thickness)	t_t	0.003175 (m)
Water Tank (Material Conductivity)	k_t	0.5 (W/mK)
Night Time Insulation Conductivity	k_{24}	0.6072 (W/m^{2}K)
Ground Reflectance Factor	ρ_g	0.3
LCR	k_{71}	10 (W/m^{2}K)

The solar fraction for the baseline was 48.36%. The nodal temperatures for the heat pipe system in Louisville, Kentucky for the selected two-week period in January are shown in Fig. 4.26.
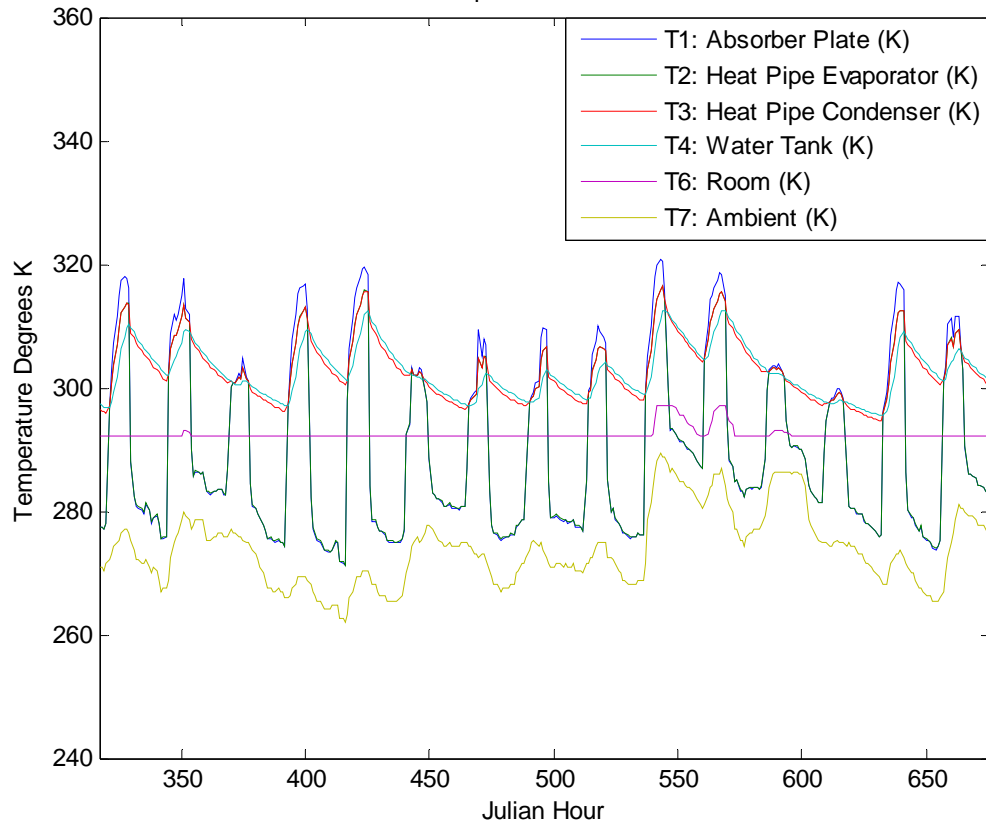
FIGURE 4.26 - Heat Pipe Wall Temperatures.

The radiation for this trial is plotted below (Fig. 4.27).
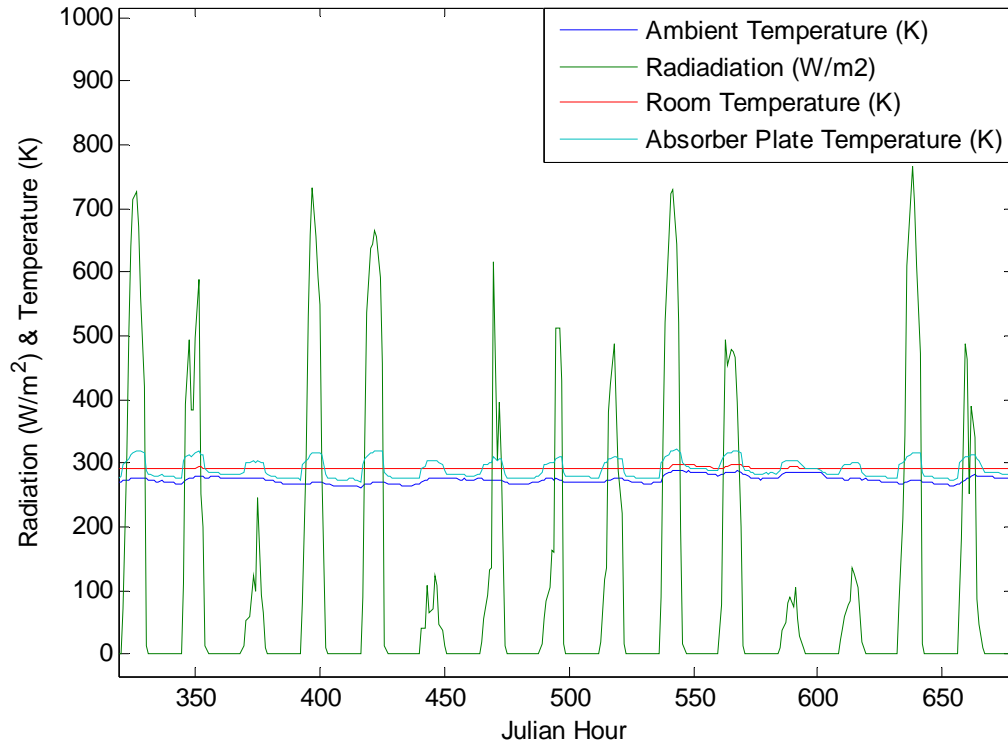
FIGURE 4.27 – Computer Simulation Radiation and Temperatures.

3. Heat Pipe Design Performance

The load to collector ratio was the first design parameter tested with the simulation. The solar fractions resulting from a range of load collector ratio values are shown in Fig. 4.28.
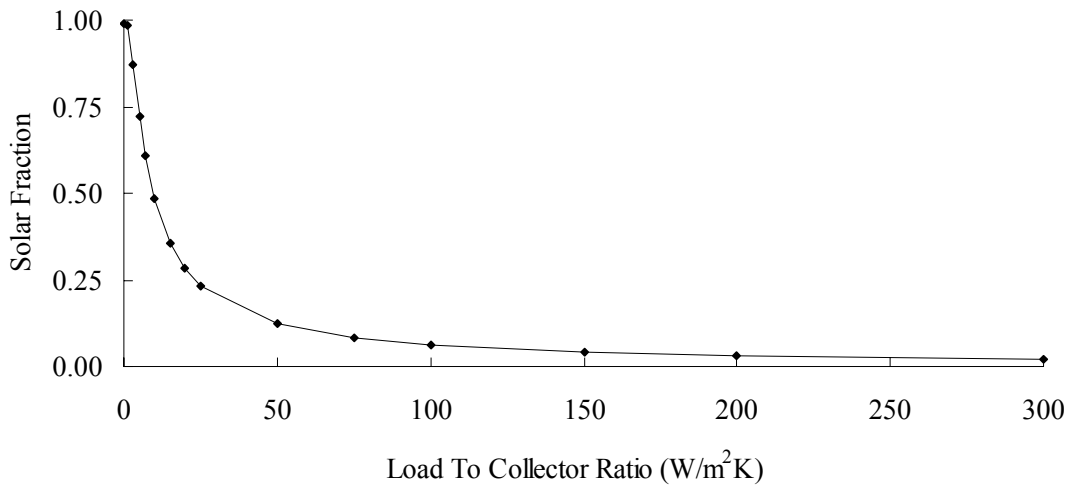
FIGURE 4.28 – Simulation Results for Load to Collector Ratio.

The baseline load to collector ratio was selected from these results. This value was

selected with an approximate solar fraction of 0.50, enabling the comparison of

performance based on design element changes. A load to collector ratio of 10 W/m^2K

and a solar fraction of 0.4836 was chosen as the simulation baseline. The baseline

parameter value is marked with an asterisk for the following computer simulations. The

next design element evaluated was the number of covers (Fig. 4.29).
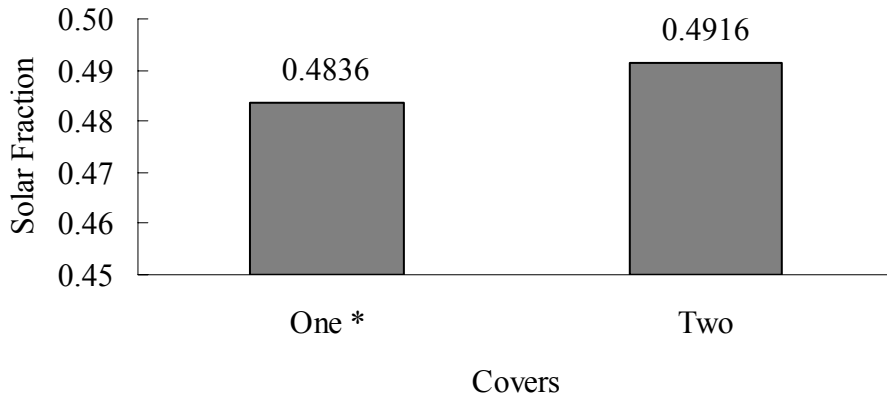
FIGURE 4.29 – Simulation Results for Number of Collector Covers.

The variation in solar fraction with respect to changes in cover thickness is shown in Fig. 4.30. Typical window glass is 3.175 mm thick (1/8 inch), while solar collectors typically use 2.38 mm glass (3/32 inch).
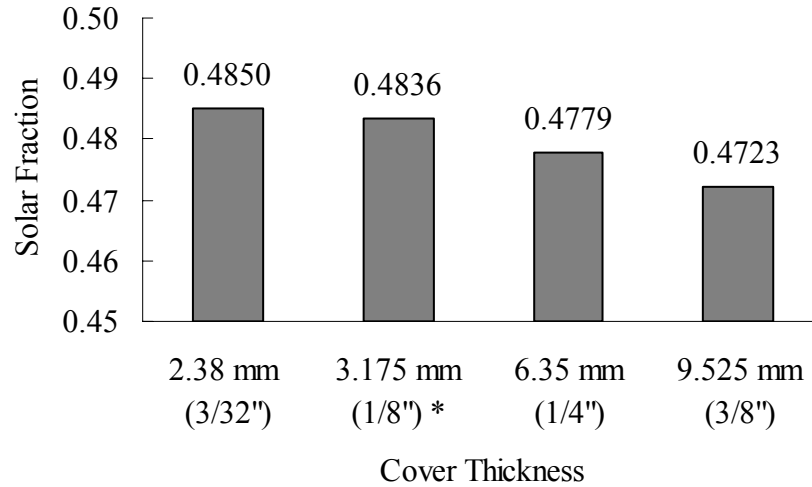
FIGURE 4.30 – Simulation Results For Collector Cover Thickness.

Fig. 4.31 shows the effects of changing the glass extinction coefficient. The extinction coefficient of the solar cover is changed by regulating the amount of iron in the glass. "Water white" glass has an extinction coefficient of 4 m^{-1}. Glass that has a greenish cast along its edge has a higher extinction coefficient and can be 32 m^{-1}. Many windows are made from "soda-lime" glass which has an extinction coefficient of 13 m^{-1}.
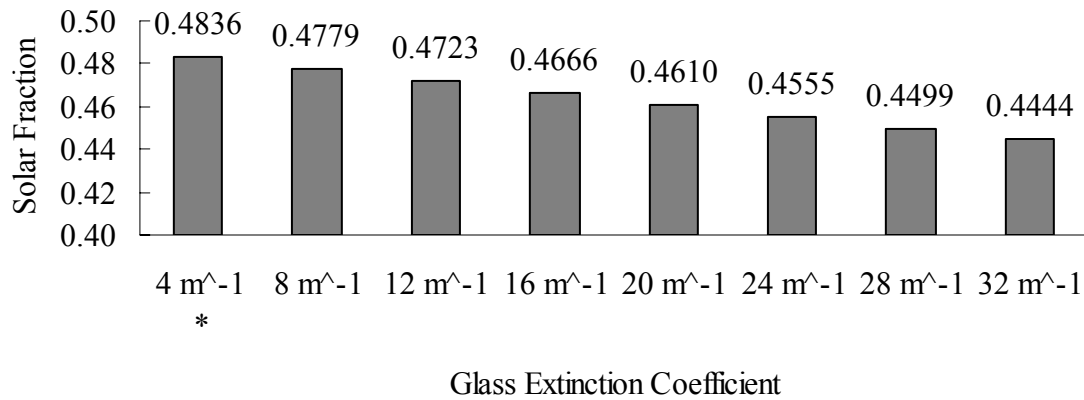
FIGURE 4.31 – Simulation Results For Glass Extinction Coefficient.

Changing the absorber plate material and the selective surface impacts the overall solar

fraction (Fig. 4.32). The selective surface changes both the absorptance and the

emissivity of the absorber plate. The absorptance of common solar plate surfaces is

shown below in Table XVII.

TABLE XVII

ABSORPTANCE OF SELECTIVE SURFACES

Selective Surface	α
Polished Aluminum	0.1
Polished Copper	0.18
Flat Black Paint	0.98
Black Nickel	0.91
Black Chrome	0.96
Black Copper	0.98
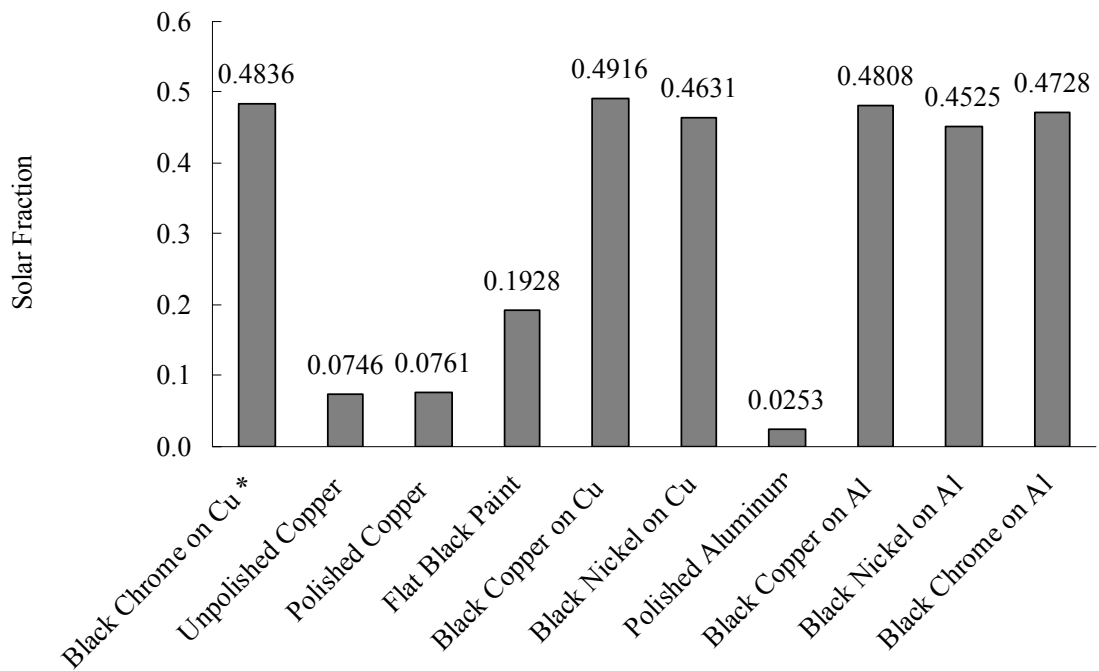
FIGURE 4.32 – Simulation Results For Absorber Plate Material And Selective Surfaces.

Fig. 4.33 shows the performance changes associated with adjusting the absorber plate

thickness. Typical active collector absorber plate thicknesses range from 1.58 mm (1/16

inch) to 3.175 mm (1/8 inch).
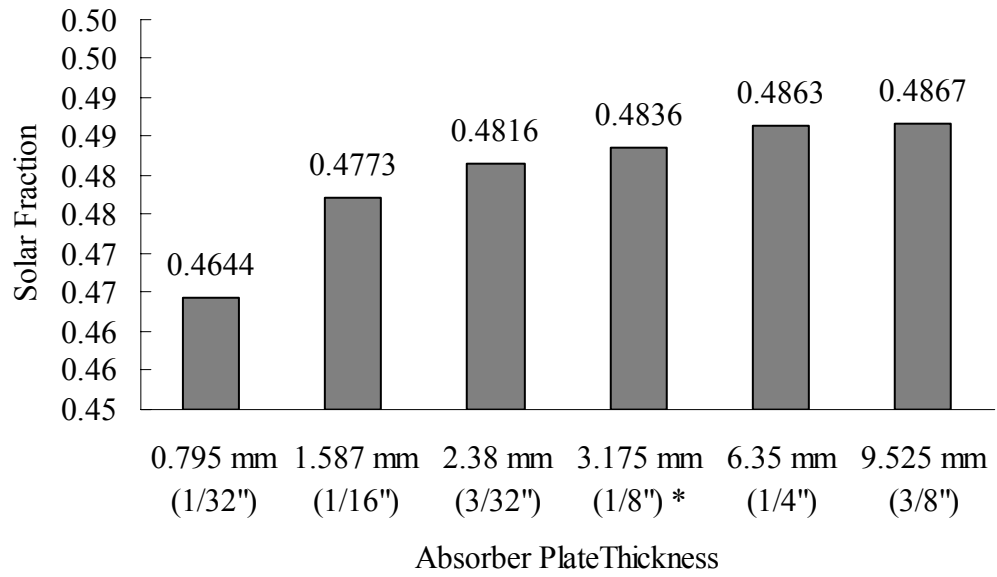
FIGURE 4.33 – Simulation Results For Absorber Plate Thickness.

Solar fraction differences with changing the thickness of the insulation surrounding the edges and bottom of the collector are shown in Fig. 4.34. Typical active solar collector insulation thickness ranges from 25 mm to 50 mm.
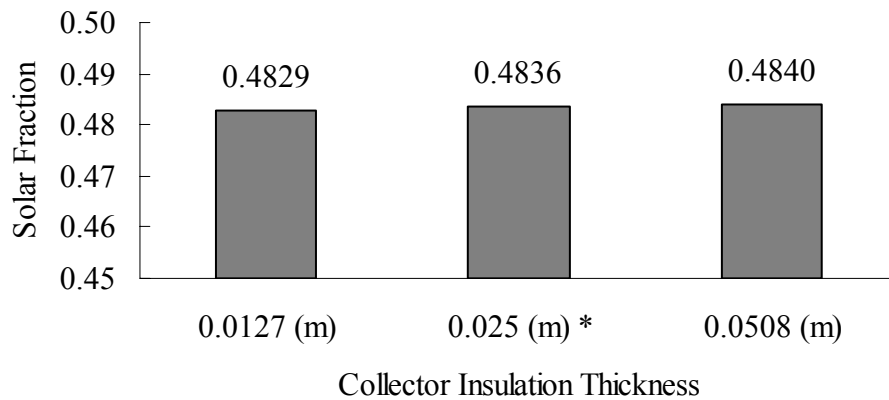
FIGURE 4.34 – Simulation Results For Collector Insulation Thickness.

The performance differences in changing the conductivity of the insulation are shown in

Fig. 4.35. Typical insulation conductivity is 0.05 W/mK.
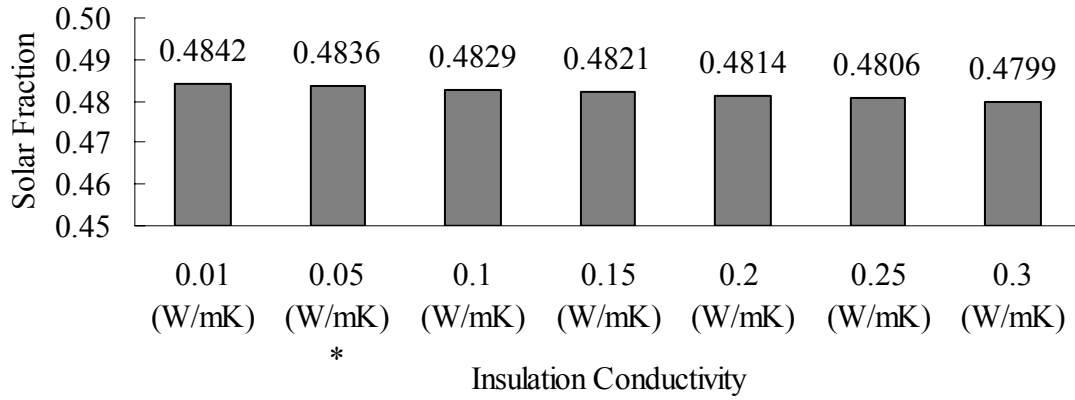
FIGURE 4.35 – Simulation Results For Insulation Ratings.

Solar fraction differences based on adjusting the heat pipe material are shown in Fig.

4.36.
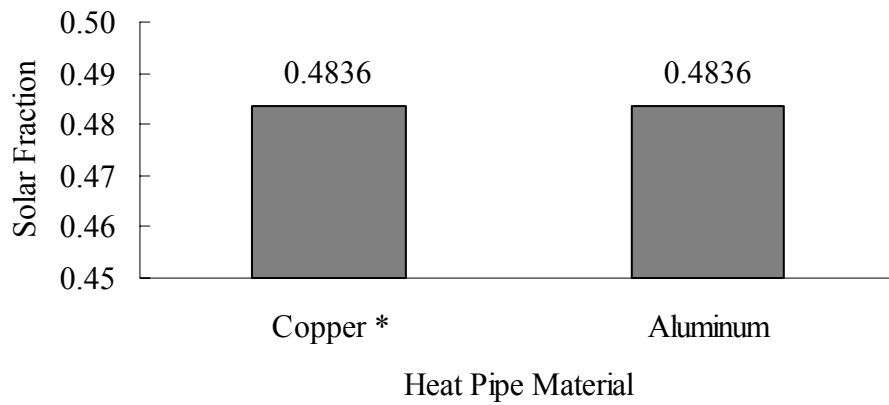
FIGURE 4.36 – Simulation Results For Heat Pipe Material.

Varying the number of heat pipes, while keeping the collector area constant, affects the solar fraction and is shown in Fig. 4.37.
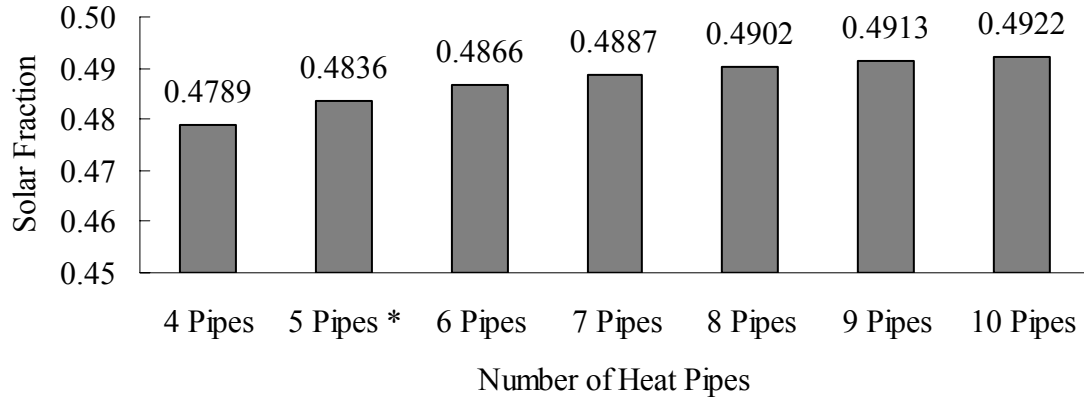
FIGURE 4.37 – Simulation Results For Heat Pipe Quantity.

The effect of increasing the volume of the mass storage device is shown in Fig. 4.38. The volume is changed by increasing the width (perpendicular to the surface of the wall) of the water wall.
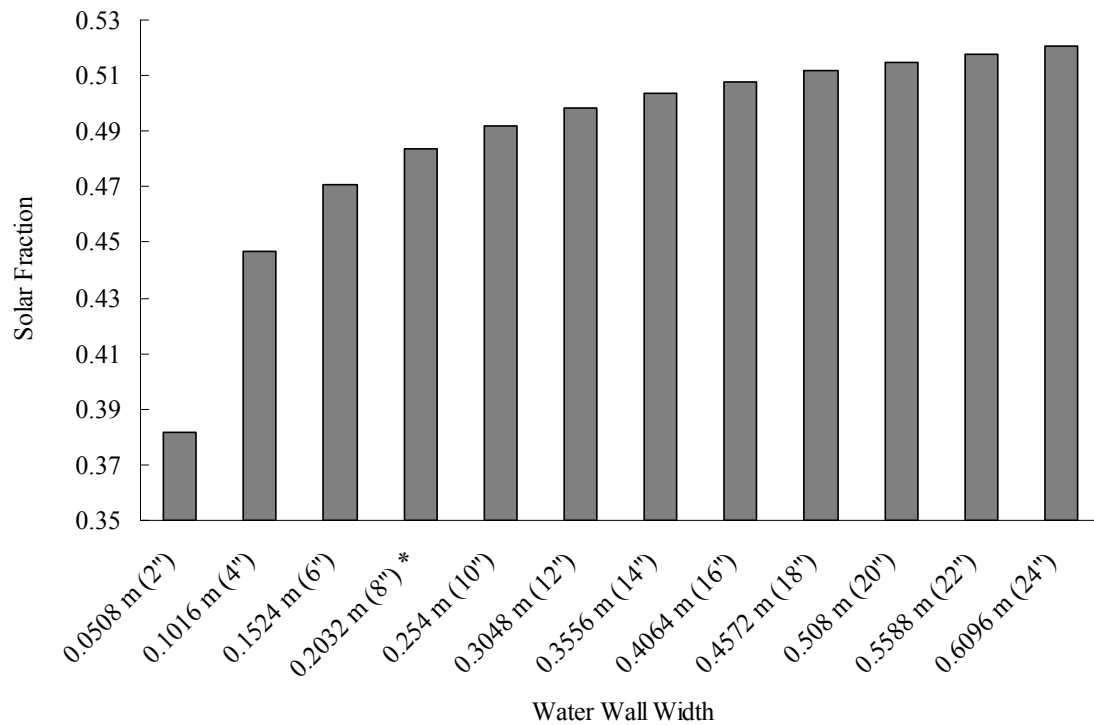
FIGURE 4.38 – Simulation Results For Water Wall Width.

By changing the types of plastic used to construct the water tanks the tank conductivity is changed. Typical water tanks are constructed of polyethylene and the thermal conductivity varies between 0.42 and 0.51 W/mK. The simulated results for tank conductivity changes are shown in Fig. 4.39.
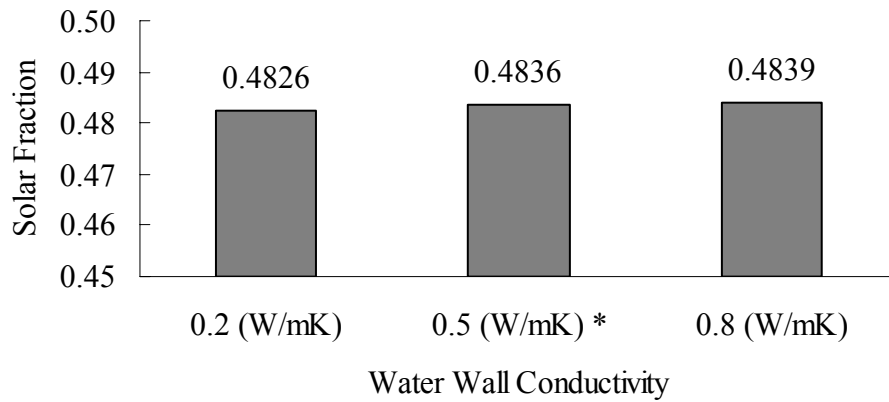
FIGURE 4.39 – Simulation Results For Water Wall Conductivity.

The results for changes in water tank wall thickness are shown below in Fig 4.40.
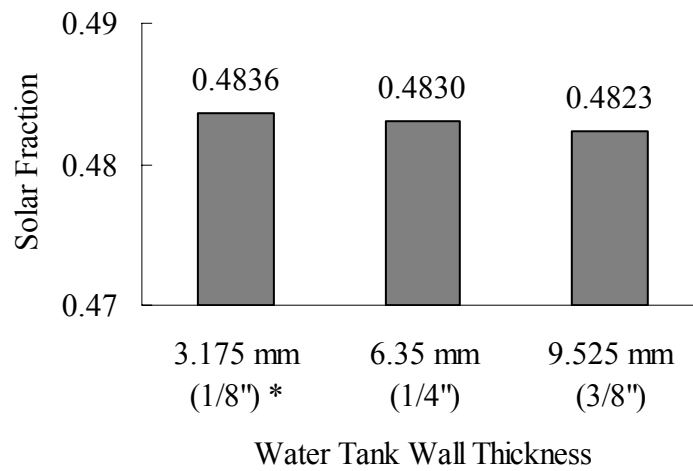
FIGURE 4.40 – Simulation Results for Water Tank Wall Thickness.

The convection coefficient varies for the water tanks as the shape of the water tank changes. The convection coefficient also varies with temperature, but typical values can

range from 0.5 W/m^{2}K to 10 W/m^{2}K. The impact of the convection coefficient on solar fraction is shown in Fig. 4.41.
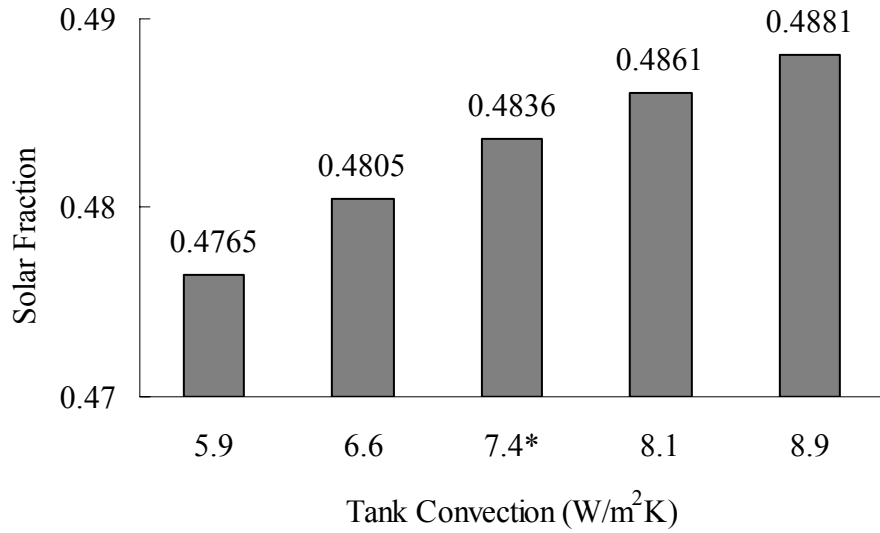
FIGURE 4.41 – Simulation Results For Tank Convection Coefficient.

To possibly improve the heat transfer between the heat pipe and the water tank external radial condenser fins were tested. The effects of condenser fins and changes in fin design are shown below (Fig. 4.42 -4.44).
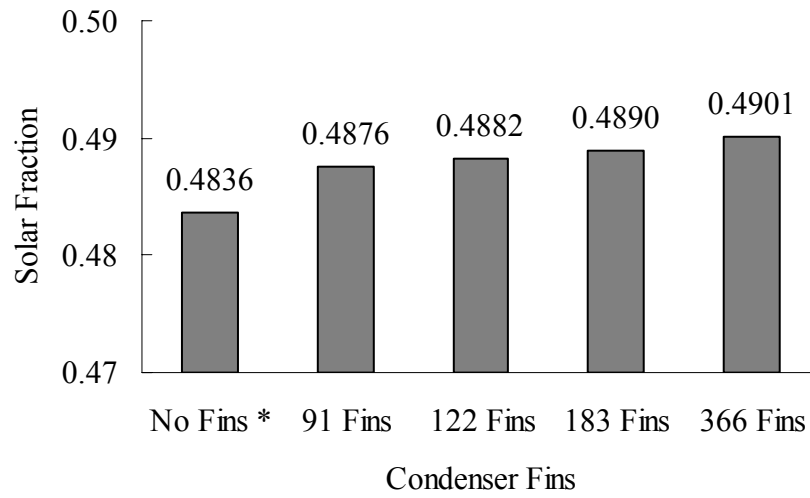
FIGURE 4.42 – Simulation Results For Number of Condenser Fins.
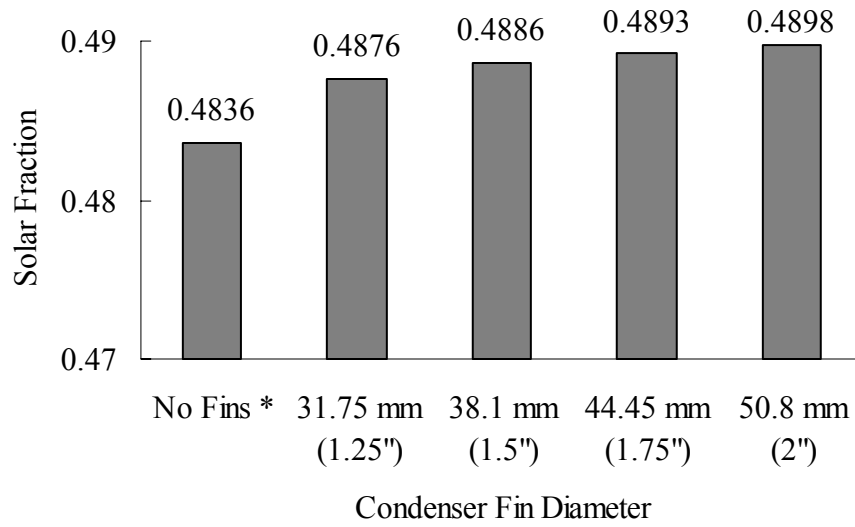
FIGURE 4.43 – Simulation Results For Condenser Fin Diameter.
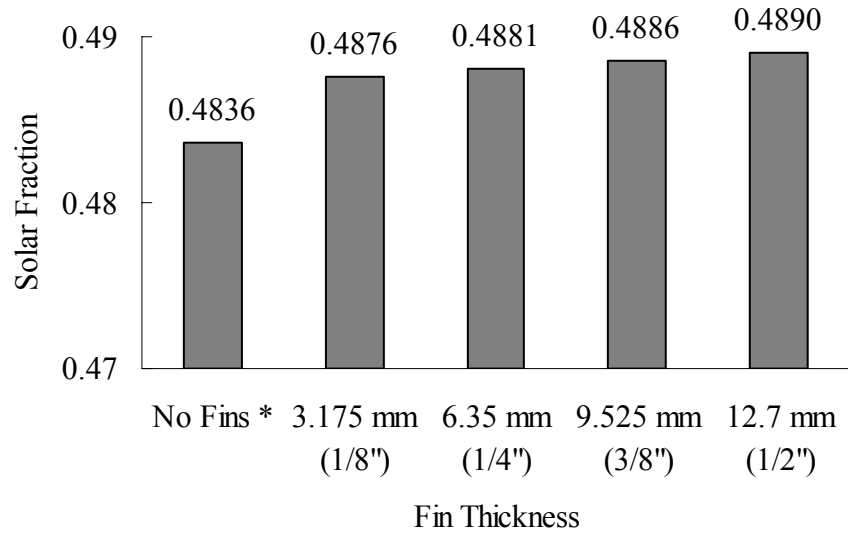
FIGURE 4.44 – Simulation Results For Condensers Fin Thickness.

Changing the thickness and design of the wall between the absorber plate and the water tanks, changes the nighttime insulation value. A typical value for nighttime insulation conductivity is 0.6072 W/m^{2}K. The effects of the nighttime insulation conductance are shown in Fig. 4.45.
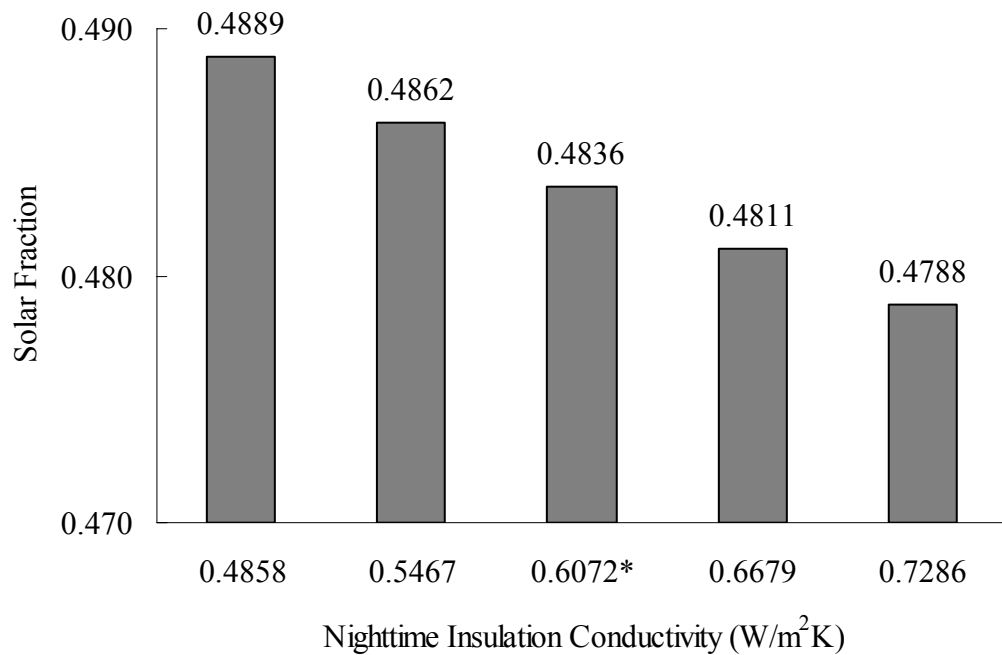
FIGURE 4.45 – *Simulation Results For Nighttime Insulation.*

C. Experimental And Simulation Matching

Validation of the computer simulation was achieved by matching the calculated

nodal temperatures of the computer simulation to the measured data from the laboratory

experiments. The computer simulation does not calculate performance variations

associated with fluid fill level. Therefore, the experiment with the best performance was

chosen for matching the simulation. Inputs for the simulation were adjusted to directly

mimic the experiment. These included changing the absorber plate area, number of heat

pipes, insulating the water tank, and changing the input radiation. Starting nodal

temperatures were also adjusted so that they were the same for both the simulation and

experiment. Nodal conductances were then adjusted to achieve the appropriate

temperatures. In the simulation the nodal mass is set at zero for each node excluding the

water tank. The nodal temperatures heat up quickly because there is no thermal mass associated with that respective node. The mass specific heat product of the water tank was calculated as 816920 J/m^{2}K and dampens the temperature rise. Fig. 4.46 shows the temperature data from the experiment and the simulation results after matching
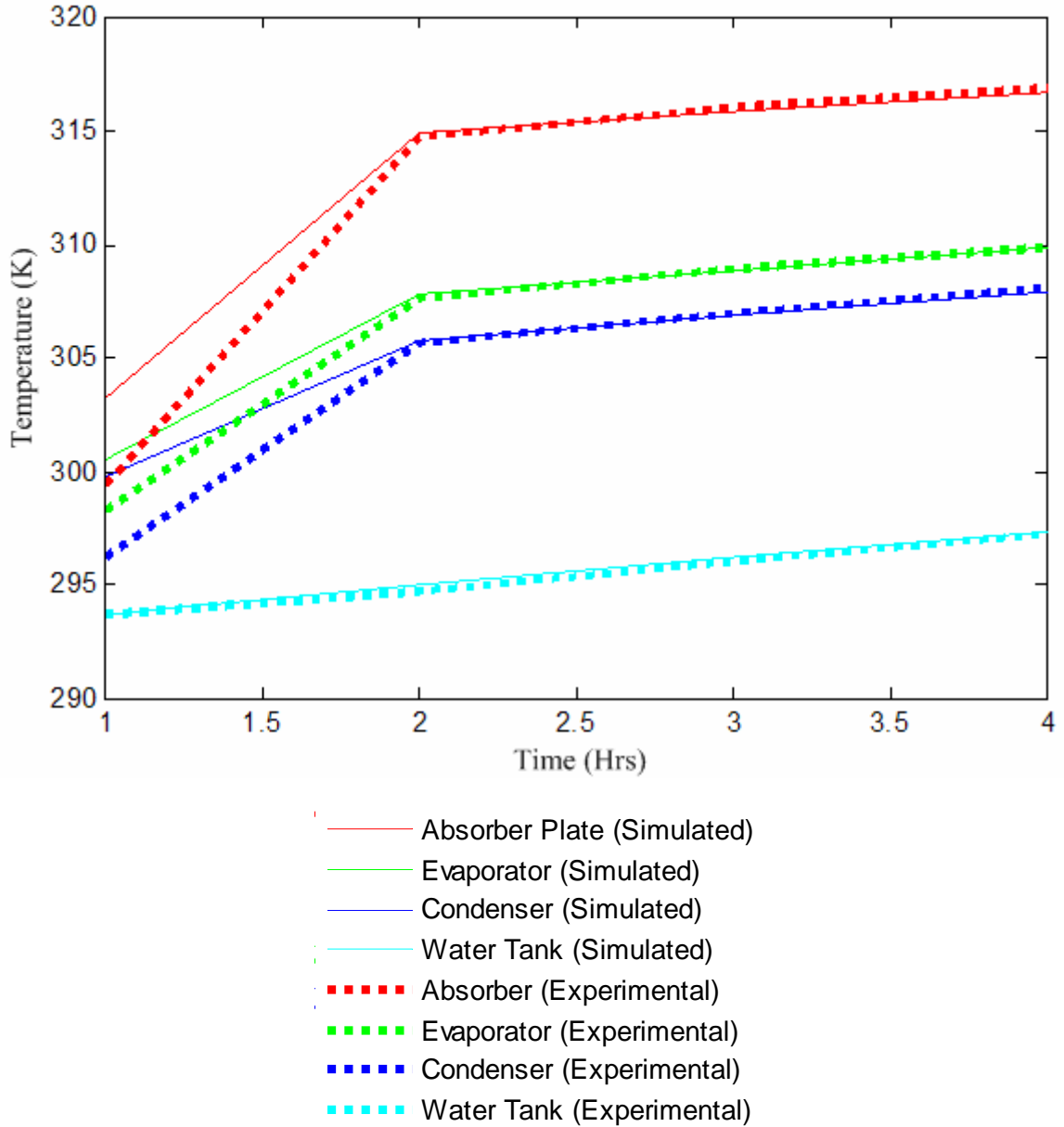
FIGURE 4.46- Matched Experimental and Simulated Temperature Data.

The conductances resulting from the matching process are shown in Table XVIII. The conductances that are temperature dependent are calculated iteratively using the temperatures of their adjacent nodes. The conductance k_{71} is calculated as the overall loss coefficient of the collector. The ambient temperature and collector temperature are used to calculate the collector top and edge losses shown by equations $6 - 25$ in the methods section. The temperature drop between the heat pipe condenser and the water tank temperature is used to calculate the conductance k_{34}. Equation 18 in the methods section calculates the Rayleigh number for convection inside the water tank. The temperature drop between nodes 5 and 6 is used to calculate the Rayleigh number shown in equation 25 in the methods section. The Rayleigh number is used to calculate the free convection off the water tank and the conductance k_{56}. The conductance k_{12}, k_{23}, and k_{45} are not temperature dependent. The conductance between the nodal temperature of the room and the ambient temperature outside is expressed as the load to collector area ratio and is also constant.

TABLE XVIII

CONDUCTANCES AND TEMPERATURES BEFORE AND AFTER MATCHING

Temperature (K)	T_1	T_2	T_3	T_4	T_5	T_6	T_7
Before Matching							
Minimum	267.51	267.68	291.26	291.86	291.86	292.15	257.05
Mean	298.48	297.81	306.01	305.40	305.19	294.84	286.35
Maximum	328.37	323.94	323.91	320.70	320.14	297.15	307.05
After Matching							
Minimum	293.63	293.62	293.62	293.50	292.25	294.25	294.25
Mean	311.27	305.70	304.12	295.07	293.25	294.25	294.25
Maximum	316.71	309.86	307.91	297.38	294.25	294.25	294.25
Conductance (W/m^{2}K)	k_{71}	k_{12}	k_{23}	k_{34}	k_{45}	k_{56}	k_{67}
Before Matching							
Minimum	1.256	118.55	0.607	5.679	385.18	0.433	10
Mean	1.926	118.55	4929.3	63.585	385.18	7.387	10
Maximum	2.838	118.55	11554	136.67	385.18	9.485	10
After Matching							
Minimum	0.901	39.517	138.64	5.265	3.85E-07	0.062	10
Mean	1.858	39.517	138.64	22.635	3.85E-07	0.130	10
Maximum	2.187	39.517	138.64	26.691	3.85E-07	0.188	10

The conductance k_{23} is not constant in the table because of the thermal diode effect of the

heat pipe. During the simulation the conductance between nodes 2 and 3 switches

between the high conductance of the heat pipe and the low conductance through the wall

insulation. The insulation conductance takes effect when the absorber plate temperature

is lower than the water tank temperature. During the experiment the absorber plate

temperature never drops below the water tank temperature. The conductance k_{45} was

decreased to a billionth of its calculated value in the matching process, to simulate the

high insulation level around the water tank in the experiment. The overall loss

coefficient, k_{71}, was decreased by 10% in the matching process. The conductance between the evaporator and condenser, k_{23}, was decreased to 6% of the calculated value. The conductance k_{34} was decreased by 2% during the matching process. The conductance between the absorber plate and the evaporator section of the heat pipe, k_{12}, was not adjusted in the matching process.

D. Economic Analysis

The economic analysis allowed the heat pipe system to be optimized for cost and performance. A basic design was developed to handle the design constraints and considerations of the system. The overall cost was determined based on manufacturing and material cost. The present worth of fuel cost was considered and a life cycle cost analysis was performed.

1. Design Considerations

A 3-D model of a heat pipe wall was created. The main concerns in development were cost, manufacturability, performance, maintenance, and ease of installation. Corliss, originally designed his heat pipe wall using a frame constructed of wood. An aluminum frame was investigated for the design of this heat pipe wall. The labor and material cost are shown in Table XIX for a wood, aluminum, and plastic frame and casing. Total cost shown is for single non-optimized unit production.

TABLE XIX

LABOR AND MATERIAL COST FOR SINGLE NON OPTIMIZED UNIT FRAME

DESIGN

Unit Frame Material	Labor Cost	Material Cost	Total
Wood	$265.59	$3,286.59	$3,539.88
Aluminum	$208.43	$3,481.23	$3,684.49
Plastic	$171.50	$3,248.59	$3,420.09

Labor cost are highest for the wood frame unit and include a total of 11.15 man hours.

The aluminum frame labor cost account for 8.5 man hours and the plastic unit has the

lowest labor time with 7.2 man hours. The extra time for a wood constructed unit is due

to the number of cuts required on the lumber and the time to square and fasten the

components. The aluminum constructed unit has additional sheet metal work that must

be completed when compared to a plastic molded unit. The increased price of aluminum

raises the material cost when compared to a plastic unit. The wood unit is $38.00 more

than the plastic unit. The wood unit also contains lumber, plywood, fasteners, tanks, and

tank straps; these components would all need to be purchased from a vendor. The plastic

unit limits the number of outsourced components, and has the lowest labor and material

cost. Plastics allow for greater versatility and material selection, and durability. Limiting

the total number of pieces used to construct the unit would also help lower the future

maintenance cost. A plastic frame could be constructed using an open main casing and a

cap to seal the contents together. Fig. 4.47 shows both the plastic main casing and the

cap. This type of construction would allow for the easiest assembly of the entire unit.

Using a cap would allow access to the insulation section, allow the absorber plate to be

slid into position, the heat pipes to be slid into the water tanks, and the bulk heads

attached to the water tanks. The adiabatic section would be insulated, and once the cap

is fastened into position the entire unit will be self contained. One main advantage of this

design is that the water tanks are molded and part of the entire casing. This cuts down on

the labor of attaching water tanks and tank straps, and the number of purchased

components. Holes could also be fabricated into the plastic mold for any fasteners used

during assembly. Once the unit is installed the cap could be removed to allow for any

future maintenance. The plastic mold could be made through an injection modeling

process. The main casing could be fabricated in two separate pieces if needed and joined

together with ultrasonic laser or infrared welding.
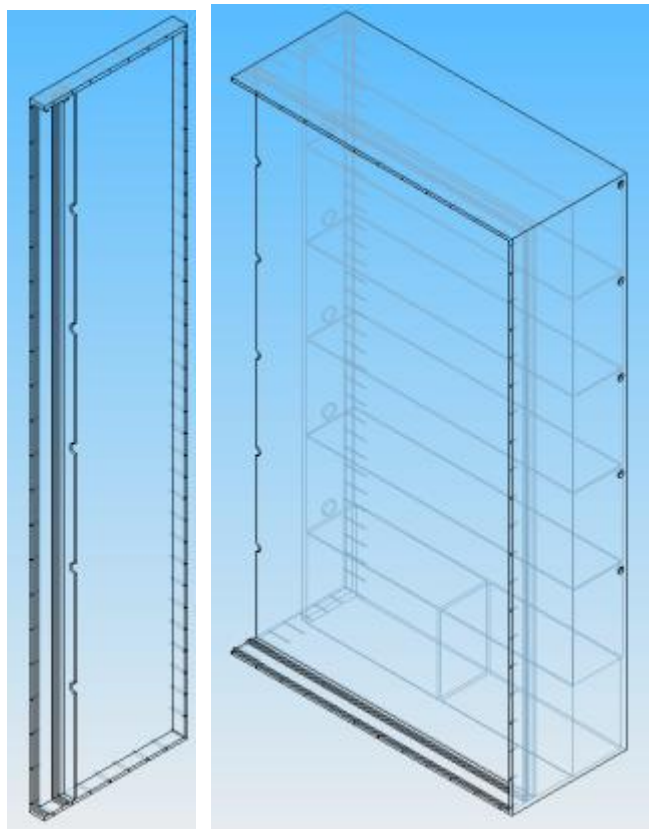
FIGURE 4.47 - Heat Pipe Wall Main Casing And Cap.

Notable features include: pre-fabricated water tanks that are a part of the injection mold, grooves or ridges to aid in the assembly and placement of the glazing and absorber plate, pre-drilled holes for the attachment of the main casing cap and aluminum mounting flange, external water tank access holes for filling and cleaning, insulation region between water tanks and absorber plate, insulation region for heat pipe adiabatic section, and heat pipe and bulk head access.

The absorber plate would be fabricated with attached heat pipes. The heat pipes would be soldered or welded into position and the entire unit would be slid into the frame casing. Fig. 4.48 shows an absorber plate/heat pipe assembly.
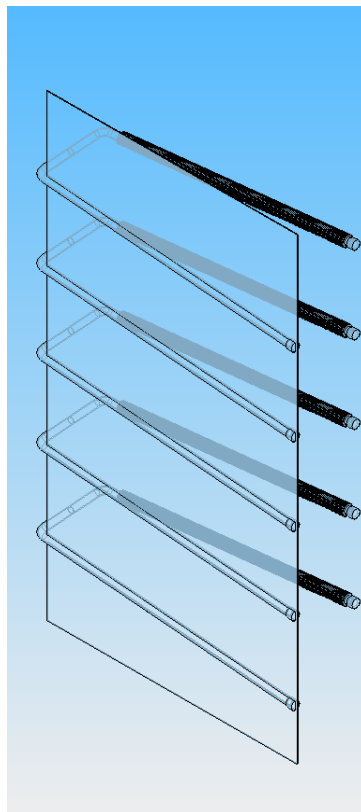
FIGURE 4.48 - Absorber Plate Heat Pipe Assembly.

The heat pipes are positioned at a five degree incline and the condenser sections shown include radial fins. The absorber plate would be fabricated of aluminum or copper. After the absorber plate has been inserted, insulation will be placed between the absorber plate and water tanks. Fiberglass insulation could be sprayed into the insulation region of the main casing cap or batt insulation could be manually inserted. The density and type of insulation would determine the R factor of the insulated region. There is enough space to allow for an R factor of 49 to be achieved. The adiabatic section would first be insulated with standard Styrofoam pipe insulation and then fiberglass insulation could be sprayed around the heat pipes or batt insulation placed in this area. The main casing cap will be sealed to contain all components of the design. The solar glazing could be installed onsite and an aluminum flange screwed on top of a gasket to seal the glazing. This flange will allow the unit to be nailed into a framed section of the building and prevent moisture from entering the passive solar heater. The aluminum flange is shown in Fig. 4.49.
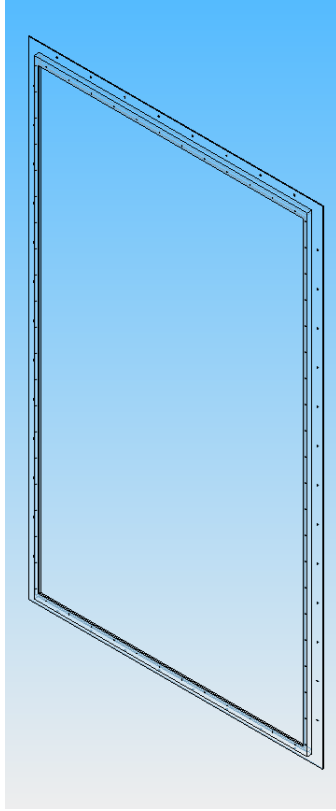
FIGURE 4.49 - Aluminum Flange.

The entire assembly is shown in Fig. 4.50.
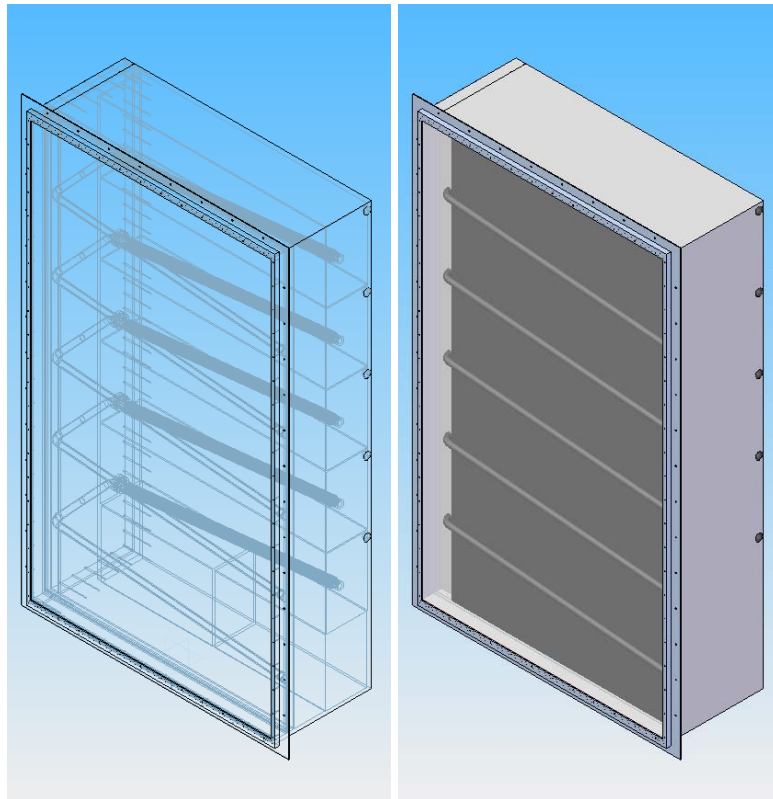
FIGURE 4.50 - Heat Pipe Passive Solar Space Heater.

2. Unit Cost

The unit cost was broken down into labor cost (Table XX) and material cost. The labor cost included the cleaning and charging of the heat pipe. The fabrication of the absorber plate and the complete final assembly are also included. The labor cost associated with fabricating the plastic frame and electroplating the absorber plate are included in the material cost. For the unit assembly the heat pipes would be fabricated first. Pipe would be cut to length and soldered or welded together. End caps would be attached to seal the heat pipes and refrigerant line would be attached for heat pipe filling. The heat pipes would then be washed, and fired to dry and sterilize. The absorber plate would then be fabricated with a machine press and the heat pipes would be soldered or welded into place. Once the entire absorber plate is assembled the piece can be

electroplated. The heat pipes would then be evacuated and charged with refrigerant.

After the selective surface has been applied and the heat pipes charged, this assembly can

be slid into the plastic main casing. The bulkheads can then be attached to seal the water

tanks. Styrofoam pipe insulation would then be placed around all exposed sections of the

heat pipe. Spray or batt insulation could then be placed into the insulation regions of the

plastic casing. The main casing cap could then be screwed into the main casing to

contain the entire unit. The gasketing, glazing, and aluminum mounting frame could then

be attached either onsite or at the manufacturing facility. The gasketing would contain an

adhesive side for easy application, and the aluminum mounting frame would screw into

the prefabricated holes to fasten to the unit. Tools needed to assemble the unit include:

machine press, acetylene torch, tig-welder, band saw or pipe cutter, grinder, hand drill,

utility knife, vacuum pump, oven, and insulation sprayer.

TABLE XX

LABOR COST FOR THE HEAT PIPE PASSIVE SOLAR HEATER

Integrated Heat Pipe Cost Analysis			
Labor Cost	$23.82	Per Hour	
Task	Number	Time (minutes)	Cost
Solder / Weld End Caps	10	2.5	$9.93
Solder / Weld Absorber Plates	10	15	$59.55
Wash Heat Pipe	5	10	$19.85
Fire (Dry and Sterilize) Heat Pipe	5	10	$19.85
Vacuum Pump Heat Pipe	5	3	$5.96
Fill Heat Pipe With Working Fluid	5	5	$9.93
Break Absorber Plates Into Fitted Sections	10	3	$11.91
Cut Heat Pipe	5	2	$3.97
Bend Heat Pipe	5	3	$5.96
Insert Absorber Plate and Heat pipe Into Main Casing	1	2	$0.79
Attach Bulk Heads	5	2	$3.97
Insert Water Tank Caps	5	1	$1.99
Insert Insulation	1	10	$3.97
Screw And Attach the Main Casing Cap	1	10	$3.97
Insert Gasketing	1	5	$1.99
Insert Glass	1	5	$1.99
Screw And Attach Flange to the Casing	1	15	$5.96
Labor Total			*$171.50*

The complete material cost is tabulated below.

TABLE XXI

MATERIAL COST FOR THE HEAT PIPE PASSIVE SOLAR HEATER

Integrated Heat Pipe Cost Analysis			
Item	Number / Weight	Item Cost	Total Cost Weight (kg , *lbs*)
Copper Absorber Plate	6	$237.28	$1,423.68 (69.25 , *152.35*)
Copper Heat Pipe	5	$73.00	$365.00 (16.82 , *37.01*)
Copper End Caps	10	$3.50	$35.00 (0.56 , *1.24*)
Bulk Heads	5	$5.00	$25.00 (3.59 , *7.9*)
Water Tank Caps	5	$0.50	$2.50 (0.34 , *0.75*)
Plastic Main Casing	1	$135.00	$135.00 (28.53 , *62.89*)
Plastic Casing Cap	1	$48.00	$48.00 (7.28 , *16.05*)
Injection Molding Tooling	1/1000	$22,000.00	$22.00 N/A
Gasketing	1	$18.20	$18.20 (5.81 , *12.79*)
Casing Screws	1	$3.64	$3.64 (0.45 , *1*)
Aluminum Flange	1	$46.94	$46.94 (9.91 , *21.8*)
Flange Screws	1	$7.27	$7.27 (0.45 , *1*)
Low Iron Glass	1	$45.20	$45.20 (19.29 , *42.44*)
Black Chroming	6	$50.00	$300.00 N/A
Insulation	4	$14.56	$58.24 (11 , *24.2*)
Emory Cloth	1	$8.94	$8.94 N/A
Flux	1	$2.68	$2.68 N/A
Solder	1	$3.25	$3.25 N/A
Refrigerant	1/10	$90.00	$9.00 N/A
Material Total			*$2,559.53* (176.85 , *389.07*)

The material cost is based on making 1000 units. The tooling cost associated with the injection modeling is divided over these 1000 units. A tenth of a tank of refrigerant will be required to charge five heat pipes. The baseline parameters used in the computer simulation were also used in the cost analysis for consistency. These material cost include the use of copper, a low iron glazing, and a black chrome selective surface. The refrigerant quoted was SUVA-124.

The overall unit cost also includes the shipping and installation cost associated with the passive solar unit. The total time allotted for installation includes demolition and framing of an existing wall, the placement of the unit, and finishing trim around the structure. Four different housing constructions were considered for installation. The installation steps and times are shown in Table XXII.

TABLE XXII

INSTALLATION STEPS AND TIMES

	Number of Laborers	Masonry Brick Straight Saw Cut	Masonry Brick Toothed Jambs	Aluminum / Vinyl Siding	Poured Concrete Foundation
Exterior Layout	2	30	30	30	30
Mount Saw	2	N/A	N/A	N/A	60
Saw Cut	2	60	60	45	60
Remove Material	2	60	60	15	60
Saw Cut Individual Courses	2	N/A	30	N/A	N/A
Remove and Clean Brick	2	N/A	30	N/A	N/A
Relay Jambs	2	N/A	60	N/A	N/A
Cut For Header Angle	2	N/A	15	N/A	45
Install Angle	2	45	30	N/A	15
Relay Brick	2	N/A	30	N/A	N/A
Interior Layout	2	45	45	45	45
Saw Cut Drywall	2	30	30	30	N/A
Remove Wall Section	2	45	45	45	N/A
Install Header	2	30	30	30	N/A
Move and Set Unit	4	120	120	120	120
Trim and Finish Interior	2	60	60	60	60
Trim and Finish Exterior	2	60	60	60	60
Clean Up	2	60	60	60	180
Time Required (min.)		645	795	540	735
Total Paid Labor Time (min.)		1530	1830	1320	1710
Total Paid Labor Time (hrs.)		25.5	30.5	22	28.5

The maximum installation time will be used for calculating the total cost which is shown in the table below.

TABLE XXIII

TOTAL UNIT COST FOR A NON OPTIMIZED HEAT PIPE PASSIVE SOLAR

HEATER

Integrated Heat Pipe Cost Analysis	
Labor Total	$171.50
Material Total	$2,559.53
Unit Cost Total	$2,731.03
Shipping	$100.00
Installation Cost	$726.51
Total	$3,557.54

3. Cost Optimization

Cost optimization was accomplished using the computer simulation and varying

design parameters. The cost for each design change was calculated and compared. The

solar fraction was divided by the cost of the unit to normalize each design change. Both

copper and aluminum absorber plates and heat pipes were analyzed. The material cost

for copper heat pipes was $80.00 each. Aluminum heat pipes cost less and at $52.00 a

piece. Below (Table XXIV) shows the change in performance and cost associated with

changing heat pipe and absorber plate material along with absorber plate thickness.

TABLE XXIV

PERFORMANCE AND COST OF ABSORBER PLATE AND HEAT PIPE DESIGN

Integrated Heat Pipe System Variable Costing				
	Solar Fraction	Absorber Cost	Unit Cost	Solar Fraction / Cost
Copper Absorber Plate With Copper Heat Pipes				
0.00079502 m (1/32 inch)	0.4644	$474.87	$2,608.73	1.78E-04
0.0015875 m (1/16 inch)	0.4773	$822.22	$2,956.08	1.61E-04
0.003175 m (1/8 inch)	0.4836	$1,423.68	$3,557.54	1.36E-04
0.00635 m (1/4 inch)	0.4863	$2,465.05	$4,598.91	1.06E-04
0.008255 m (3/8 inch)	0.4867	$4,268.16	$6,402.02	7.60E-05
Aluminum Absorber Plate With Aluminum Heat Pipes				
0.00079502 m (1/32 inch)	0.4365	$102.37	$2,096.23	2.08E-04
0.0015875 m (1/16 inch)	0.4604	$307.10	$2,300.96	2.00E-04
0.003175 m (1/8 inch)	0.4728	$532.21	$2,526.07	1.87E-04
0.00635 m (1/4 inch)	0.4759	$922.32	$2,916.18	1.63E-04
0.008255 m (3/8 inch)	0.4765	$1,216.04	$3,209.90	1.48E-04
Aluminum Absorber Plate With Copper Heat Pipes				
0.00079502 m (1/32 inch)	0.4365	$102.37	$2,236.23	1.95E-04
0.0015875 m (1/16 inch)	0.4604	$307.10	$2,440.96	1.89E-04
0.003175 m (1/8 inch)	0.4728	$532.21	$2,666.07	1.77E-04
0.00635 m (1/4 inch)	0.4759	$922.32	$3,056.18	1.56E-04
0.008255 m (3/8 inch)	0.4765	$1,216.04	$3,349.90	1.42E-04

The glazing selection was also compared and is shown in Table XXV.

TABLE XXV

SOLAR GLAZING NUMBER, TYPE, AND THICKNESS COST

Integrated Heat Pipe System Variable Costing			
	Unit Cost	Solar Fraction	Fraction / Cost
Number of Covers			
1	$3,557.54	0.4836	1.36E-04
2	$3,684.34	0.4916	1.33E-04
Glass Type			
Window Glass	$3,534.94	0.4444	1.26E-04
Low Iron Glass	$3,557.54	0.4836	1.36E-04
Glass Thickness			
0.00238 m (3/32 inch)	$3,550.18	0.4850	1.37E-04
0.003175 m (1/8 inch)	$3,557.54	0.4836	1.36E-04
0.00635 m (1/4 inch)	$3,572.26	0.4779	1.34E-04
0.008255 m (3/8 inch)	$3,586.10	0.4723	1.32E-04

The selective surfaces chosen were then compared, and the results tabulated in Table XXVI.

TABLE XXVI

SELECTIVE SURFACE COST

Integrated Heat Pipe System Variable Costing			
Selective Surface	Unit Cost	Solar Fraction	Fraction / Cost
Black Nickel	$3,527.54	0.4631	1.31E-04
Black Chrome	$3,557.54	0.4836	1.36E-04
Black Copper	$3,887.54	0.4916	1.26E-04
Flat Black Paint	$3,265.54	0.1928	5.90E-05
Polished Surface	$3,257.54	0.0761	2.34E-05

The number of heat pipes drastically effects the labor and material cost. The results are
shown in Table XXVII.

TABLE XXVII

COST OF NUMBER OF HEAT PIPES

Integrated Heat Pipe System Variable Costing			
	Unit Cost	Solar Fraction	Fraction / Cost
Number of Heat Pipes			
4	$3,264.04	0.4789	1.47E-04
5	$3,557.54	0.4836	1.36E-04
6	$3,851.04	0.4866	1.26E-04
7	$4,144.54	0.4887	1.18E-04
8	$4,438.04	0.4902	1.10E-04
9	$4,731.54	0.4913	1.04E-04
10	$5,025.04	0.4922	9.79E-05

The size of the water tanks (Table XXVIII) can affect the performance, cost and

installation price.

TABLE XXVIII

COST AND PERFORMANCE OF WATER TANK WIDTH

Tank Width	Solar Fraction	Dead Load (kg , lbs.)	Cost	Fraction / Cost
0.0508 m (2")	0.3815	(82.18 , *180.80*)	$3,523.45	1.08E-04
0.1016 m (4")	0.4469	(164.36 , *361.59*)	$3,534.81	1.26E-04
0.1524 m (6")	0.4708	(246.54 , *542.39*)	$3,546.18	1.33E-04
0.2032 m (8")	0.4836	(328.72 , *723.19*)	$3,557.54	1.36E-04
0.254 m (10")	0.4921	(410.90 , *903.99*)	$3,568.90	1.38E-04
0.3048 m (12")	0.4986	(493.08 , *1084.78*)	$3,580.27	1.39E-04
0.3556 m (14")	0.5037	(575.26 , *1265.58*)	$3,591.63	1.40E-04
0.4064 m (16")	0.5080	(657.44 , *1446.38*)	$3,603.00	1.41E-04
0.4572 m (18")	0.5116	(739.62 , *1627.17*)	$3,614.36	1.42E-04
0.508 m (20")	0.5149	(821.81 , *1807.97*)	$3,625.72	1.42E-04
0.5588 m (22")	0.5178	(903.99 , *1988.77*)	$3,637.09	1.42E-04
0.6096 m (24")	0.5204	(986.17 , *2169.57*)	$3,648.45	1.43E-04

The increased volume of the water tank creates an increased dead load that must be supported by the floor joist. Specific details of the installation location would change any result of the structural analysis. The floor joist span, wood size, grade, and species would be needed for any calculation. Details of the floor joist would allow for the bearing length, force in bending and modulus of elasticity to be found. Building codes also vary by municipality and the exact design requirements for live load, dead load and deflection limits would need to be researched. The International Residential Code is used as a basic guideline for many buildings codes and suggest limits of 195.2971 kg/m^2 (40 psf) for live loads, 48.82428 kg/m^2 (10 psf) for dead loads and a deflection limit of (Span in inches)/360. If the limits of the building code are exceeded then the structural joist need to be improved. To accomplish this the floor joist could be doubled, the joist replaced, or

a structural column installed.   If the location of the unit already has finished floors and living spaces then replacing or modifying the existing floor joist can be difficult and expensive. The most versatile and inexpensive method of supporting the solar unit would be to install a structural column. In this method 4x4's would be anchored to the existing floor joist. Then 4x4 columns would be braced underneath the ends of the anchored 4x4 floor joist. This would then be framed and finished to match the existing finish. The material cost and labor cost for this installation method are shown in Table XXIX.

TABLE XXIX

MATERIAL AND LABOR COST OF SUPPORT COLUMN

Material	Cost
Lumber 4x4	$20.91
Lumber 2x4	$33.90
Dry Wall	$16.50
Dry Wall Plaster	$4.99
Dry Wall Tape	$3.50
Paint	$18.00
Trim	$20.00
Fasteners	$5.94
Material Cost	$123.74
Labor	Time
Saw Cut Lumber	20
Anchor 4x4 to Joist	10
Set 4x4 Support Columns	20
Frame Walls	60
Anchor Dry Wall	45
Finish Dry Wall	60
Paint	45
Trim	30
Cleanup	30
Time (min.)	320
Time (hrs.)	5.33
Labor Cost	151.04
Installation Cost	$274.78

Adding this additional installation cost will raise the cost of the unit based on water tank width. Assuming the span of an installed unit is 3.6576 m (12 feet) and the suggested building code limits defined by International Residential Code are used the cost effectiveness of the water tank width (Fig. 4.51) is shown below.
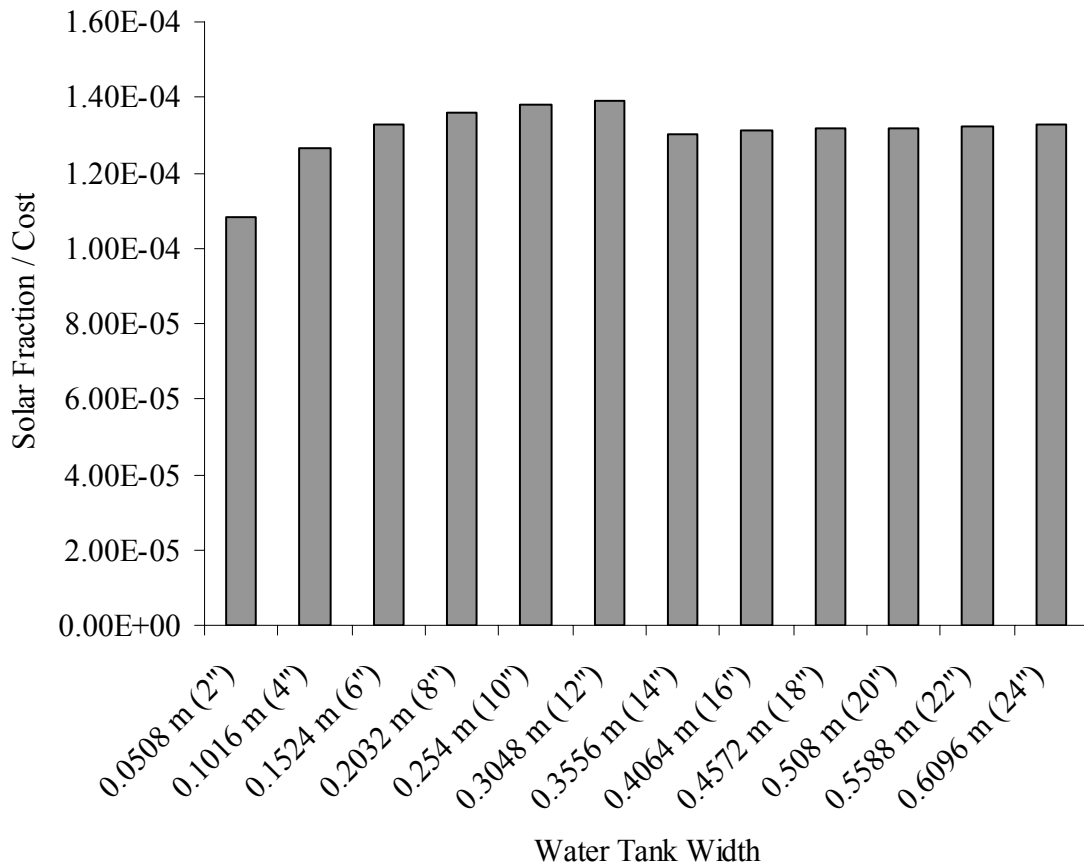
FIGURE 4.51– Cost Effectiveness Of Water Tank Width.

When filled, the water tank width of 0.3048 m (12 inches) does not exceed the assumed

dead load limit and the extra installation cost is not required. After each design change

was compared by cost, the parameters were optimized to achieve the most cost effective

design. Using a single low iron glass cover, aluminum absorber plate 0.00079502 m

(1/32 inch) thick with four aluminum heat pipes, and a water tank width of 0.3048 m (12

inches), provides the most cost effective design. The cost for this design and solar

fraction are $1825.46 and 0.4267 respectively.

4. Life Cycle Cost Analysis

The life cycle cost analysis calculates the present worth of future fuel cost based on usage, interest rate and discount rate. The entire life cycle cost analysis is calculated based on a thirty year mortgage and uses the optimized design. The initial parameters are shown in the table below.

TABLE XXX

LIFE CYCLE COST PARAMETERS

Reduction of Fuel Purchase	42.67%	
Cost of Collector and Equipment	$1825.46	
Length of Mortgage	30	Years
Mortgage Interest Rate	5.75%	
Down Payment	20%	
Inflation Rate	4.00%	
Cost of Fuel	0.1	$/kWh
Yearly Fuel Requirement	8426.44	kWh
Discount Rate	2.50%	
Fuel Cost Inflation	4.00%	
Resale Value	30.00%	
Tax Inflation Rate	4.00%	
Effective Income Tax Rate	28.00%	
First Year Maint. Insu. Etc.	$50	
Extra Property Tax	$0	
Monthly Mortgage Payment	$42.61	

The amount of fuel used is calculated from the simulation using a load to collector ratio of 10 W/m^{2}K. Using the collector area and the load to collector ratio, the load for the room can be calculated. The equations outlined in the Methods section can then be used to calculate the number of units needed. For an area of 179.86 m^2 (1936 ft^2), a total of five collectors would be needed. The details of the room construction can be seen in Appendix VIII. Over a 30 year mortgage the total present worth value of the future fuel

cost is $30,687.18. A year by year table of this present worth value is shown in Appendix IX. Solar savings is calculated by subtracting the financing, extra tax, insurance, and maintenance from the fuel savings. The total undiscounted solar savings over the 30 year period is $5,291.89. The life cycle solar savings is $1,825.67. The year by year calculation of the life cycle cost is shown in Appendix X. By dividing the first years fuel savings by the cost of the optimized design the simple payback period is 25.38 years. The discounted payback period on the optimized heat pipe passive solar heater is 22.21 years. Federal and state tax credits incentives the installation of alternative energy systems. Federal tax incentives currently are 30% of the project cost and residential Kentucky State tax credits are 30% of the project up to $500. The payback periods for projects using tax incentives applied to the cost of the system are shown in Table XXXI.

TABLE XXXI

TAX INCENTIVE PAYBACK PERIODS

	Optimized Design
Initial Cost	$1,825.46
State Tax Credit KY	$500.00
Federal Tax Credit	$547.64
Unit Cost (w/ Tax Deductions)	$777.82
Simple Payback (w/out Tax Deductions)	25.38
Discounted Payback (w/out Tax Deductions)	22.21
Undiscounted Payback (w/out Tax Deductions)	8.23
Simple Payback (w/ Tax Deductions)	10.82
Discounted Payback (w/ Tax Deductions)	10.35
Undiscounted Payback (w/ Tax Deductions)	3.83

V. DISCUSSION

A. Experimental Results

1. Radiation Experiments

To achieve uniform radiation on the absorber plate, three solar lamps were used. The blinders and reflectors described in the procedure section helped eliminate large radiation differences. It was hoped to achieve a standard deviation normalized by the mean during the radiation sampling of 5%. The standard deviation of the 15 locations measured across the absorber plate was 31.65 W/m^2. The final design setup for the solar lamps achieved a standard deviation over mean of 4.46%, thus the radiation differences across the absorber plate were within the acceptable ranges. The maximum percentage difference across the absorber plate is 14.7%. TMY2 data for Louisville showed maximum radiation values during winter periods do not exceed 850 W/m^2. While some days do not experience hourly radiation values this high, the average value measured across the absorber plate of 709.4 W/m^2 would be experienced during many sunny winter days in Louisville, Kentucky. The peak hourly radiation values for January from TMY2 data have an average radiation value of 707.3 W/m^2. Thus the peak hourly radiation value for January was 99.7% of the measured radiation value across the absorber plate.

2. Fill Level and Adiabatic Insulation Experiments

The first experimental setup used a heat pipe charged to 80% volume of the evaporator section with an un-insulated adiabatic section. Table II of the results section showed that the minimum, mean, and maximum radiation value measured during the three test runs was 666.50 W/m^2, 700.45 W/m^2, 734.88 W/m^2 respectively. The standard deviation for this test setup was 10.66 W/m^2 and was 1.52% of the measured mean radiation value. The percentage difference among the radiation values in all three runs is small.

The rate of temperature change of the thermal storage device was calculated to determine the power output of the system. Using the rate of temperature change for each test run the standard deviation was calculated and divided by the mean rate of temperature change. This percentage showed the difference in rate of temperature change between individual test runs. The mean rate of temperature change for the un-insulated heat pipe charged to 80% volume of the evaporator section was 1.136°C/hr. The standard deviation was 0.5% of the mean rate of temperature change, showing a small difference between the rate of temperature change in the test runs.

Insulating the adiabatic section produced a 2.51% percentage increase in the rate of temperature change. This is attributed to the short length of the adiabatic section, less than 15%, when compared to the overall length of the heat pipe. There is limited surface area at this location to produce a larger percentage increase in performance. The 80% fill volume performed the worst with an average temperature change of 1.153°C/hr. The 120% fill volume performed the best at 1.223°C/hr. This was 2.34% better than the 100% fill level and 1.75% better than the 140% fill volume.

The rate of temperature change of the water tank did not increase when radial fins were added to the condenser section of the heat pipe. The rate of temperature change for both the non-finned and finned condenser with 120% fill and insulated adiabatic section was 1.223°C/hr. The standard deviation of the rate of temperature change between the finned condenser runs was 0.0049°C/hr. This standard deviation is 0.4% of the mean rate of temperature change. While adding fins dramatically increases the surface area of the condenser, it does not increase the rate of temperature change of the mass storage system. This suggest that the fins are not performing correctly, and the heat transfer between the condenser section of the heat pipe and the finning section is limited. This may be attributed to the thermal connection between the fin and the condenser section. Reasons the thermal connection might be poor at this junction include: machined grooves on the inside diameter of the fins created through fabrication; imperfect soldered connections between fin and condenser; inconsistent placement and spacing of condenser fins.

The test setup with the lowest overall system efficiency, 79.33%, was the 80% fill level with an un-insulated adiabatic section. Insulating the adiabatic section improved the overall system efficiency to 80.89%. When the heat pipe was charged to its highest tested fill level, 140%, the overall system efficiency was 83.9% with an insulated adiabatic section. Insulating the adiabatic section and charging the heat pipe to 120% volume of the evaporator section provided the highest overall system efficiency of 85.1%.

The computer simulation was used to estimate possible performance improvements. The overall loss coefficient of the collector should have a significant impact on the overall system efficiency. With a tighter fitting collector box the overall

system efficiency might increase by 3.5% for absorber plate areas that are 97% of the glazing area. Adding an additional 0.0508m (2 inches) of insulation around the edge of the collector would decrease the conductivity between the absorber plate and ambient by 11% and the overall system efficiency might increase by 1%. Heat pipe design such as fill fraction also has a significant impact on the systems performance. To improve the overall performance the system the technique of attaching the copper plates to the copper heat pipe could be improved. The plates were soldered on for this experiment, however a brazing or welding technique could improve the thermal connection by 30%. Brazing and welding are performed at higher temperatures and filler materials with higher thermal conductivities can be used. Higher operating temperatures make brazing and welding easier to join the round surface of the heat pipe with the flat sections of the absorber plate. An increase in the conductivity between the absorber plate and the heat pipe by 30% could improve the system efficiency by 1.5%. To fill the heat pipe a hole was drawn through the adiabatic section and a refrigerant line with a valve was attached. A better understanding of the effects of this heat pipe charging point might also improve performance.

The first one-way ANOVA test analyzed the null hypothesis, that the mean system efficiencies from each fill level during the experiment were equal. The ratio of variance between groups over variance within groups was greater than one with the F-value equal to 5.87. The conventional alpha value when analyzing the p-value is 0.05. If the p-value is lower than the alpha value the null hypothesis is rejected. The p-value for one-way ANOVA testing system efficiency versus fill level percentage was 0.005. The null hypothesis for the first test was false and the mean system efficiencies from each

fill level were not equal. We may conclude that the system efficiency does depend on the fill level.

Another one-way ANOVA test analyzed system efficiency versus an insulated adiabatic section. The calculated F-value was 11.69 and the probability of obtaining this ratio, the p-value, was equal to 0.002. Thus the system efficiency is dependent on whether or not the adiabatic section of the heat pipe is insulated. Even though the overall system efficiency difference is small because of the limited surface area of the adiabatic section, it remains dependent on this design variable.

A one-way ANOVA was again used to calculate the null hypothesis that the mean system efficiency between a non-finned condenser and finned condenser are equal. The calculated F-value for this test was 0.11 with a probability of obtaining an F-value equal or greater than 0.11 as 76.0%. The p-value was 0.76, consequently the system efficiency is not dependent on the fining on the condenser section.

3. Error Propagation

The data acquisition system was calibrated and the absolute accuracy was then calculated. The absolute accuracy of the entire data acquisition system was ± 3.6 mV. The uncertainty in the measurements included $\pm 0.27\%$ for the mass of the water tank, $\pm 2.13\%$ for the radiation measured across the absorber plate, and $\pm 0.79\%$ for the measured temperature at each thermocouple. Using the maximum radiation level measured in all experiments, 735.17 W/m^2, the uncertainty of this measurement is ± 15.66 W/m^2. Water tank temperatures were calculated between the 23 °C and 26.5 °C. Using 26.5 °C the uncertainty in the measured water tank temperatures was ± 0.2 °C. The uncertainty in the calculated system efficiency is 0.72%. The greatest system

efficiency, 85.1%, was achieved with an insulated adiabatic section and a fill level of 120% of evaporator volume. Therefore with uncertainty the system efficiency of this setup was between 84.49% and 85.71%.

<u>B. Simulated Results</u>

<u>1. Climate Comparison</u>

Of the four climates studied in the passive solar comparison, Albuquerque experienced the warmest winters and highest levels of radiation. Direct gain systems have faster reaction times when compared to the Trombe and water walls. In addition, however, direct gain systems also have the largest losses during nighttime and cloudy periods. The direct gain system performed the best in Albuquerque, because these losses were offset by large gains during sunny days. The lower radiation values and cooler temperatures in the other climates provided decreased gains and increased losses, shifting the advantage to the storage wall systems in these climates.

The storage wall systems, water and concrete Trombe walls, allow for more even delivery of heat throughout the day, compared to the direct gain system. Losses in these systems are experienced through the solar glazing during cloudy and nighttime periods. Faster reaction times are seen in the water walls due to the free convection in the tanks. The water wall system outperformed the concrete wall system in all climates.

Higher gains could be experienced in these systems if insulation were installed during lower solar radiation periods. Moveable insulation however is cumbersome and manual operation is not practical for most homeowners. Automatic systems are

commercially available, but the insulation ratings they provide are low when compared to a structural wall.

The heat pipe system outperformed all other passive solar systems in all climates. The thermal diode effect of the heat pipes and insulation layers between the mass storage and solar glazing eliminated many of the losses experienced in the other systems. The city of Madison experienced the lowest winter temperatures. Here, losses through the solar glazing of the direct gain system provided a negative solar fraction. The storage walls also experienced their lowest performance in this climate.

Despite the lower solar radiation values experienced in Louisville when compared to Rock Springs, the heat pipe system performance was slightly better. The solar fraction achieved in Louisville was 48.36% and in Rock Springs the solar fraction was 47.85%. The milder winter time temperatures in Louisville allows for lower losses. Solar fractions in Louisville for each solar system were higher than performances in Rock Springs and Madison. The water wall system in Louisville achieved the second highest solar fraction, 38.84%, when comparing the passive solar systems. The concrete wall system in Louisville had a solar fraction of 30.77% and the direct gain system had a solar fraction of 22.39%. Thus the heat pipe system in Louisville performed 24.51% better than water wall system, 57.16% better than the concrete trombe wall system, and 115.98% better than the direct gain system.

The direct gain system performed best in the warm and sunny climate, when auxiliary heating is not required for early morning load. The lowest solar fraction achieved amongst all passive solar systems tested was the direct gain system in Madison. The higher losses of a direct gain system combined with the lower radiation values and

colder temperatures accounted for the -4.51% solar fraction. For each climate tested the water wall system had the second highest solar fraction. In the climate with the highest solar radiation values, Albuquerque, the heat pipe system performed 26.7% better than the water wall system. In the climate with the lowest solar radiation values, Madison, the heat pipe system performed 23.7% better than the water wall system in this climate. In the four climates tested, the heat pipe system outperformed the other passive solar options.

2. Heat Pipe Nodal Data

The parameters outlined for the base case scenario were chosen on initial performance estimates. The parameters were not based on economic considerations, and sizing was comparable to previous heat pipe designs by Susheela and Sharp [2001] and Corliss [1979]. The simulation data in Fig. 4.24 shows the temperature fluctuations across the system. The levels of radiation in Fig. 4.25 show that for this time period there were both cloudy and sunny days. The absorber plate and evaporator sections of the system experienced high temperature swings throughout the day. The thermal diode effect of the system is evident in comparatively slow decreases in temperature experienced by the condenser and water tank during the night. The largest gains to the room can be seen during consecutive days of high radiation.

3. Heat Pipe Design Results

The design parameters simulated by the computer model show differences in performance based on solar fraction. As defined earlier, the solar fraction is the ratio of the amount of energy supplied by the heat pipe system, to that required by the load of the room. The load to collector ratio was the first parameter simulated and is the ratio of the

load of the room to that of the collector area. As the water tank temperature rises heat is

transferred, through the thermal network, from the mass storage device to the room. An

increase in solar fraction means heat is being transferred from the water tank to the room

resulting in an increase in the amount of energy supplied to the load when compared to

the required load. An increase in the solar fraction decreases the energy cost. Room

temperature fluctuates due to both the heat transfer from the water tank to the room, k_{56},

and from the room to the ambient temperature, k_{67}. Figure 4.26 shows the rise and fall of

room temperature during a two week period. Supplementary space conditioning would

provide heating and cooling when the room temperature becomes undesirable. The

computer simulation accounts for these conditions, therefore, temperature change alone is

not a valid parameter to evaluate performance of the solar system. However, despite the

temperature of the room, the solar system can be transferring heat to the load. Solar

fraction describes the amount of the required heating load that is being supplied and is a

better measure of performance.

The load to collector ratio is also the conductance between the room and ambient

temperature. Controlling the load to collector ratio allows a designer to correctly size a

system for a number of different loads. Increasing the load of the system in relation to

the size of the collector decreases the solar fraction for a particular climate. For solar

fraction of 25%, the required ratio for Louisville is 25 W/m^2K. A load to collector ratio

of 10 W/m^2K in Louisville produced a solar fraction of 48.36%.

Adding additional covers was expected to improve the solar fraction. Additional

covers on the system reduce convective losses from the solar collector and decrease the

overall loss coefficient. Adding a second cover increased the solar fraction by 1.7%. The

extra cover does improve the performance of the system, but also adds extra cost.

Increasing the thickness of the cover was then analyzed using the computer

simulation. The thickness of the cover has to be designed based on performance and

durability. While a thinner cover increases performance, the cover needs to withstand

weather conditions and minor impacts without failure. Increasing the thickness of the

collector by an eighth of an inch decreases the overall solar fraction by 1.2%.

The type of glass used in the collector also affects the solar fraction supplied by

the system. Window glass contains high levels of iron and exhibits a glass extinction

coefficient of 32 m^{-1}. Glass specifically created for solar applications has lower levels of

iron. Lowering the iron level in glass will increase transmissivity, and lower the

absorptance. Low iron glass for solar applications has an extinction coefficient of 4 m^{-1}.

The performance of the heat pipe system is improved by 8.1% by using low iron glass

rather than window glass.

The absorptance and emmisivity of the absorber plate can be changed by applying

a selective surface. By painting a copper absorber plate with black paint the absorptance

is increased from 0.18 to 0.96, however, the emissivity is also raised from 0.07 to 0.96.

While the overall performance is improved, the high emissivity keeps the solar fraction at

a low value, 0.1928. Applying an electroplated surface such as black chrome, black

nickel, or black copper can raise the absorptance of the selective surface and still keep the

emmisivity at a low value, but costs more than paint. Black chroming absorber plates is a

common practice in the solar industry. Black chrome surfaces provide absorptance of

0.96 and emmisivity of 0.02. Black copper and nickel electroplating is not as common in

industry, more expensive to apply, and provide similar emmisivities. Black chroming the surface of the absorber plate produces a 60.1% increase in solar fraction compared to a flat black paint finish. When comparing to a black chromed surface, a black copper surface improves solar fraction by 1.7% , and the black nickel surface decreases performance by 4.2%.

The absorber plate material affects the solar fraction because the thermal conductivity is different among the materials. The emittance of the absorber plate is also affected by the material type. Having flexibility in material choice is important when designing a commercial unit due to differences in material prices. The solar fraction for a polished copper absorber plate was 7.61% and when the absorber was made with polished aluminum the solar fraction is 2.53%. Switching absorber plate material results in a decrease in solar fraction of 66.75%. This is a significant decrease in solar fraction which can be improved by applying a selective surface to the absorber plate.

Applying a black chrome surface to a copper absorber plate has a solar fraction of 48.36%. Using an aluminum absorber plate and a black chrome surface the solar fraction decreases to 47.28%, a percent difference of 2.23%. Changing the absorber plate thickness also has a minimal impact on overall solar fraction. Solar fraction decreases with thinner absorber plates. The simulation calculated the solar fraction for a 1.587 mm (1/16 inch) absorber plate to be 47.73%, a decrease of 1.3% of solar fraction. For a 0.795 mm (1/32 inch) absorber plate the solar fraction was decreased by 3.97% with a value of 46.44%.

Changing the type and thickness of the insulation around the solar collector affects the overall loss coefficient. The overall loss coefficient is the conductance

between the ambient temperature and the absorber plate temperature. The baseline case

for the simulation used an insulation thickness of 0.025 m (1 inch) and a conductivity of

0.05 W/mK. R-value is a measure of the thermal resistance of the insulation. By

increasing the insulation thickness and decreasing the conductivity the overall resistance

of the insulation value increases. Inversely, the conductance decreases with an increased

insulation R-value. By doubling the baseline insulation thickness the conductivity was

decreased by half and the R-value was doubled. The solar fraction for a collector with

0.0508 m (2 inches) insulation was 48.4%. This was less than a 1% improvement in solar

fraction. Collector performance was then tested by modifying the collector insulation

conductivity. By decreasing the conductivity of the insulation from 0.05 W/mK to 0.01

W/mK the R-value of the insulation was raised by a factor of 5. The solar fraction was

increased from 48.36% to 48.42%. This is a 0.12% improvement in solar fraction.

Switching the copper heat pipes to aluminum pipes did not change the solar

fraction value. Changing from a five heat pipe system to four heat pipe system decreased

the solar fraction to 0.4789, a decrease of 1.0%   Four heat pipes adequately conduct the

heat from the absorber plate. Additional heat pipes did not improve the performance by a

significant amount. Doubling the number of heat pipes increased the performance by

1.8%.

The baseline water tank used a water tank width of 0.2032 m (8 inches) and had a

solar fraction of 48.36%. Reducing the water tank volume by one half decreased the

solar fraction by 7.6%. A reduction in mass storage of 75% decreased the solar fraction

by 21.1%. Doubling the water tank volume increased the solar fraction by 5.0%.

Changing tank wall thickness and material conductivity did not significantly affect the

solar fraction and performance of the system. Decreasing the convection coefficient on the walls of the water tank by 20% decreased the solar fraction by 1.5%. Increasing the convection coefficient by 20% increase the solar fraction by 1%.

It was hypothesized that increasing the surface area of the condenser through the addition of fins would increase the overall solar fraction. Experimental tests showed little improvement in the performance of the heat pipe system through the addition of fins. Simulation results analyzed the addition of condenser fins, and variations in fin diameter and thickness. The addition of fins increased the solar fraction by 0.8%. Increasing the number of fins from 91 to 366 increased the solar fraction by 0.5%. Changing the fin diameter also did not significantly improve this performance.

Changing the amount of insulation between the mass storage device and the absorber plate adjusts the losses between the two. These variations enable the construction of the separating wall to be chosen based on thermal and economic performance. Increasing or decreasing the conductivity between the water tank and absorber plate by 20% affected the solar fraction by 1.0%.

C. Matching Results

The computer simulation was modified to simulate the experimental test. To simulate the experimental results, radiation values were input from the experiment in one minute increments. The simulation accounts for no heat losses to ambient from the heat pipe. No losses from the heat pipe assumes that the adiabatic section of the heat pipe is well insulated. Differences between the experimental runs and the simulation also include the lack of mass at each thermal node in the computer simulation. The only

thermal node in the computer simulation that has a mass, is the water tank mass storage node. For the experimental test, temperature data was measured at the absorber plate, heat pipe evaporator section, heat pipe adiabatic section, heat pipe condenser section, and water tank. Thermal nodes in the computer simulation included the outside ambient temperature, the absorber plate temperature, the heat pipe evaporator section, heat pipe condenser section, water tank, water tank wall, and room temperature. The simulation was used to match the corresponding measured temperature data.

The measured experimental temperatures rise quickly in the first hour of the test. This is because the radiation value is not constant as the lamps warm up. The initial temperatures from the experiment were matched in the simulation at the start. The lack of thermal mass in the simulation causes the temperatures of nodes other than the water tank to rise quickly, thus the simulated temperatures in the first hour do not directly match with the measured experimental values for the simulated nodes without mass. The water tank temperature from the simulation matches the experimental data throughout the test. The water tank temperature does not rise as quickly as the absorber plate and heat pipe temperatures due to the mass at that node.

After the simulation inputs were adjusted to match the experiment, the conductances were adjusted until the temperatures matched. The calculated heat transfer coefficient, k_{71}, the overall loss coefficient of the collector was decreased by 10% in the simulation. After matching, the maximum conductance was 2.187 W/m^{2}K. The conductance between the absorber plate and the evaporator section of the heat pipe was not adjusted during the matching process. The calculated conductance between the evaporator and the condenser was decreased to 6% of the original value to match the

measured temperatures. This suggests that either the heat pipe should have performed significantly better during the experiment, or that the simulation is not accurately calculating the conductance between the evaporator and condenser section of the heat pipe. The calculated conductance between the condenser section of the heat pipe and the water tank was decreased by 2% to match the measured values. The maximum conductance for k_{34} was 26.691 W/m^{2}K after matching.

To improve the matching process the heat pipe conductance should be further investigated. The charging point of the heat pipe in the adiabatic section could have reduced the performance of the heat pipe. The simulation does not account for heat loss in the system and if improved upon could more accurately match the conductance of the experiment. The simulation does not model the fluid behavior inside the heat pipe, and if accounted for could also more accurately model the conductance of the heat pipe.

Before matching, the highest conductance in the heat pipe system is k_{23}, the heat pipe conductance. After matching k_{23} was still the highest conductance. Because of this, the system performance is not sensitive to k_{23}, and the value of this conductance cannot be determined with any accuracy during matching. The second lowest conductance both before and after matching was k_{12}, the conductance between the absorber plate and the heat pipe. The experimental conductance could be improved by insuring a better thermal connection. This could be accomplished by brazing or welding the absorber plate to the heat pipe instead of soldering. The lowest conductance before and after matching was k_{34}, the conductance between the condenser of the heat pipe and the water tank. This remains as the thermal bottleneck of the system. Improving this conductance could greatly improve the overall performance of the heat pipe system. Radial fins were

analyzed in both the experiment and the computer simulation. Increasing the number of fins in the computer simulation increased solar fraction performance by 1.5%. In the experiment the fins were manually soldered to the heat pipe. Adjusting the design and fabrication techniques of the condenser fins could increase performance.

D. Economic Results

1. Design Cost and Recommendations

Fabricating the units out of plastic allows for lower manufacturing cost, low shipping weights, modular design, and customizability. Plastic units would be easier to manufacture and the design could ease the overall assembly. The design outlined would allow for prefabricated grooves for the absorber plate and glazing. Water tanks would be constructed as part of the prefabricated plastic structure with access for bulk heads and filling ports. The main casing and main casing cap could be fabricated through injection modeling. Table XVIII outlined the differences in single unit non optimized design cost. Based on labor and material cost the plastic unit is also the most cost effective option. The wood frame construction is $119.79 more than the plastic unit and the aluminum frame construction is the most expensive design $264.44 more than the plastic unit. These advantages and the overall flexibility allowed through injection molding make this design superior.

The labor cost accounts for 4% of the total cost of the unit. The material cost for the unit is 71.2% of the cost of the unit. The metal material used in the unit accounts for 52.1% of the overall cost. 8.3% of the cost of the unit is in the selective surface coating. 5.7% of the overall cost is made up of the plastics used and cost for tooling and dies.

Reducing the amount of metal or changing the metal from copper to aluminum would lower the overall cost of the unit.

2. Cost Optimization

The solar fraction of each design change was divided by the overall cost of the unit including the changes made. These values allowed for an accurate cost comparison. The material type and thickness of the absorber was first analyzed. The 0.000795 m (1/32 inch) aluminum absorber plate has the best performance for the cost. Switching from a copper to aluminum absorber plate reduces the overall cost of the unit by 26.7%.

The use of an additional cover improved the solar fraction of the system, however, this design change is not cost effective. The use of low iron glass with a thin thickness also improves the cost effectiveness of the design. This design setup was used in the base case scenario, therefore, there is no overall cost reduction.

The application of a selective surface of black chrome increased the overall price of the unit by $300.00 and increased the solar fraction from 7.61% to 48.36%. The extra expense in black copper surface did not provide a more cost effective design than the black chrome surface. Applying a black chrome surface is more common than the black nickel and black copper surfaces, and is the most cost effective option.

Changing the number of heat pipes on the absorber plate increase or decrease both the labor cost and material cost of the unit. Each additional heat pipe adds $293.50 to the cost of the system. Lowering the number of heat pipes below four significantly drops the solar fraction of the system. The addition of extra heat pipes does not increase the solar fraction enough to increase the cost effectiveness of the design.

The size of the mass storage device is an important decision in the cost optimization of the system. Increasing the width of the unit adds additional material and weight to the system. Heat pipe systems with a larger mass storage device have higher solar fractions. If additional structural support needs to be installed to accommodate the higher dead loads, then the installation cost would rise by $274.78. If the span of the floor joist is assumed to be 3.6576 m (12 ft) and the International Residential Codes are used, then additional support would be required at dead loads higher than 500 kg. The most cost effective water wall width when the additional installation requirements are considered, is 0.3048 m (12 inch).

The most cost effective design would incorporate an aluminum absorber plate with four heat pipes. The solar glazing would have one cover and be made with low iron glass (3/32 inch) thick. The total cost of the unit would be $1825.46 and have a solar fraction of 42.67%.

3. Life Cycle Analysis

The overall cost of the unit is high when compared to the total load it can replace. Rising fuel cost will ultimately lower the payback period of the unit, but design changes should be made to eliminate some of the cost. Currently the high price of copper and aluminum encompass a large percentage of the overall price. The most cost effective design was used for life cycle cost analysis. This unit is constructed of 4 aluminum heat pipes on a 0.00079502 m (1/32 inch) aluminum absorber plate that is black chromed. The absorber plate glazing would consist of a 2.38 mm (3/32 inch) low iron glass cover. The water tank on the unit would be 0.3048 m (12 inches) thick. The overall unit price is 48.19% of the present worth of the future fuel cost. The payback period of 22.21 years is

high. The cost of the unit can be mortgaged over a 30 year period if multiplied units are

purchased. Installation cost of each unit accounted for $726.51. If the system integrated

heat pipe system is installed in a new construction this cost is drastically reduced. There

is also material savings associated with sections of previous wall that would not be

constructed. These savings are estimated to be $176. A price difference of $592.85

would exist between a retrofit installation and new construction installation. The

payback period for new construction systems consisting of the optimized design would

drop to 15.75 years. The use of tax incentives to offset the initial cost of the system

decrease the payback period. The discounted payback period for the optimized design

using the $1,047.64 in tax incentives is 10.35 years.   For new construction installations

the payback period with tax incentives is 6.74 years. This payback period is more

reasonable from a consumer perspective.

VI. CONCLUSION

A prototype heat pipe wall was constructed and instrumented. One of the objectives of the project was to test the effects of fluid fill level and insulating the adiabatic section of the heat pipe. The average radiation on the absorber plate was 709.4 W/m^2. The experimental heat pipe performance was affected by the fluid fill level of the heat pipe. A fluid fill level of 120% of the evaporator section volume delivered the best performance, and efficiency. The average rate of water tank temperature change was 1.190 °C/hr, and the overall efficiency was 83.41%. Insulating the adiabatic section of the heat pipe proved to be an easy way to improve the overall performance. The efficiency with an insulated adiabatic section was 85.09%. Condenser fins did not significantly improve the overall efficiency of the system.

A computer program was written to simulate the performance of a heat pipe wall. A goal of the simulation was to test the performance of passive solar systems in different climate regions. Climate comparisons of simulated passive solar systems showed that the water wall indirect gain system outperformed the concrete wall in all four climates, and that the heat pipe wall outperformed all other designs in all climates. The water wall system in Louisville (cloudy and cool) had a solar fraction of 38.84%. Indirect gain systems performed better than the direct gain systems in all climates except Albuquerque

(sunny and cool). The thermal losses of the direct gain system delivered a negative solar

fraction, -4.51%, in Madison , which has low winter radiation and cold ambient

temperatures. The solar heat pipe wall performed well in Louisville, and even better

relative to the other systems in the colder and cloudier climates. The heat pipe wall in

Rock Springs (sunny and cool) was 47.85% and in Louisville the solar fraction was

48.36%. Regardless of the passive solar system chosen, Louisville's climate is

advantageous for effect solar energy use. All systems performed better in Louisville than

in Rock Springs (sunny and cold) and Madison (cloudy and cold). The thermal diode

effect of the heat pipe wall provides an effective and convenient means to eliminate

losses in a passive solar system. It is a design that is aesthetically pleasing and offers the

benefits of excellent nighttime insulation without the need to remove and replace the

insulation daily.

Another objective of the project was to use computer simulations to study the

effects of design changes on overall system performance. The computer simulations for

the passive solar heat pipe wall with parameter variations showed the most effective ways

to improve the overall thermal performance of the system. Low iron glass should be used

when designing passive solar systems and performance was improved by using smaller

glass thickness. Decreasing the collector thickness from 3.175 mm (1/8 inch) to 2.38 mm

(3/32 inch) increased the solar fraction to 48.5%. Adding an additional cover decreased

the collector overall loss coefficient and slightly increased the solar fraction of the design

to 49.16%. Painting the absorber plate with flat black paint more than doubled the

performance of the collector compared to bare copper, but the application of a selective

surface provided a further dramatic increase in solar fraction. Unpolished copper had a

solar fraction of 7.46% and a flat black paint increased the solar fraction to 19.28%. As expected, thicker absorber plates improved the solar fraction because they improve the heat transfer between the plate and heat pipe. Increasing the insulation rating around the absorber plate also reduces the heat losses of the collector.

Using aluminum or copper heat pipes did not significantly affect the thermal performance of the heat pipe. At a minimum, four heat pipes should be used for this size collector. Additional heat pipes did help transfer heat from the absorber plate to the water tank, but with decreasing margins. The solar fraction was improved by increasing the mass of the water tank. A water tank 0.1019 m (4 inch) wide had a solar fraction of 44.69%, and when the width was increased to 0.3048 m (12 inch) the solar fraction was 49.86%. A point of diminishing returns was exhibited with increased water wall width. Water tank thickness and material conductivity did not significantly improve the solar fraction of the unit. As seen in the experiment, adding fins on the condenser end of the heat pipe did not significantly improve performance. The solar fraction only increased by 0.8% when 91 radial fins were added. Increasing the insulation level between the mass storage device and absorber plate beyond the baseline value also did not significantly increase performance.

A main goal of the project was to match the performance of the laboratory model with the results of the computer simulation. The computer simulation accurately matched the temperatures of the experiment. The lack of nodal mass in the simulation caused the temperatures to rise quicker than the experimental values. The conductance between the absorber plate temperature and the ambient temperature was reduced by 10% in the matching process. The heat pipe conductance operated significantly lower than the

calculated values of the simulation. This value was reduced to 6% of its original value to match the experimental temperatures. The heat pipe conductance during matching was 138.46 W/m^{2}K. The conductance between the water tank and the condenser of the heat pipe was reduced by 2% to match the experimental values. The conductance between the absorber plate and the heat pipe was not adjusted.

The final goals of the project were to complete an economic assessment and give recommendations on the units design with regards to the future development of a commercial unit. Design recommendations were made to improved manufacturing, assembly, shipping and installation. Compared to a wood or aluminum frame construction, using plastic injection modeling was more cost effective. Labor cost and material prices were both reduced with this design. Labor cost during unit assembly was also reduced with the plastic frame. The adiabatic section of the heat pipe was fully insulated, and the absorber plate and water tanks were isolated with insulation for nighttime conditions. Grooves in the plastic frame allow for the absorber plate and glazing to be slid into position. This reduces the need to mount these parts and provides a secure fit. Prefabricated and structurally attached water tanks are one of the most important features of a plastic design. Tanks of this design reduce labor, parts, cost and maintenance. The cost of the optimized design is $1825.46 and the material cost was $827.45.

The absorber plate comprises a majority of the units cost. The optimized design includes the use of four aluminum heat pipes and a black chromed aluminum absorber plate that is 0.79502 mm (1/32 inch). One solar glazing made of low iron glass that is 2.38252 mm (3/32 inch) provides the most cost effective cover. The fabricated water

tank width would be 0.3048 m (12 inches) long. Life cycle costing shows that the

payback period is 22.21 years for a retrofit application and 15.75 years for new

construction. Federal and state tax credits can alleviate $1047.64 from the cost of the

unit. The discounted payback period when including tax incentives is 10.35 years.

VII. RECOMENDATIONS

While the computer simulation models passive solar systems effectively, a significant amount of insight could be gained by improving the model. One of the limitations of the model is that it does not simulate performance changes based on fluid fill levels. Improvement could be seen in the overall design by modeling the phase change interactions inside the heat pipe. With these adjustments heat pipe wick design, fluid type, and overall limitations could be explored. Modeling the heat pipe fluid behavior would also improve the analysis of the startup of the system. By calculating the viscous, sonic, entrainment, capillary and boiling limits, heat pipe behavior could be better understood in a passive solar application. Experimental analysis could be further improved with full scale testing. This would provide greater insight into the performance of this system with Louisville, Kentucky's latitude and climate.

The computer simulation should also be matched to the performance of full scale tests in Louisville, Kentucky. This comparison could show differences in performance with the simulation based on heat pipe startup and heat pipe operational limits. Furthermore the full scale test should also be conducted in different climate regions. This way the comparisons can be made with the variations in climates. A limitation of the simulation is the use of typical meteorological data. Extreme conditions in temperature,

wind speeds, rain, and snow will have an impact of the systems performance. These

topics can all be investigated with full scale test in varying climate regions.

Summertime overheating situations also need to be investigated before

commercial units are put into production. An investigation should be made into the

design of the unit and the architectural design installation point. The simulation could

then be adjusted to handle the summer heat through both air conditioning and venting.

Possibly by inverting the unit during summer conditions the heating unit could be

converted into a cooling unit. The design of the unit would have to be modified to allow

this seasonal conversion to be made easily by the consumer.

VIII. REFERENCES

Abo El-Nasr, A. and El-Haggar, S. M. 1996. Effective thermal conductivity of heat pipes. *Heat and Mass Transfer* 32: 97-101.

Akyurt, Mehmet. 1984. Development Of Heat Pipes For Solar Water Heaters. *Solar Energy* Vol 32 No. 5: 625-63.

Azad, E., Bahar, F., and Moztarzadeh, F. 1987. Solar Water Heater Using Gravity-Assisted Heat Pipe. *Heat Recovery Systems and CHP* Vol. 7 No. 4: 343-350.

Chun, Wongee, Kang, Y. H., Kwak, H.Y., and Lee, Y.S. 1999. An experimental study of the utilization of heat pipes for solar water heater. *Applied Thermal Engineering* 19: 807-817.

Corliss, J.M. (1979). "Evaluation of heat pipe application for passive solar systems." *DOE Rep.*, Dept. of Energy, Washington, D.C.

Duffie, J.A. and Beckman, W.A. 1991. *Solar Engineering Of Thermal Processes*. New York: John Wiley and Sons.

Gilat, Amos. 2004. *Matlab: An Introduction with Applications*, 2nd ed. New York: John Wiley and Sons.

Hegerl, G.C., F. W. Zwiers, P. Braconnot, N.P. Gillett, Y. Luo, J.A. Marengo Orsini, N. Nicholls, J.E. Penner and P.A. Stott, 2007: Understanding and Attributing Climate Change. In: Climate Change 2007: The Physical Science Basis. Contribution of Working Group I to the Fourth Assessment Report of the Intergovernmental Panel on Climate Change [Solomon, S., D. Qin, M. Manning, Z. Chen, M. Marquis, K.B. Averyt, M. Tignor and H.L. Miller (eds.)]. Cambridge University Press, Cambridge, United Kingdom and New York, NY, USA.

Incropera, Frank P. and Dewitt, David P. 2002. *Introduction to Heat Transfer*. New York: John Wiley and Sons.

Kempers, R., Ewing, D., and Ching. C.Y. 2006. Effect of number of mesh layers and fluif loading on the performance of screen mesh wicked heat pipes. *Applied Thermal Engineering* 26:589-595.

National Instruments Corporation. 2009. Austin, Texas. 26 Feb. 2009
        <http://www.ni.com/advisor/accuracy/acc_support.htm>

Peterson,G.P.1994. *An Introduction To Heat Pipes: Modeling,Testing,and
        Applications*. New York: John Wiley and Sons.

Reay,D.A., Kew, K.A.2006. *Heat Pipes: Theory, Design, and Application*, 5th ed..
        Oxford: Elsevier.

Rothman, Daniel. 2002. Atmospheric Carbon Dioxide Levels For The Last 500 Million
        Years. *Proceedings of the National Academy of Science of the United States of
        America* Vol. 99, No. 7:4167-4171.

Saatci, A.M., Olwi, R.R., et. al.1989. Passive Transport Of Solar Energy Downward By
        Heat Pipes. *Energy* Vol 14 No. 7: 383-392.

Siegel, R., Howell, J.R..*Thermal Radiation Heat Transfer*, 4th ed. New York: Taylor and
        Francis.

Susheela, Narasimhan, Sharp, M. Keith. 2001. Heat Pipe Augmented Passive Solar
        System For Heating of Buildings. *Journal of Energy Engineering* Vol. 127, No
        l:18-36.

Van Dijk HAL, *et al*. (1983). High Performance passive solar heating system with heat
        pipe energy transfer and latent heat storage. *Solar energyto applications to
        dwellings,* Proceedings EC contractor's meeting, Brussels, 1-3 June, D. Reidel
        Publishing Company, pp. 118-130.

Vasilev, L.L., Avakyan, Y.V., Grakovich, L.P., Khrustalev, D.K., and Dabagyan, T.N.
        1987. Investigating the Parameters of a Flat Solar Energy Receiver with Heat
        Pipes. *Thermal Engineering* 34: 479-481.

Wang, H.Y., Yan, H.F., Xing, B.B., and Wang, Y.L. 1985. Optimization of Parameters
        For Solar Plane-Plate Collector With Gravity Heat Pipes. Proceedings of the
        International Simposium on Thermal Application of Solar Energy
        (Hakone,Japan), 111-114.

W.Y. Saman, N.J. Yaseen & R.A. Abdulla. The use of heat pipes to reduce heating and
        cooling loads in buildings. Proc. International Conference on heating ventilating
        and air-conditioning, Copenhagen,1985.

Zittel, Werner. and Schindler, Jörg. 2007. Crude Oil The Supply Outlook. *Report to the
        Energy Watch Group* EWG-Series No. 3/2007

TMY2 DATA

TABLE XXII

TMY2 DATA FOR JULIAN HOURS 300-348

Time		Global Horizontal Radiation $\frac{W*h/}{m^2}$		Direct Normal Radiation $\frac{W*h/}{m^2}$		Diffuse Horizontal Radiation $\frac{W*h/}{m^2}$		Dry Bulb Temperature °C*10		Wind Speed m/s	
Day	Hour	Data Value	F. Data Uncertainty	Data Value	F. Data Uncertainty	Data Value	F. Data Uncertainty	Data Value	F. Data Uncertainty	Data Value	F. Data Uncertainty
13	12	131	4	11	4	126	5	106	7	67	7
13	13	193	4	2	4	192	5	133	7	108	7
13	14	123	4	8	4	119	5	144	7	103	7
13	15	127	4	0	4	127	5	150	7	124	7
13	16	99	4	4	4	98	5	161	7	113	7
13	17	98	5	182	5	62	5	128	7	103	7
13	18	29	5	17	5	27	5	89	7	180	7
13	19	0	0	0	0	0	0	50	7	144	7
13	20	0	0	0	0	0	0	39	7	103	7
13	21	0	0	0	0	0	0	39	7	93	7
13	22	0	0	0	0	0	0	33	7	82	7
13	23	0	0	0	0	0	0	28	7	77	7
13	24	0	0	0	0	0	0	22	7	41	7
14	1	0	0	0	0	0	0	11	7	31	7
14	2	0	0	0	0	0	0	0	7	26	7
14	3	0	0	0	0	0	0	-11	7	41	7
14	4	0	0	0	0	0	0	-17	7	21	7

14	5	0	0	0	0	0	0	-22	7	21	7
14	6	0	0	0	0	0	0	-22	7	26	7
14	7	0	0	0	0	0	0	-28	7	36	7
14	8	0	0	0	0	0	0	-17	7	46	7
14	9	44	5	203	4	26	5	-11	7	52	7
14	10	189	5	562	4	53	5	0	7	52	7
14	11	338	4	718	4	71	5	11	7	57	7
14	12	446	4	788	4	83	5	17	7	57	7
14	13	500	4	818	4	89	5	22	7	46	7
14	14	496	4	823	4	88	5	33	7	62	7
14	15	424	4	783	4	80	5	39	7	41	7
14	16	299	4	690	4	66	5	39	7	52	7
14	17	144	5	491	4	47	5	33	7	52	7
14	18	29	5	99	4	19	5	22	7	41	7
14	19	0	0	0	0	0	0	6	7	36	7
14	20	0	0	0	0	0	0	-11	7	36	7
14	21	0	0	0	0	0	0	-11	7	31	7
14	22	0	0	0	0	0	0	-17	7	41	7
14	23	0	0	0	0	0	0	-17	7	21	7
14	24	0	0	0	0	0	0	-11	7	0	7
15	1	0	0	0	0	0	0	-22	7	0	7
15	2	0	0	0	0	0	0	-33	7	21	7
15	3	0	0	0	0	0	0	-22	7	26	7
15	4	0	0	0	0	0	0	-28	7	0	7
15	5	0	0	0	0	0	0	-44	7	0	7
15	6	0	0	0	0	0	0	-61	7	26	7
15	7	0	0	0	0	0	0	-56	7	15	7
15	8	0	0	0	0	0	0	-56	7	26	7
15	9	52	5	350	4	20	5	-44	7	21	7
15	10	213	5	752	4	30	5	-6	7	36	7
15	11	323	4	704	4	60	5	17	7	52	7
15	12	342	5	381	5	166	5	28	7	52	7

APPENDIX II

MATLAB COMPUTER SIMULATION CODE

```
% Augmented Passive Solar Heat Pipe Wall Computer Model

% Formatting Matlab
clc;                          % Clears Command Window
%clear;                       % Deleting all variables from workspace
format compact;              % Removes extra line spacing from
output
format short;                % Short Engineering Output
tic;                          % Starts Clock
Trial=1
% City location data
latitude = 38.18; longitude = 85.73; Lst = 75.0;          % Louisville
% latitude = 43.13; longitude = 89.33; Lst = 90.0;        %
Albuquerque
% latitude = 35.05; longitude = 106.6; Lst = 105;         % Madison
% latitude = 41.6; longitude = 109.22; Lst = 105;         % Rock
Springs

% Constants
density_water=1000;          % Density of Water (kg/m^3)
cp_water=4190;               % Specific Heat of Water (J/kgK)
deltat=60;                   % Delta t is the time step
St=5.67*10^-8;               % Steffan Boltzman Constant
k_cu=385;                    % T. Conductivity, copper (W/m*K)
k_al=205;                    % T. Conductivity, aluminum (W/m*K)
g=9.81;                      % Acceleration of Gravity (m/s^2);
Gsc = 1367;                  % Watts/meter^2

% Building & Collector Properties
beta=90.0;                   % Slope of the collector (degrees)

N=1;                         % Number of Glass Covers
eg=0.88;                     % Emittance of glass
ep=0.02;                     % Emittance of plate 0.02 &0.095

L_glass=0.003175;            % Thickness of the glass (m)
K_ex_glass=4;                % Extinction coefficient of glass (m^-1)
KL=K_ex_glass*L_glass;
```

135

```
rho_g=0.3;                          % ground reflectance

an=0.96;                            % normal absorptivity
n1=1.0;                             % index of refraction for air
n2=1.526;                           % index of refraction for glass

L_abp=2.0828;                       % Length of the Absorber Plate (m)
W_abp=1.165225;                     % Width of the Absorber Plate (m)
Area=L_abp*W_abp;                     % area of the collector (m^2)
P=2*L_abp+2*W_abp;                  % Perimeter of the Collector (m)
thick=0.003175;                     % Collector Thickness (m)
k_collector=k_cu;                   % T. Conductivity, collector (W/m*K)
k_cic=0.05;                         % Insulation Conductivity (W/m*K)
% k_cic_=205;
L_bl=0.005;                         % Back Insulation Thickness (m)
Ledge=0.025;                        % Edge Insulation Thickness (m)

% Heat Pipe and Wicking Structure Details
Numberof_HeatPipes=5;               % Number of Heat Pipes
W_hp=0.34713212;                     % Distance between the centers of
two adjacent heat pipes (m)
% Numberof_HeatPipes=4;               % Number of Heat Pipes
% W_hp=0.41656;                      % Distance between the centers of
two adjacent heat pipes (m)
OD=0.028575;                        % Outer Diameter of the Copper heat
pipe (m)
ID=0.022225;                        % I.D. of Copper heat Pipe (m)
Le=1.165225;                        % Length of evaporator section (m)
La=.365125;                         % Length of adiabatic section (m)
Lc=1.165225;                        % Length of condenser section (m)
Length=Le+La+Lc;                    % Overall Length of the Heat Pipe
(m)
kp=k_cu;                            % Pipe Wall Thermal Conductivity
(W/m*K)
% Conductances, non temperature dependent
% K71
if beta>0 & beta<70;
    C=520*(1-.000051*beta^2);
else beta>70;
    C=520*(1-.000051*70^2);
end
% Bottom Loss Coefficient
%Ub=k_cic/L_bl;                               % (W/m^2*K)
% Edge Loss Coefficient
UA_edge=(k_cic/Ledge)*(2*(L_abp)+2*(W_abp))*thick;
% Ue=UA_edge/((L_abp+0.1524)*(W_abp+0.1524));  % (W/m^2*K)
Ue=UA_edge/((L_abp)*(W_abp));
% k12
Nfins=Numberof_HeatPipes+1;
      % Number of fins
heff=1/((1/(3*k_collector*thick))*((W_hp-OD)/2)^2);          % (W/m^2*K)
% Normalizing the value
k12=heff*(Nfins/2)*(W_hp-OD)*L_abp/Area;        % (W/m^2*K)


% Wall Material Thicknesses
```

```
L_Brick=0.0508; L_Plywood=0.01905; L_Insulation=0.1524;
L_Sheetrock=0.00635;
% Wall Material Conductances
k_Brick=0.72; k_Plywood=0.120; k_Insulation=0.370; k_Sheetrock=0.170;
NIC=(1/Area/(L_Brick/k_Brick+L_Plywood/k_Plywood+L_Insulation/k_Insulat
ion+L_Sheetrock/k_Sheetrock)*(1+0.0)));

% k34
radfin=0.01905;                         % Radius of fin (m)
tfin=0.003175;
r2c=radfin+(tfin/2);
Number_condenserfins=91;            % Number of fins
Area_fin=2*pi*((r2c^2-(OD/2)^2));   % Area of fins (m^2)
Area_condenser=OD*pi*Lc;            % Area of condenser section (m^2)
Area_condensertotal=Number_condenserfins*Area_fin+Area_condenser;
nf=1;
no=1-(Number_condenserfins*Area_fin/Area_condensertotal)*(1-nf);

% k56 Free Convection Off The Water Tank
% Vertical Side
NumberofTanks=1;
TankWidth=0.2032; % (m)
TankHeight=1.9558; % (m)
TankLength=1.190625; % (m)

% Vertical Sides
VCL=TankHeight;         % Characteristic Length (m)
% Horizontal Side Top
TCL=(TankWidth*TankLength)/(2*TankWidth+2*TankLength);          %
Characteristic Length (m)
% Horizontal Side Bottom
BCL=(TankWidth*TankLength)/(2*TankWidth+2*TankLength);          %
Characteristic Length (m)

Tanksurface=NumberofTanks*2*((TankWidth*TankHeight)+(TankWidth*TankLeng
th)+(TankHeight*TankLength));

% k45
% Conduction Through The Tank Wall
L_Tank=0.003175;                        % Thickness of Water Tank Wall
k_Tank=0.5;                             % Tank Wall Thermal Conductivity
(W/m*K)

k45=(1/(L_Tank/k_Tank))/Area*Tanksurface;         % (W/m^2*K)

% k67 Reciprical of Collector Area to Load Ratio
% Infiltration
V=5.465151;                             % Room Volume (m^3)
k67=10;


% Total Number of TMY2 Hours imported
Xsize_Array=size(Gt);
Xsize=Xsize_Array(1,1);

% Initialize the variables
% Mass of the system
```

```
m1=0.0; m2=0.0; m3=0.0; m5=0.0; m6=0.0; m7=0.0; % (J/m^2K)
m4=density_water*cp_water*TankWidth*TankHeight*TankLength/Area;
% m4=0.0;

% Iterate variable used in while loop
Iterate=1;
IterationCount=(zeros(Xsize,60));
Plotcheck=0;

% Temperatures
T1old=292.15; T2old=292.15; T3old=292.15; T4old=292.15; T5old=292.15;
T6old=292.15;
T1=292.15; T2=292.15; T3=292.15; T4=292.15; T5=292.15; T6=292.15;

% Auxiliary heating to keep room at 19C
Qaux1=0.0; Qaux2=0.0; Qaux3=0.0;
Qaux4=0.0;Qaux5=0.0;Qaux6=0.0;Qaux7=0.0;Qaux8=0.0;Qaux9=0.0;Qaux10=0.0;
Qaux11=0.0;Qaux12=0.0; Qaux=0.0;

% Heat lost over the year to maintain room temperature of 19C (W*hr)
Qreqd1=0.0; Qreqd2=0.0; Qreqd3=0.0;
Qreqd4=0.0;Qreqd5=0.0;Qreqd6=0.0;Qreqd7=0.0;Qreqd8=0.0;Qreqd9=0.0;Qreqd
10=0.0;Qreqd11=0.0;Qreqd12=0.0; Qreqd=0.0;

% Calculation of n for the ith day of the year
for i=1:1:Xsize;
    if month(i)==1;
        n(i)=day(i);
    elseif month(i)==2;
        n(i)=31.+day(i);
    elseif month(i)==3;
        n(i)=59.+day(i);
    elseif month(i)==4;
        n(i)=90.+day(i);
    elseif month(i)==5;
        n(i)=120.+day(i);
    elseif month(i)==6;
        n(i)=151.+day(i);
    elseif month(i)==7;
        n(i)=181.+day(i);
    elseif month(i)==8;
        n(i)=212.+day(i);
    elseif month(i)==9;
        n(i)=243.+day(i);
    elseif month(i)==10;
        n(i)=273.+day(i);
    elseif month(i)==11;
        n(i)=304.+day(i);
    elseif month(i)==12;
        n(i)=334.+day(i);
    end
end;

% Diffuse (equation 5.4.2 of Duffie & Beckman)
theta_d=59.7-0.1388*beta+0.001497*beta^2;
theta2_d = asind(n1*sind(theta_d)/n2);
rperp_d =(sind(theta2_d-theta_d))^2/((sind(theta2_d+theta_d))^2);
```

```matlab
rparl_d=(tand(theta2_d-theta_d))^2/((tand(theta2_d+theta_d))^2);
ta_d=exp(-KL/(cosd(theta2_d)));
tr_d=.5*((1-rparl_d)/(1+(2*N-1)*rparl_d)+(1-rperp_d)/(1+(2*N-
1)*rperp_d));
t_d=ta_d*tr_d;
a_d=(1+2.0345*10^(-3)*theta_d-1.990*10^(-4)*theta_d^2+5.324*10^(-6)...
    *theta_d^3-4.799*10^(-8)*theta_d^4)*an;
talpha_d = 1.01*t_d*a_d;


% Ground Reflected (equation 5.4.1 of Duffie & Beckman)
theta_g = 90.0-0.5788*beta+.002693*beta^2;
theta2_g = asind(n1*sind(theta_g)/n2);
rperp_g = (sind(theta2_g-theta_g))^2/((sind(theta2_g+theta_g))^2);
rparl_g = (tand(theta2_g-theta_g))^2/((tand(theta2_g+theta_g))^2);
ta_g = exp(-KL/(cosd(theta2_g)));
tr_g = .5*((1-rparl_g)/(1+(2*N-1)*rparl_g)+(1-rperp_g)/(1+(2*N-
1)*rperp_g));
t_g = ta_g*tr_g;
a_g = (1+2.0345*10^(-3)*theta_g-1.990*10^(-4)*theta_g^2+5.324*10^(-
6)...
    *theta_g^3-4.799*10^(-8)*theta_g^4)*an;
talpha_g = 1.01*t_g*a_g;



% Start the big loop that is incremented at each hour
for j = 1:Xsize;
    declination(j) = 23.45 * sind(360.0*((284+n(j))/365));
    B(j) = (n(j)-1)*360./365.;  %(degrees)
    EOT(j) = 229.2*(0.000075 + 0.001868*cosd(B(j)) -
0.032077*sind(B(j))...
          - 0.014615*cosd(2*B(j)) - 0.04089*sind(2*B(j)));
    solartime(j) = hour(j) + ((4*(Lst-longitude) + EOT(j))/60);
%(hours)
    omega2(j) = (solartime(j) - 12.0)*15.0;  % (degrees)
    omega1 = omega2(j)-15; % (degrees)
    costheta(j) =  -sind(declination(j))*cosd(latitude)...
                    +
cosd(declination(j))*sind(latitude)*cosd(omega2(j));
    theta(j) = acosd(costheta(j));
    costhetaz(j) =
cosd(latitude)*cosd(declination(j))*cosd(omega2(j))...
                    + sind(latitude)*sind(declination(j));
    thetaz(j) = acosd(costhetaz(j));
    if (theta(j) > 90. | thetaz(j) > 90.);
        Rb(j) = 0.0;
    else
        Rb(j) = costheta(j)/costhetaz(j);
    end;

    % Rb is capped when thetaz is close to 90 degrees. This eliminates
    % irregularities associated with calculations during sunrise and
sunset
    if Rb(j) > 10.0
        Rb(j) = 10.0;
    end;

% Calculating Beam Transmisivity (Ch. 5 of Duffie & Beckman)
```

```
    theta2_b(j) = asind(n1*sind(theta(j))/n2);
    rperp_b = (sind(theta2_b(j)-
theta(j)))^2/((sind(theta2_b(j)+theta(j)))^2);
    rparl_b = (tand(theta2_b(j)-
theta(j)))^2/((tand(theta2_b(j)+theta(j)))^2);
    ta_b = exp(-KL/(cosd(theta2_b(j))));
    tr_b =.5*((1-rparl_b)/(1+(2*N-1)*rparl_b)+(1-rperp_b)/(1+(2*N-
1)*rperp_b));
    t_b = ta_b *tr_b;

% Calculating absorbtivity (eq 4.11.1 of Duffie & Beckman)
    a_b =(1+2.0345*10^(-3)*theta2_b(j)-1.990*10^(-
4)*theta2_b(j)^2+5.324*10^(-6)*theta2_b(j)^3-4.799*10^(-
8)*theta2_b(j)^4)*an;
    talpha_b(j)= 1.01 * t_b * a_b;
    if theta(j) > 90.0
        talpha_b(j) = 0.0;
    end;

    if Gt(j)<=0;
        Io=0;
    else

Io=((12*3600)/pi)*Gsc*(1+(0.033*cosd((360*n(j))/365)))*(cosd(latitude)*
cosd(declination(j))*(sind(omega2(j))-sind(omega1)) + ((pi*(omega2(j)-
omega1))/180) * sind(latitude) * sind(declination(j)));
    end

    if Gt(j)<=0;
        Ib=0;
    else
        Ib=Gt(j)-Id(j);
    end
%     if Gt(j)<=0;
%         Ib=0;
%     elseif Id(j)>Gt(j);
%         Ib=0;
%     else
%         Ib=Gt(j)-Id(j);
%     end

    if Gt(j)<=0;
        Ai=0;
    else
        Ai=Ib/Io;
    end

    if Gt(j)<=0;
        fff=0;
    else
        fff=(Ib/Gt(j))^0.5;
    end

% ANISOTROPIC
    E1(j)=(Ib+Id(j)*Ai)*Rb(j)*talpha_b(j)+Id(j)*(1-
Ai)*talpha_d*((1+cosd(beta))/2)*(1+fff*(sind(beta/2))^3)+Gt(j)*rho_g*ta
lpha_g*((1-cosd(beta))/2);
```

```
% Isotropic and Anisotropic Performance Comparison
%
ISO(j)=Ib*Rb(j)*talpha_b(j)+Id(j)*talpha_d*((1+cos(beta))/2)+rho_g*(Ib+
Id(j))*talpha_g*((1-cos(beta))/2);
%      ANISO(j)=(Ib+Id(j)*Ai)*Rb(j)*talpha_b(j)+Id(j)*(1-
Ai)*talpha_d*((1+cosd(beta))/2)*(1+fff*(sind(beta/2))^3)+Gt(j)*rho_g*ta
lpha_g*((1-cosd(beta))/2);

% Calculate the Wind Heat Transfer Coefficient for the Hour.
    V3=V^(1/3);                             % Cubed root of building
Volume (meters)
    hw(j)=max(5,8.6*WVS(j)^0.6/V3^.4);  % Wind heat transfer
coefficient (W/m^2*K) (eq (3.15.10))
    f(j)=(1+0.089*hw(j)-0.1166*hw(j)*ep).*(1+0.07866*N);


% Start the small loop that is incremented at each minute
    for i = 1:60
        % Reset "Iterate" for next calculation
        if Iterate==0
            Iterate=1;
        end

      while Iterate==1
            % Temperatures from the previous iteration

T1prev=T1;T2prev=T2;T3prev=T3;T4prev=T4;T5prev=T5;T6prev=T6;

% Resistance Calculation
            R_pipe_e=log(OD/ID)/(2*pi*Le*kp);              %
Resistance through the evaporator pipe wall
            R_pipe_c=log(OD/ID)/(2*pi*Lc*kp);              %
Resistance through the condenser pipe wall

      % k23 Heat Pipe Wall and Wick Evaporator End
          k23=Numberof_HeatPipes/(R_pipe_e+R_pipe_c)/Area;

      % k71
            e_ut=((0.430*(1-100/T1)));
            Ut=(N./abs(C./T1*((T1-T7(j))./(N+f(j))).^e_ut)+1/hw(j)).^(-
1)+St*(T1+T7(j))*(T1^2+T7(j).^2)/((ep+0.00591*N*hw(j)).^(-
1)+((2*N+f(j)-1+0.133*ep)/eg)-N);
            Ul=(Ut+Ue);        %  Overall Loss Coefficient (W/m^2*K)
            k71=Ul;                  % (W/m^2*K)

      % k34
            Tf34=(T3+T4)/2;    % (K)
            Tfc34=(ceil(Tf34/10))*10;
            Tff34=(floor(Tf34/10))*10;
            Tfc34Loc=find(T_Water==Tfc34);
            Tff34Loc=find(T_Water==Tff34);

            BETA34W1=BETA_Water(Tfc34Loc,1);
            BETA34W2=BETA_Water(Tff34Loc,1);
            BETA34=(BETA34W1-((Tfc34-Tff34)*(BETA34W1-BETA34W2)/(Tfc34-
Tff34)))*10^(-6); % (m^2/s)
```

```
        if BETA34<=0;
            BETA34=1;
        end

        NU34W1=NU_Water(Tfc34Loc,1);
        NU34W2=NU_Water(Tff34Loc,1);
        NU34=(NU34W1-((Tfc34-Tff34)*(NU34W1-NU34W2)/(Tfc34-
Tff34)))*10^(-7); % (m^2/s)

        ALPHA34W1=ALPHA_Water(Tfc34Loc,1);
        ALPHA34W2=ALPHA_Water(Tff34Loc,1);
        ALPHA34=(ALPHA34W1-((Tfc34-Tff34)*(ALPHA34W1-
ALPHA34W2)/(Tfc34-Tff34)))*10^(-7); % (m^2/s)

        Pr34W1=Pr_Water(Tfc34Loc,1);
        Pr34W2=Pr_Water(Tff34Loc,1);
        Pr34=(Pr34W1-((Tfc34-Tff34)*(Pr34W1-Pr34W2)/(Tfc34-
Tff34)));

        kk34W1=k_Water(Tfc34Loc,1);
        kk34W2=k_Water(Tff34Loc,1);
        kk34=(kk34W1-((Tfc34-Tff34)*(kk34W1-kk34W2)/(Tfc34-
Tff34))); % (W/m*K)

        CR34=g.*BETA34*abs(T3-T4)*OD^3/(NU34.*ALPHA34);
        CNu34= (0.60 + (0.387 *
CR34.^(1/6))/((1+(0.559/Pr34).^(9/16)).^(8/27))).^2;

k34=(Numberof_HeatPipes*(kk34*CNu34/OD)*Area_condenser/Area);
% (W/m^2*K)

% For Finning on Condenser End Use...
%
k34=Numberof_HeatPipes*(kk34*CNu34/OD)*no*Area_condensertotal/Area;

    % k56
        Tf56=(T5+T6)/2;     % (K)
        Tfc56=(ceil(Tf56/100))*100;
        Tff56=(floor(Tf56/100))*100;
        Tfc56Loc=find(T_Air==Tfc56);
        Tff56Loc=find(T_Air==Tff56);

        BETA56=1/Tf56;          % (1/K)

        NU56W1=NU_Air(Tfc56Loc,1);
        NU56W2=NU_Air(Tff56Loc,1);
        NU56=(NU56W1-((Tfc56-Tf56)*(NU56W1-NU56W2)/(Tfc56-
Tff56)))*10^(-6); % (m^2/s)

        ALPHA56W1=ALPHA_Air(Tfc56Loc,1);
        ALPHA56W2=ALPHA_Air(Tff56Loc,1);
        ALPHA56=(ALPHA56W1-((Tfc56-Tf56)*(ALPHA56W1-
ALPHA56W2)/(Tfc56-Tff56)))*10^(-6); % (m^2/s)

        Pr56W1=Pr_Air(Tfc56Loc,1);
        Pr56W2=Pr_Air(Tff56Loc,1);
        Pr56=(Pr56W1-((Tfc56-Tf56)*(Pr56W1-Pr56W2)/(Tfc56-Tff56)));
```

142

```
            kk56W1=k_Air(Tfc56Loc,1);
            kk56W2=k_Air(Tff56Loc,1);
            kk56=(kk56W1-((Tfc56-Tf56)*(kk56W1-kk56W2)/(Tfc56-
Tff56)))*10^(-3); % (W/m*K)

     % Water Tank Sides
            % Vertical Side
            VR=g*BETA56*abs(T5-T6)*VCL^3/(NU56.*ALPHA56);   %Rayleigh
Number (eq 9.25) Incropera, Dewitt

            if VR<10^9;

VNu=(0.68+(0.670*VR.^(1/4))/((1+(0.492/Pr56).^(9/16)).^(4/9)));
%Nusselt Number Incropera & Dewitt eq(9.26)
            else

VNu=(0.825+(0.387*VR.^(1/6))/((1+(0.492/Pr56).^(9/16)).^(8/27))).^2;
     %Nusselt Number (eq 11) Susheela, Sharp & Incropera,Dewitt
eq(9.26)
            end

            Vh=VNu*kk56/VCL;   % Convection Coefficient (W/m^2*K)

            % Top Side
            TR=g*BETA56*abs(T5-T6)*TCL^3/(NU56.*ALPHA56);   %Rayleigh
Number (eq 9.25) Incropera, Dewitt

            % Nusselt Number Calculation (eq 13) Susheela, Sharp
            if TR>10^4 & TR<10^7;
                 TNu=(0.54*TR.^0.25);
            else TR>10^7 & TR<10^11;
                 TNu=(0.15*TR.^0.333);
            end

            Th= TNu*kk56/TCL; % Convection Coefficient (W/m^2*K)

            % Bottom Side
            BR=g*BETA56*abs(T5-T6)*BCL^3/(NU56.*ALPHA56);   %Rayleigh
Number (eq 9.25) Incropera, Dewitt
            BNu=0.27*BR.^0.25;       %Nusselt Number Calculation (eq 13)
Susheela, Sharp
            Bh=BNu*kk56/BCL;         % Convection Coefficient (W/m^2*K)


k56=(1+0.0)*NumberofTanks*((Vh*(2*TankHeight*TankWidth+2*TankHeight*Tan
kLength)/Area)+(Th*(TankWidth*TankLength/Area))+(Bh*(TankWidth*TankLeng
th/Area)));

% Calculate Nodal Temperatures
                 B1 = (m1/deltat)*T1old + k71*T7(j) + E1(j);
                 B2 = (m2/deltat)*T2old;
                 B3 = (m3/deltat)*T3old;
                 B4 = (m4/deltat)*T4old;
                 B5 = (m5/deltat)*T5old;
                 B6 = (m6/deltat)*T6old + k67*T7(j);
```

```
                        A11 = (m1/deltat) + k71 + k12; A12 = -k12;  A13 =
0.0; A14 = 0.0; A15 = 0.0; A16 = 0.0;
                        A21 = -k12; A22 = (m2/deltat) + k12 + k23; A23 = -
k23; A24 = 0.0; A25 = 0.0; A26 = 0.0;
                        A31 = 0.0; A32 = -k23; A33 = (m3/deltat) + k23 +
k34; A34 = -k34; A35 = 0.0; A36 = 0.0;
                        A41 = 0.0; A42 = 0.0; A43 = -k34; A44 = (m4/deltat)
+ k34 + k45; A45 = -k45; A46 = 0.0;
                        A51 = 0.0; A52 = 0.0; A53 = 0.0; A54 = -k45; A55 =
(m5/deltat) + k45 + k56; A56 = -k56;
                        A61 = 0.0; A62 = 0.0; A63 = 0.0; A64 = 0.0; A65 = -
k56; A66 = (m6/deltat) + k56 +k67;

                        A = [A11,A12,A13,A14,A15,A16;
                             A21,A22,A23,A24,A25,A26;
                             A31,A32,A33,A34,A35,A36;
                             A41,A42,A43,A44,A45,A46;
                             A51,A52,A53,A54,A55,A56;
                             A61,A62,A63,A64,A65,A66];

                        B = [B1;B2;B3;B4;B5;B6];
                        X= [inv(A)* B];
                        T1 = X(1); T2 = X(2); T3 = X(3); T4 = X(4); T5 =
X(5); T6 = X(6);

% Recalculate Nodal Temperatures with AUX heating if T6<19 C
                        if T6 < 292.15;
                        T6 = 292.15;
                        B1 = (m1/deltat)*T1old + k71*T7(j) + E1(j);
                        B2 = (m2/deltat)*T2old;
                        B3 = (m3/deltat)*T3old;
                        B4 = (m4/deltat)*T4old;
                        B5 = (m5/deltat)*T5old + k56*T6;

                        A11 = (m1/deltat) + k71 + k12; A12 = -k12;  A13 =
0.0; A14 = 0.0; A15 = 0.0;
                        A21 = -k12; A22 = (m2/deltat) + k12 + k23; A23 = -
k23; A24 = 0.0; A25 = 0.0;
                        A31 = 0.0; A32 = -k23; A33 = (m3/deltat) + k23 +
k34; A34 = -k34; A35 = 0.0;
                        A41 = 0.0; A42 = 0.0; A43 = -k34; A44 = (m4/deltat)
+ k34 + k45; A45 = -k45;
                        A51 = 0.0; A52 = 0.0; A53 = 0.0; A54 = -k45; A55 =
(m5/deltat) + k45 +k56;

                        A = [A11,A12,A13,A14,A15;
                             A21,A22,A23,A24,A25;
                             A31,A32,A33,A34,A35;
                             A41,A42,A43,A44,A45;
                             A51,A52,A53,A54,A55];

                        B = [B1;B2;B3;B4;B5];
                        X= [inv(A)* B];
                        T1 = X(1); T2 = X(2); T3 = X(3); T4 = X(4); T5 =
X(5);
                        end;
% Recalculate Temperatures for Nighttime Insulation T4>T1!
```

144

```matlab
                                if T1 < T4
                                    k23 = NIC;     % Nighttime Insulation

                                    B1 = (m1/deltat)*T1old + k71*T7(j) + E1(j);
                                    B2 = (m2/deltat)*T2old;
                                    B3 = (m4/deltat)*T4old;
                                    B4 = (m5/deltat)*T5old;
                                    B5 = (m6/deltat)*T6old + k67*T7(j);

                                    A11 = (m1/deltat) + k71 + k12; A12 = -k12;
A13 = 0.0; A14 = 0.0; A15 = 0.0;
                                    A21 = -k12; A22 = (m2/deltat) + k12 + k23;
A23 = -k23; A24 = 0.0; A25 = 0.0;
                                    A31 = 0.0; A32 = -k23; A33 = (m4/deltat) +
k23 + k45; A34 = -k45; A35 = 0.0;
                                    A41 = 0.0; A42 = 0.0; A43 = -k45; A44 =
(m5/deltat) + k45 + k56; A45 = -k56;
                                    A51 = 0.0; A52 = 0.0; A53 = 0.0; A54 = -
k56; A55 = (m6/deltat) + k56 + k67;

                                    A = [A11,A12,A13,A14,A15;
                                         A21,A22,A23,A24,A25;
                                         A31,A32,A33,A34,A35;
                                         A41,A42,A43,A44,A45;
                                         A51,A52,A53,A54,A55];

                                    B = [B1;  B2;  B3; B4; B5];
                                    X= [inv(A)* B];
                                    T1 = X(1); T2 = X(2); T4 = X(3); T5 = X(4);
T6 = X(5);

% Recalculate the temperatures in the.. if the room temperature
                                    % T6 goes below 19C.
                                        if T6 < 292.15
                                            T6 = 292.15;
                                            B1 = (m1/deltat)*T1old + k71*T7(j)
+ E1(j);

                                            B2 = (m2/deltat)*T2old;
                                            B3 = (m4/deltat)*T4old;
                                            B4 = (m5/deltat)*T5old + k56*T6;

                                            A11 = (m1/deltat) + k71 + k12; A12
= -k12;   A13 = 0.0; A14 = 0.0;

                                            A21 = -k12; A22 = (m2/deltat) + k12
+ k23; A23 = -k23; A24 = 0.0;

                                            A31 = 0.0; A32 = -k23; A33 =
(m4/deltat) + k23 + k45; A34 = -k45;
                                            A41 = 0.0; A42 = 0.0; A43 = -k45;
A44 = (m5/deltat) + k45 + k56;

                                            A = [A11,A12,A13,A14;
                                                 A21,A22,A23,A24;
                                                 A31,A32,A33,A34;
                                                 A41,A42,A43,A44];

                                            B = [B1;  B2;  B3; B4];
                                            X= [inv(A)* B];
```

145

```matlab
                                        T1 = X(1); T2 = X(2); T4 = X(3); T5
= X(4);
                            end;
                        end;

                if T6 > 297.15;
                    T6 = 297.15;
                    B1 = (m1/deltat)*T1old + k71*T7(j) + E1(j);
                    B2 = (m2/deltat)*T2old;
                    B3 = (m3/deltat)*T3old;
                    B4 = (m4/deltat)*T4old;
                    B5 = (m5/deltat)*T5old + k56*T6;

                    A11 = (m1/deltat) + k71 + k12; A12 = -k12;  A13 =
0.0; A14 = 0.0; A15 = 0.0;
                    A21 = -k12; A22 = (m2/deltat) + k12 + k23; A23 = -
k23; A24 = 0.0; A25 = 0.0;
                    A31 = 0.0; A32 = -k23; A33 = (m3/deltat) + k23 +
k34; A34 = -k34; A35 = 0.0;
                    A41 = 0.0; A42 = 0.0; A43 = -k34; A44 = (m4/deltat)
+ k34 + k45; A45 = -k45;
                    A51 = 0.0; A52 = 0.0; A53 = 0.0; A54 = -k45; A55 =
(m5/deltat) + k45 +k56;

                    A = [A11,A12,A13,A14,A15;
                         A21,A22,A23,A24,A25;
                         A31,A32,A33,A34,A35;
                         A41,A42,A43,A44,A45;
                         A51,A52,A53,A54,A55];

                    B = [B1;B2;B3;B4;B5];
                    X= [inv(A)* B];
                    T1 = X(1); T2 = X(2); T3 = X(3); T4 = X(4); T5 =
X(5);
                end;

                    if (abs(T1-T1prev)<=0.5 & ...
                            abs(T2-T2prev)<=0.5 & ...
                            abs(T3-T3prev)<=0.5 & ...
                       abs(T4-T4prev)<=0.5 & ...
                       abs(T5-T5prev)<=0.5 & ...
                       abs(T6-T6prev)<=0.5);

                       Iterate=0;      %  Iterations are complete
                   else
                       Iterate=1;      % Need to iterate again
                   end;          % end if statement for "Iterate"
Variable

% Counts the Number of Iterations before Temperatures are Saved
                IterationCount(j,i)=IterationCount(j,i)+1;

% Average Temperature values incase of runaway iterations
                q=IterationCount(j,i);
                if j~=1 | i~=1;

                    T1iteration(q,:)=T1;
```

146

```
        T2iteration(q,:)=T2;
        T3iteration(q,:)=T3;
        T4iteration(q,:)=T4;
        T5iteration(q,:)=T5;
        T6iteration(q,:)=T6;

    if q >= 25
        T1=(T1iteration(q-1,:)+T1iteration(q,:))/2;
        T2=(T2iteration(q-1,:)+T2iteration(q,:))/2;
        T3=(T3iteration(q-1,:)+T3iteration(q,:))/2;
        T4=(T4iteration(q-1,:)+T4iteration(q,:))/2;
        T5=(T5iteration(q-1,:)+T5iteration(q,:))/2;
        T6=(T6iteration(q-1,:)+T6iteration(q,:))/2;
        end
end  % end AVG Temp to prevent Runaway

% Provide check in program for runaway iterations
if q > 1000;
        if (round(abs(T1-T1prev)*1000000)==0.0 & ...
            round(abs(T2-T2prev)*1000000)==0.0 & ...
            round(abs(T3-T3prev)*1000000)==0.0 & ...
            round(abs(T4-T4prev)*1000000)==0.0 & ...
            round(abs(T5-T5prev)*1000000)==0.0 & ...
            round(abs(T6-T6prev)*1000000)==0.0);

            Iterate=0; % Iterations are complete
        end

 if q > 10000 & q < 10100;
     T1check(q)=T1;T2check(q)=T2;T3check(q)=T3;
     T4check(q)=T4;T5check(q)=T5;T6check(q)=T6;
 end

 if q == 10101 & Plotcheck == 0;
     subplot(2,3,1);
     plot(T1check);
     xlabel('Iteration')
     ylabel('Temperature Degrees K')
     axis([10001 10099 240 360])
     title('T1 : Absorber');
     subplot(2,3,2);
     plot(T2check);
     xlabel('Iteration')
     ylabel('Temperature Degrees K')
     axis([10001 10099 240 360])
     title('T2 : Evaporator End');
     subplot(2,3,3);
     plot(T3check);
     xlabel('Iteration')
     ylabel('Temperature Degrees K')
     axis([10001 10099 240 360])
     title('T3 : Heat Pipe Condenser End');
     subplot(2,3,4);
     plot(T4check);
     xlabel('Iteration')
     ylabel('Temperature Degrees K')
     axis([10001 10099 240 360])
```

```
                        title('T4 : Water Temperature');
                        subplot(2,3,5);
                        plot(T5check);
                        xlabel('Iteration')
                        ylabel('Temperature Degrees K')
                        axis([10001 10099 240 360])
                        title('T5 : Water Wall');
                        subplot(2,3,6);
                        plot(T6check);
                        xlabel('Iteration')
                        ylabel('Temperature Degrees K')
                        axis([10001 10099 240 360])
                        title('T6 : Room');
                        suptitle('Temperature Convergence')
                        Plotcheck=1;
                        pause
                    end

                if q > 30000;

                        AVERAGING=wavread('notify');
                        sound(AVERAGING,24000);
                        Warning=max([abs(T1-T1prev),abs(T2-T2prev),abs(T3-
T3prev),abs(T4-T4prev),abs(T5-T5prev),abs(T6-T6prev)]);
                        if Warning<0.7;
                            if (abs(T1-T1prev)<=Warning & ...
                                abs(T2-T2prev)<=Warning & ...
                                abs(T3-T3prev)<=Warning & ...
                                abs(T4-T4prev)<=Warning & ...
                                abs(T5-T5prev)<=Warning & ...
                                abs(T6-T6prev)<=Warning);

                            Iterate=0;        % Iterations are complete
                            end
                        end

                        disp('             ')
                        disp('             ')
                        disp('WARNING: Iterations Have Converged');
                        disp(' On A Temperature Above While Loop Limit');
                        disp(' While Loop Limit Was 0.5 Degrees');
                        disp(' 30,000 Iterations Have Passed');
                        disp(' New Cleareance For This ');
                        disp(' Iteration Is ');
                        Cleareance=Warning
                        disp('             ');
                        disp('       j           i                  q ');
                        [j i q]
                        disp('                              T#prev /
T#');
                        [T1prev T2prev T3prev T4prev T5prev T6prev;T1 T2 T3
T4 T5 T6]
                        disp('                              abs(T#-
T#prev)');
                        [abs(T1-T1prev),abs(T2-T2prev),abs(T3-
T3prev),abs(T4-T4prev),abs(T5-T5prev),abs(T6-T6prev)]
```

```
                            disp('
Conductances');
                            [k71 k12 k23 k34 k45 k56 k67]
                            end
                    end

                    if q >= 50000;
                        ERROR=wavread('chord');
                        sound(ERROR,24000);
                        disp('WARNING: Runaway Iterations');
                        disp('Please Press (Ctrl + C)');
                        disp('To Stop The Simulation');
                    elseif IterationCount(j,i)>50000 &
IterationCount(j,i)<50010;
                        [j i q]
                        [T1prev T2prev T3prev T4prev T5prev T6prev;T1 T2 T3
T4 T5 T6]
                        [abs(T1-T1prev),abs(T2-T2prev),abs(T3-
T3prev),abs(T4-T4prev),abs(T5-T5prev),abs(T6-T6prev)]
                        [k71 k12 k23 k34 k45 k56 k67]
                    end

        end;        % end while loop

% Saving Temperatures and Conductances
    T1_save(j,i)=T1; T2_save(j,i)=T2;
      T3_save(j,i)=T3; T4_save(j,i)=T4;
      T5_save(j,i)=T5; T6_save(j,i)=T6;

    T1old_save(j,i)=T1old; T2old_save(j,i)=T2old;
    T3old_save(j,i)=T3old; T4old_save(j,i)=T4old;
    T5old_save(j,i)=T5old; T6old_save(j,i)=T6old;

    k71_save(j,i)=k71; k12_save(j,i)=k12;
      k23_save(j,i)=k23; k34_save(j,i)=k34;
      k45_save(j,i)=k45; k56_save(j,i)=k56;
      k67_save(j,i)=k67;

              % If the room temperature (T6) falls below 19C, auxiliary
heat will
              % added to the room.  Calculate the aux. heat supplied to
the room.
              % Qaux has units of Wmin/m^2
                  if T6 <= 292.15
                  if j <= 744
                      Qaux1 = Qaux1 - k56*(T5-T6) + k67* (T6 - T7(j));
                  end;
                  if j > 744 & j <= 1416
                      Qaux2 = Qaux2 - k56*(T5-T6) + k67* (T6 - T7(j));
                  end;
                  if j > 1416 & j <= 2160
                      Qaux3 = Qaux3 - k56*(T5-T6) + k67* (T6 - T7(j));
                  end;
                  if j > 2160 & j <= 2880
                      Qaux4 = Qaux4 - k56*(T5-T6) + k67* (T6 - T7(j));
                  end;
                  if j >2880 & j <= 3624
```

```
                    Qaux5 = Qaux4 - k56*(T5-T6) + k67* (T6 - T7(j));
                end;
                if j >3624 & j <= 4344
                    Qaux6 = Qaux4 - k56*(T5-T6) + k67* (T6 - T7(j));
                end;
                if j >4344 & j <= 5088
                    Qaux7 = Qaux7 - k56*(T5-T6) + k67* (T6 - T7(j));
                end;
                if j >5088 & j <= 5802
                    Qaux8 = Qaux8 - k56*(T5-T6) + k67* (T6 - T7(j));
                end;
                if j >5802 & j <= 6552
                    Qaux9 = Qaux9 - k56*(T5-T6) + k67* (T6 - T7(j));
                end;
                if j >6552 & j <=7296
                    Qaux10 = Qaux10 - k56*(T5-T6) + k67* (T6 - T7(j));
                end;
                if j >7296 & j <=8016
                    Qaux11 = Qaux11 - k56*(T5-T6) + k67* (T6 - T7(j));
                end;
                if j >8016 & j <=8994
                    Qaux12 = Qaux12 - k56*(T5-T6) + k67* (T6 - T7(j));
                end;
                    Qaux = Qaux - k56*(T5-T6) + k67* (T6 - T7(j));
                end;


        % Rewriting Old Temperatures.
        T1old =T1; T2old =T2; T3old =T3; T4old =T4; T5old = T5; T6old
=T6;


        end;   % end of the i loop


% Save Temperatures and Conductances for j loop only
    T1_hour_save(j,:)=T1; T2_hour_save(j,:)=T2;
      T3_hour_save(j,:)=T3; T4_hour_save(j,:)=T4;
      T5_hour_save(j,:)=T5; T6_hour_save(j,:)=T6;

    k71_hour_save(j,:)=k71; k12_hour_save(j,:)=k12;
      k23_hour_save(j,:)=k23; k34_hour_save(j,:)=k34;
      k45_hour_save(j,:)=k45; k56_hour_save(j,:)=k56;
      k67_hour_save(j,:)=k67;
    TEMPCHECK(j,:)=[T1,T2,T3,T4,T5,T6];

    T1_CHECK(:,j)=T1;


% Q required for each month
    if T7(j) < 292.15
        if j <= 744
            Qreqd1 = Qreqd1 + k67*(292.15 - T7(j));
        end;
        if j > 744 & j <= 1416
            Qreqd2 = Qreqd2 + k67*(292.15 - T7(j));
        end;
        if j > 1416 & j <= 2160
            Qreqd3 = Qreqd3 + k67*(292.15 - T7(j));
        end;
```

150

```
        if j > 2160 & j <= 2880
            Qreqd4 = Qreqd4 + k67*(292.15 - T7(j));
        end;
        if j >2880 & j <= 3624
            Qreqd5 = Qreqd4 + k67*(292.15 - T7(j));
        end;
        if j >3624 & j <= 4344
            Qreqd6 = Qreqd4 + k67*(292.15 - T7(j));
        end;
        if j >4344 & j <= 5088
            Qreqd7 = Qreqd7 + k67*(292.15 - T7(j));
        end;
        if j >5088 & j <= 5802
            Qreqd8 = Qreqd8 + k67*(292.15 - T7(j));
        end;
        if j >5802 & j <= 6552
            Qreqd9 = Qreqd9 + k67*(292.15 - T7(j));
        end;
        if j >6552 & j <=7296
            Qreqd10 = Qreqd10 + k67*(292.15 - T7(j));
        end;
        if j >7296 & j <=8016
            Qreqd11 = Qreqd11 + k67*(292.15 - T7(j));
        end;
        if j >8016 & j <=8994
            Qreqd12 = Qreqd12 + k67*(292.15 - T7(j));
        end;
        Qreqd = Qreqd + k67*(292.15 - T7(j)); % Units of W/m^2
    end;

% Display Percentage of Program Complete
        if j==round(0.25*Xsize);
            disp('              ')
            disp('Simulation 25 % Complete')
            disp('              ')
        end
        if j==round(0.5*Xsize);
            disp('              ')
            disp('Simulation 50 % Complete')
            disp('              ')
        end
        if j==round(0.75*Xsize);
            disp('              ')
            disp('Simulation 75 % Complete')
            disp('              ')
        end
        if j==round(0.9*Xsize);
            disp('              ')
            disp('Simulation 90 % Complete')
            disp('              ')
        end
        if j==round(0.95*Xsize);
            disp('              ')
            disp('Simulation 95 % Complete')
            disp('              ')
        end
end;    % end of the j loop
```

```matlab
COMPLETE=wavread('ding');
sound(COMPLETE,22000);
clc;

disp('HPPSS')
disp('Michael Vincent Albanese')
disp('               ')
disp('Duration of Simulation')
Xsize
disp('               ')
disp('Trial')
Trial
disp('               ')
% Calculate Solar Fraction
Qaux1 = Qaux1/60.;
Qaux2 = Qaux2/60.;
Qaux3 = Qaux3/60.;
Qaux4 = Qaux4/60.;
Qaux5 = Qaux5/60.;
Qaux6 = Qaux6/60.;
Qaux7 = Qaux7/60.;
Qaux8 = Qaux8/60.;
Qaux9 = Qaux9/60.;
Qaux10 = Qaux10/60.;
Qaux11 = Qaux11/60.;
Qaux12 = Qaux12/60.;
Qaux = Qaux/60.;
Fraction = 1-(Qaux/Qreqd)

% Qaux1, Qreqd1, Qaux2, Qreqd2, Qaux3, Qreqd3, Qaux4, Qreqd4, Qaux5,
Qreqd5, Qaux6, Qreqd6, Qaux7, Qreqd7, Qaux8, Qreqd8, Qaux9, Qreqd9,
Qaux10, Qreqd10, Qaux11, Qreqd11, Qaux12, Qreqd12,
%
disp('           ')
disp('    T1           T2           T3           T4           T5           T6
T7 ')
[min(min(T1_save)) min(min(T2_save)) min(min(T3_save))
min(min(T4_save)) min(min(T5_save)) min(min(T6_save)) min(min(T7));
 mean(mean(T1_save)) mean(mean(T2_save)) mean(mean(T3_save))
mean(mean(T4_save)) mean(mean(T5_save)) mean(mean(T6_save))
mean(mean(T7));
 max(max(T1_save)) max(max(T2_save)) max(max(T3_save))
max(max(T4_save)) max(max(T5_save)) max(max(T6_save)) max(max(T7))]
format short e
disp('    k71           k12           k23           k34           k45
k56         k67 ')
[min(min(k71_save)) k12, min(min(k23_save)) min(min(k34_save)) , k45,
min(min(k56_save)), k67;
 mean(mean(k71_save)) k12, mean(mean(k23_save)) mean(mean(k34_save))
,k45, mean(mean(k56_save)), k67;
 max(max(k71_save)) k12, max(max(k23_save)) max(max(k34_save)) ,k45,
max(max(k56_save)), k67]

format short
% disp(' ')
% disp('Parameters')
```

```
% disp('          ')
% disp('Glass Covers')
% [N,L_glass,K_ex_glass;an,n2,eg]
% disp('Absorber Plate')
% [L_abp,W_abp,thick;k_collector,ep,Nfins]
% disp('Collector Insulation')
% [Ledge,k_cic]
% disp('Condenser Fins')
% [Number_condenserfins,nf]
% disp('Wall Insulation')
%
[L_Brick,L_Plywood,L_Insulation,L_Sheetrock;k_Brick,k_Plywood,k_Insulat
ion,k_Sheetrock]
% disp('Water Tank')
% [NumberofTanks,L_Tank,k_Tank;TankWidth,TankHeight,TankLength]
% disp('   ')

% Stopping Clock to Calculate Length of Run
toc;                      % Stops Clock
MINUTES=toc/60

%
plot(J,T1_hour_save,J,T2_hour_save,J,T3_hour_save,J,T4_hour_save,J,T6_h
our_save,J,T7)
% xlabel('Julian Hour')
% ylabel('Temperature Degrees K')
% axis([317 676 240 360])
% title('Absorber Plate - Evaporator - Condenser - Water Tank');
% legend('T1: Absorber Plate (K)','T2: Heat Pipe Evaporator (K)','T3:
Heat Pipe Condenser (K)','T4: Water Tank (K)','T6: Room (K)','T7:
Ambient (K)')
%
% pause
%
% plot(J,T7,J,E1,J,T6_hour_save,J,T1_hour_save);
% xlabel('Julian Hour')
% ylabel('Radiation (W/m^2) & Temperature (K)')
% axis([317 676 -50 1000])
% title('Ambient & Room Temperatures with Radiation');
% legend('Ambient Temperature (K)','Radiadiation (W/m2)','Room
Temperature (K)','Absorber Plate Temperature (K)');
%
% pause
%
% plot(J,T7,J,E1,J,T6_hour_save);
% xlabel('Julian Hour')
% ylabel('Temperature Degrees K')
% axis([0 2000 -50 1000])
% title('Ambient & Room Temperatures with Radiation');
% legend('Ambient Temperature (K)','Radiadiation (W/m2)','Room
Temperature (K)');
%
% pause
%
% plot(J,T7,J,E1,J,T6_hour_save);
% xlabel('Julian Hour')
% ylabel('Temperature Degrees K')
```

```
% axis([2000 4000 -50 1000])
% title('Ambient & Room Temperatures with Radiation');
% legend('Ambient Temperature (K)','Radiadiation (W/m2)','Room
Temperature (K)');
%
% pause
%
% plot(J,T7,J,E1,J,T6_hour_save);
% xlabel('Julian Hour')
% ylabel('Temperature Degrees K')
% axis([6000 8998 -50 1000])
% title('Ambient & Room Temperatures with Radiation');
% legend('Ambient Temperature (K)','Radiadiation (W/m2)','Room
Temperature (K)');
%
% pause
%
%
plot(J,T1_hour_save,J,T2_hour_save,J,T3_hour_save,J,T4_hour_save,J,T6_h
our_save,J,T7,J,E1)
% xlabel('Time ( Julian Hours )')
% ylabel('Temperature ( K )')
% axis([317 676 270 320])
% title('System Results Jan 00-00');
% legend('T1: Absorber Plate','T2: Heat Pipe Evaporator','T3: Heat Pipe
Condenser','T4: Water Tank','T6: Room','T7: Ambient','Radiation')
%
% plot(J,T1_hour_save,J,T2_hour_save,J,T3_hour_save,J,T4_hour_save)
% xlabel('Time ( Julian Hours )')
% ylabel('Temperature ( K )')
% axis([400 600 270 330])
% title('Heat Pipe Wall Experimental Results');
% legend('T1: Absorber Plate','T2: Heat Pipe Evaporator','T3: Heat Pipe
Condenser','T4: Water Tank')
%
% plot(J,T6_hour_save,J,T7)
% xlabel('Time ( Julian Hours )')
% ylabel('Temperature ( K )')
% axis([317 676 290 310])
% title('Heat Pipe Wall Experimental Results');
% legend('T6: Room','T7: Ambient')
%
%
% pause
%
% subplot(3,3,1);
% plot(J,T7);
% xlabel('Julian Hour')
% ylabel('Temperature Degrees K')
% axis([317 676 240 360])
% title('Ambient');
% subplot(3,3,2);
% plot(J,T1_hour_save);
% xlabel('Julian Hour')
% ylabel('Temperature Degrees K')
% axis([317 676 280 320])
% title('Absorber');
```

154

```
% subplot(3,3,3);
% plot(J,T2_hour_save);
% xlabel('Julian Hour')
% ylabel('Temperature Degrees K')
% axis([317 676 280 320])
% title('Evaporator End')
% subplot(3,3,4);
% plot(J,T3_hour_save);
% xlabel('Julian Hour')
% ylabel('Temperature Degrees K')
% axis([317 676 280 320])
% title('Heat Pipe Condenser End');
% subplot(3,3,5);
% plot(J,T4_hour_save);
% xlabel('Julian Hour')
% ylabel('Temperature Degrees K')
% axis([317 676 280 320])
% title('Water Temperature');
% subplot(3,3,6);
% plot(J,T5_hour_save);
% xlabel('Julian Hour')
% ylabel('Temperature Degrees K')
% axis([317 676 280 320])
% title('Water Wall');
% subplot(3,3,7);
% plot(J,T6_hour_save);
% xlabel('Julian Hour')
% ylabel('Temperature Degrees K')
% axis([317 676 280 320])
% title('Room');
% subplot(3,3,8);
% plot(J,E1);
% xlabel('Julian Hour')
% ylabel('W/m^2')
% axis([317 676 -50 1000])
% title('Radiation');
% suptitle('Heat Pipe Simulation')
```

APPENDIX III

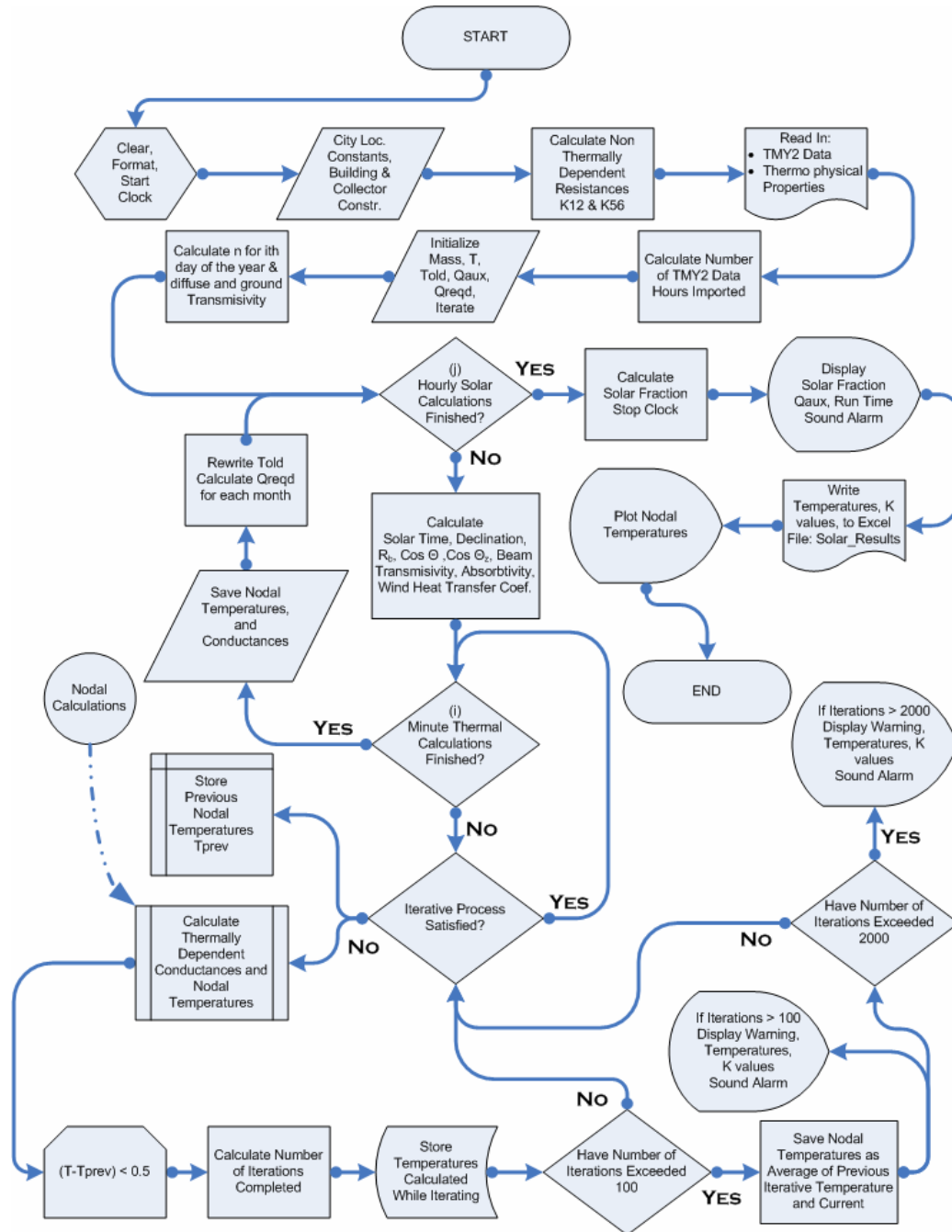## COMPUTER SIMULATION FLOW CHART

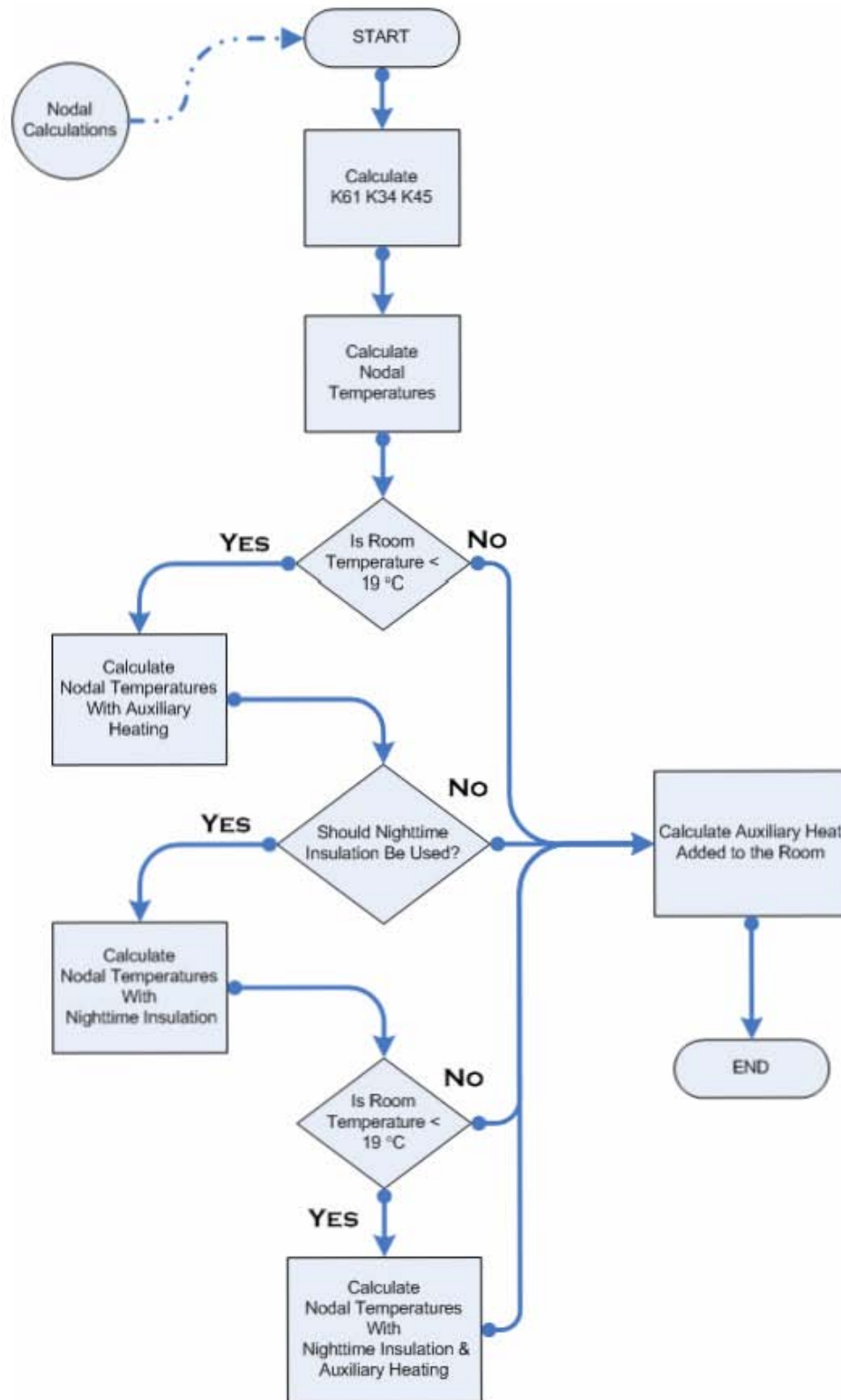
FIGURE A.1 – Computer Simulation Flow Chart.

FIGURE A.2 – Flow Chart Nodal Calculations.

APPENDIX IV

SIMULATION BASE PARAMETERS

TABLE XXXI

COMPUTER SIMULATION BASE PARAMETERS

City	Louisville, Kentucky
Cover (Number)	1
Cover (Thickness)	0.003175 (m)
Cover (Emittance)	0.88
Cover (Extinction Coefficient)	4 (m-1)
Absorber Plate (Material)	Copper
Absorber Plate (Selective Surface)	Black Chrome
Absorber Plate (Thickness)	0.003175 (m)
Absorber Plate (Insulation Thickness)	0.025 (m)
Absorber Plate (Insulation Conductivity)	0.05 (W/mK)
Absorber Plate (Height)	2.0828 (m)
Absorber Plate (Width)	1.165225 (m)
Heat Pipe (Number, Spacing)	5 , 0.3471342 (m)
Heat Pipe (Material)	Copper
Heat Pipe (Inclination Angle)	(No Vapor Column Conductance)
Heat Pipe (Wick Structure)	(None)
Condenser Fin (Number)	(None)
Water Tank (Number)	1
Water Tank (Height)	1.9558 (m)
Water Tank (Length)	1.190625 (m)
Water Tank (Width)	0.2032 (m)
Water Tank (Wall Thickness)	0.003175 (m)
Water Tank (Material Conductivity)	0.5 (W/mK)
Night Time Insulation Conductivity	0.6072 (W/m^{2}K)
Ground Reflectance Factor	0.3
LCR	10 (W/K)

APPENDIX V

RADIATION VALUES

38-3/4"

13-5/8"

678.67 701.70 697.81 700.77 645.84

732.86 736.19 757.28 751.91 700.87

715.75 722.14 733.23 707.43 658.79

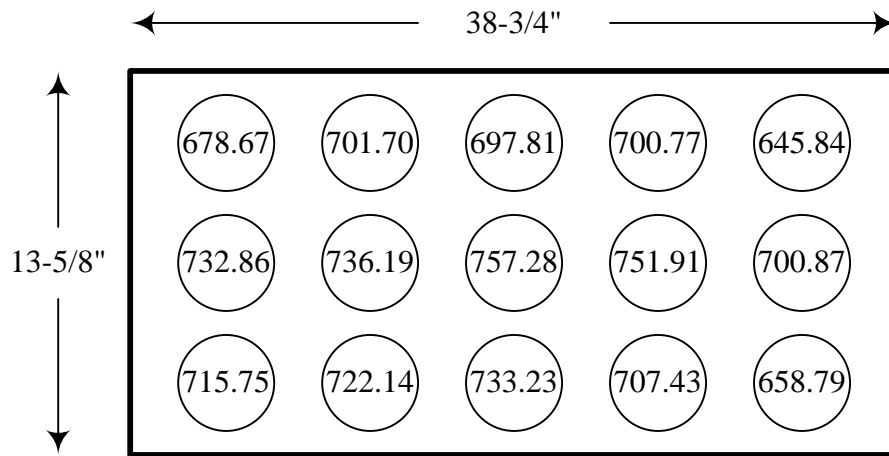*FIGURE A.3 - Radiation Distribution Test Results (W/m^2).*
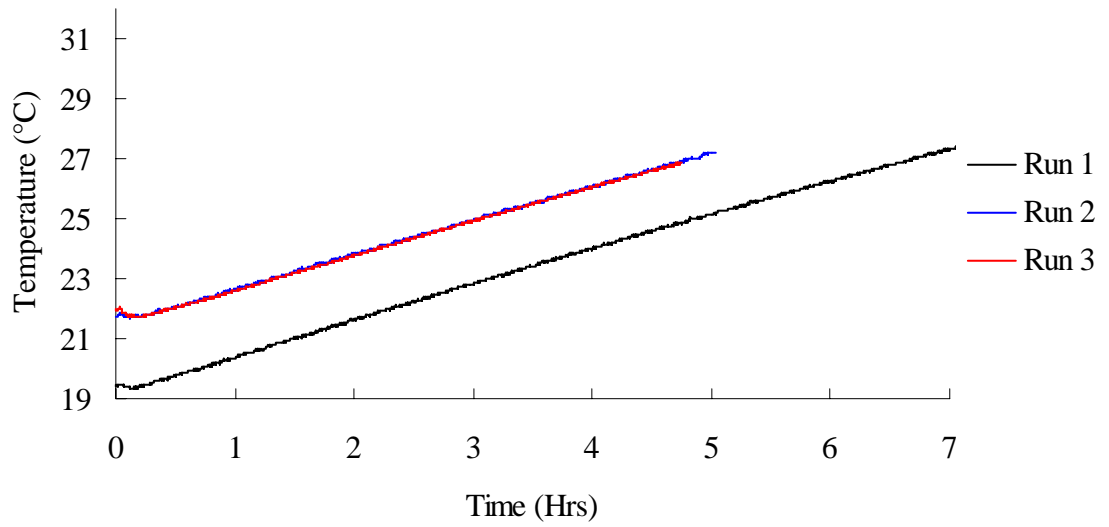
EXPERIMENT TEMPERATURE DATA

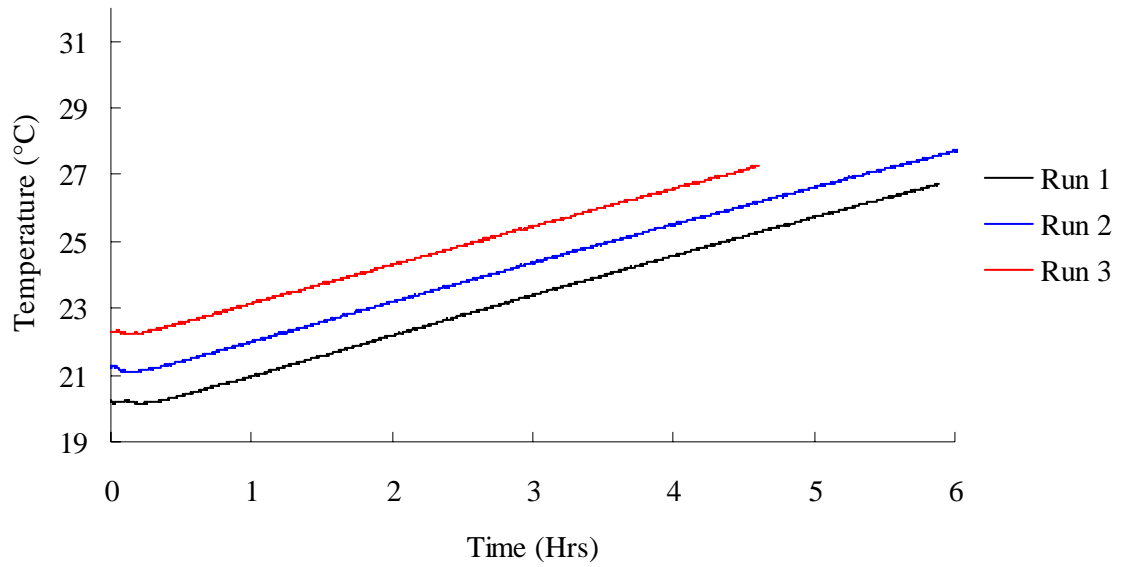*FIGURE A.4 - (Un-insulated / 80% Fill / Un-finned Condenser).*

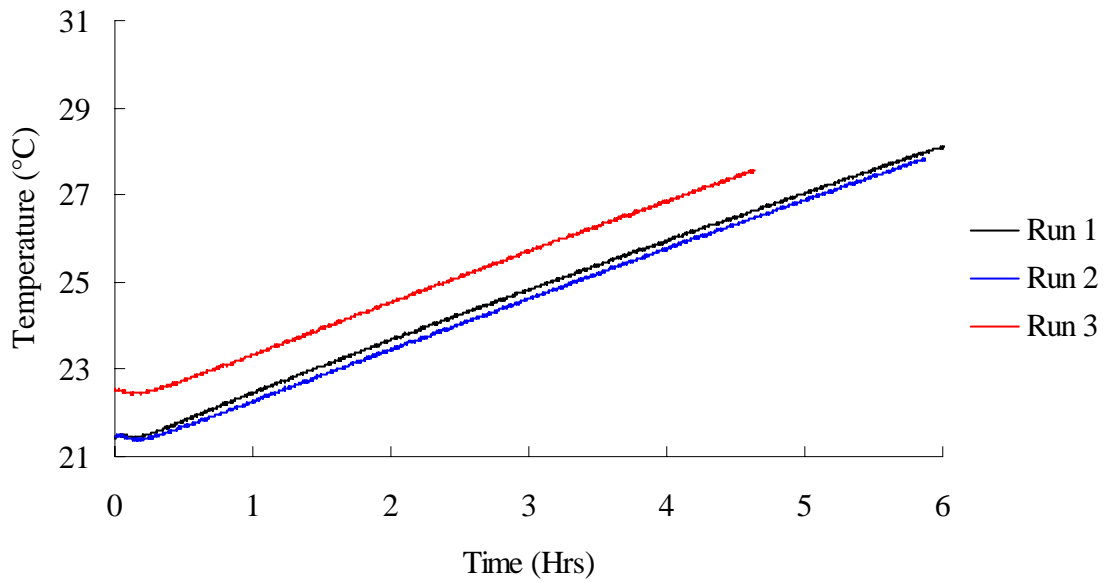*FIGURE A.5 - (Insulated / 80% Fill / Un-finned Condenser).*

FIGURE A.6 - (Un-insulated / 100% Fill / Un-finned Condenser).
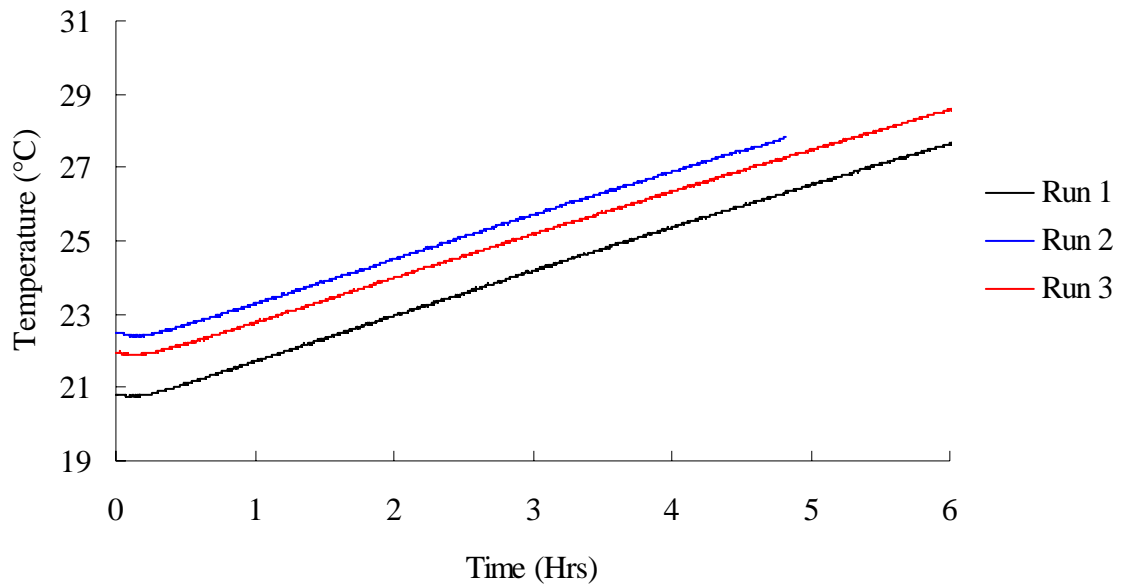
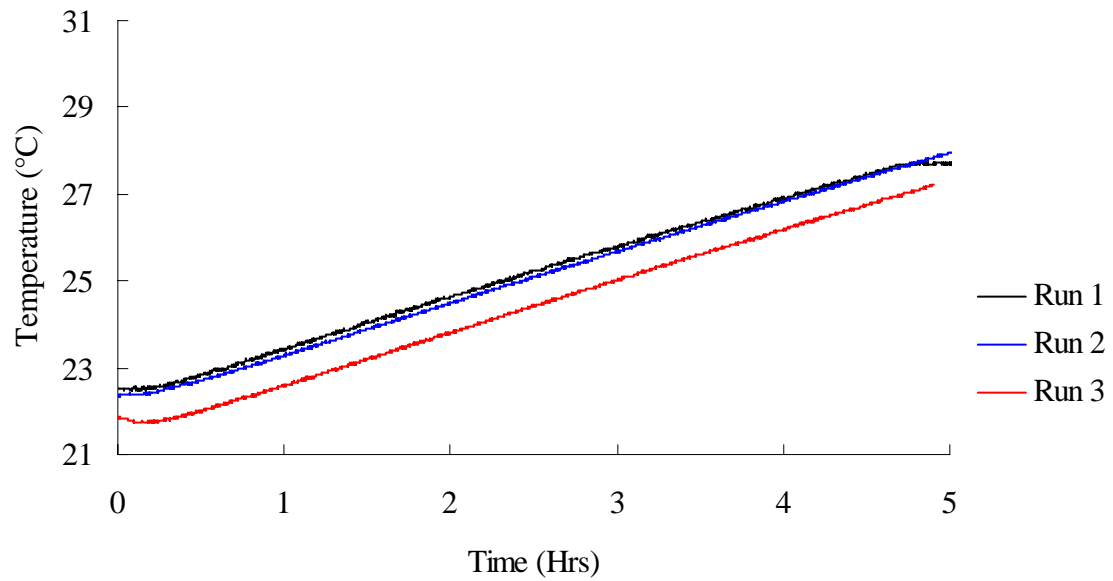*FIGURE A.7 - (Insulated / 100% Fill / Un-finned Condenser).*

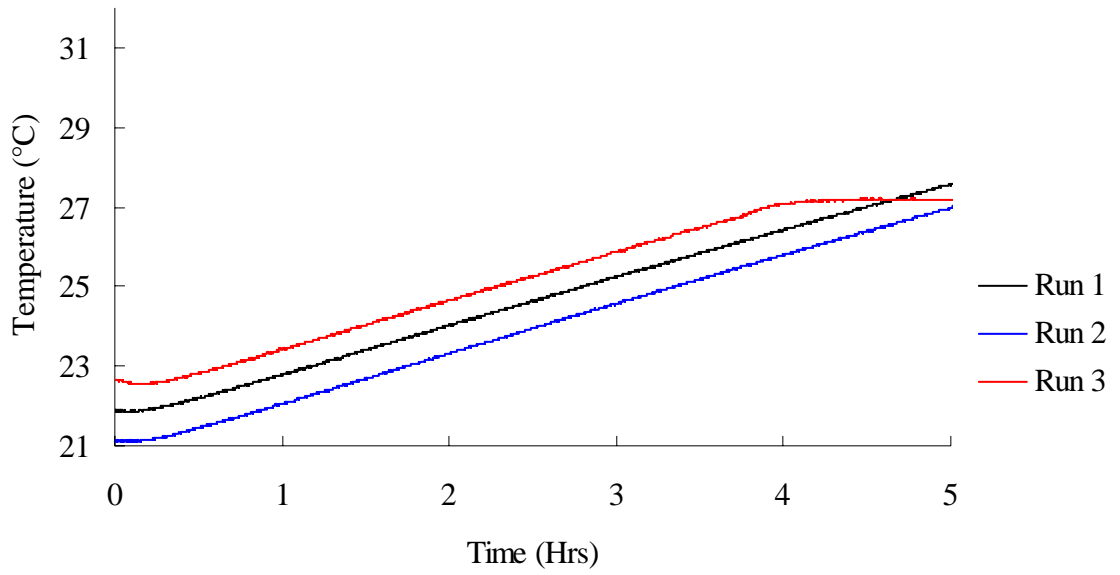*FIGURE A.8 - (Un-insulated / 120% Fill / Un-finned Condenser).*

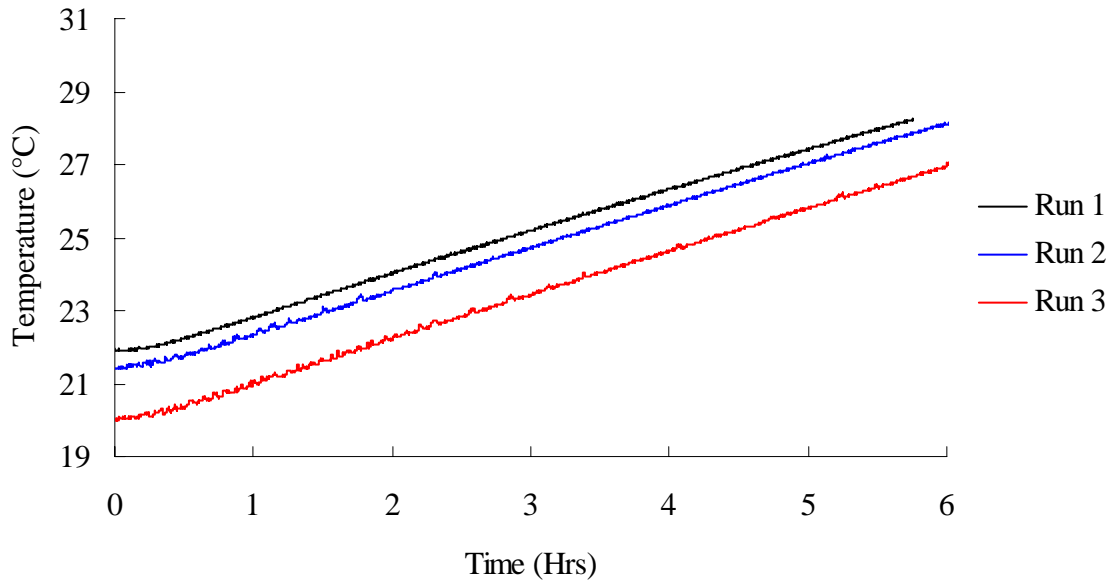*FIGURE A.9 - (Insulated / 120% Fill / Un-finned Condenser).*

FIGURE A.10 - (Un-insulated / 140% Fill / Un-finned Condenser).

163

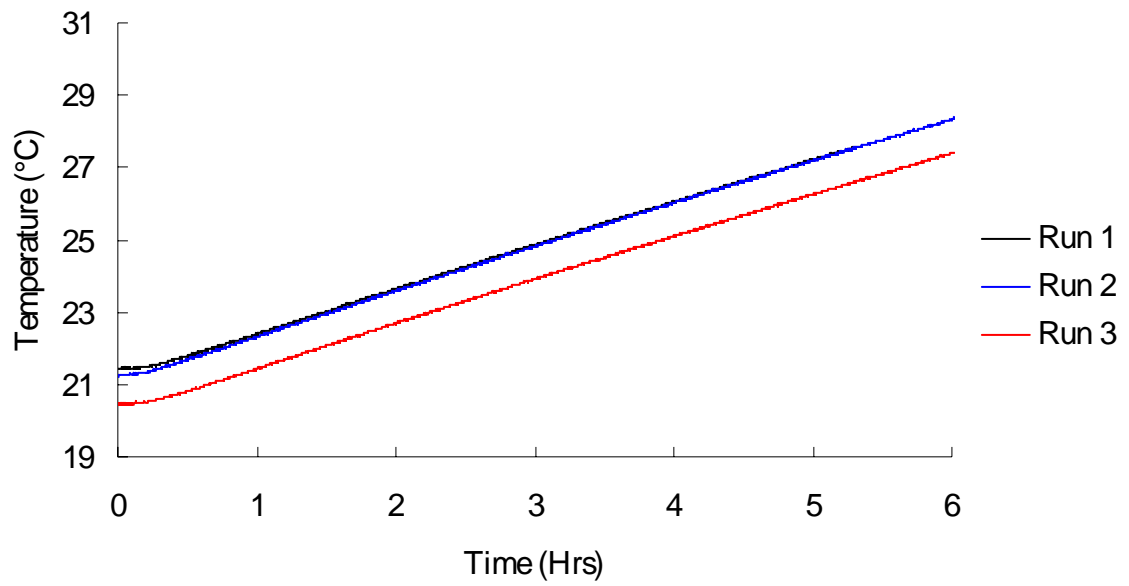*FIGURE A.11 - (Insulated / 140% Fill / Un-finned Condenser).*
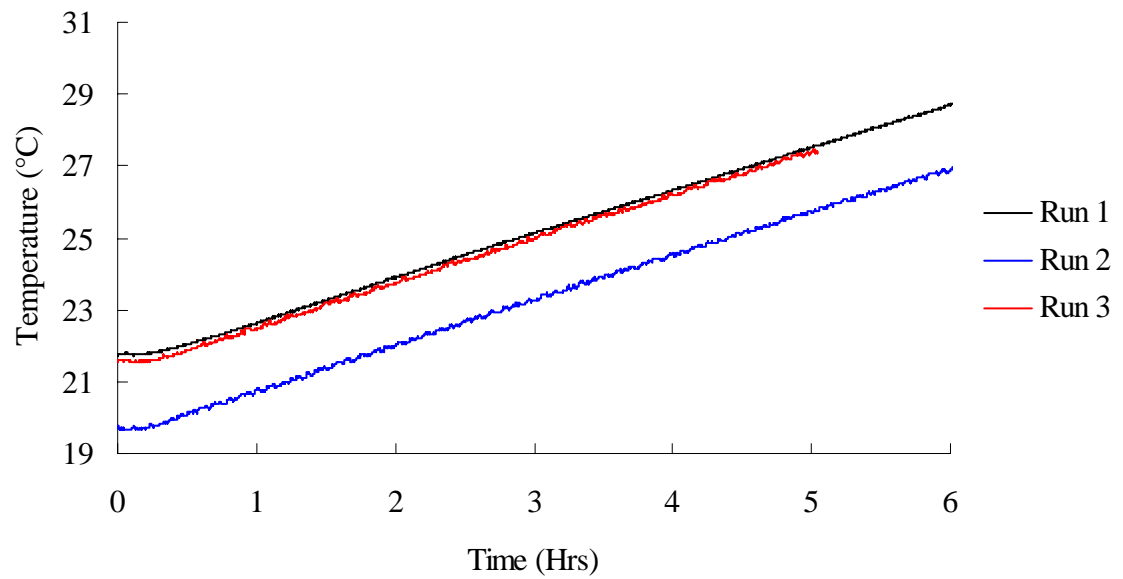
FIGURE A.12 - (Insulated / 120% Fill / Finned Condenser).

EXPERIMENT RADIATION DATA

FIGURE A.13 – Measured Radiation (Un-insulated / 80% Fill).

FIGURE A.14 – Measured Radiation (Insulated / 80% Fill).

FIGURE A.15 – Measured Radiation (Un-insulated / 100% Fill).

FIGURE A.16 – Measured Radiation (Insulated / 100% Fill).

FIGURE A.17 – Measured Radiation (Un-insulated / 120% Fill).
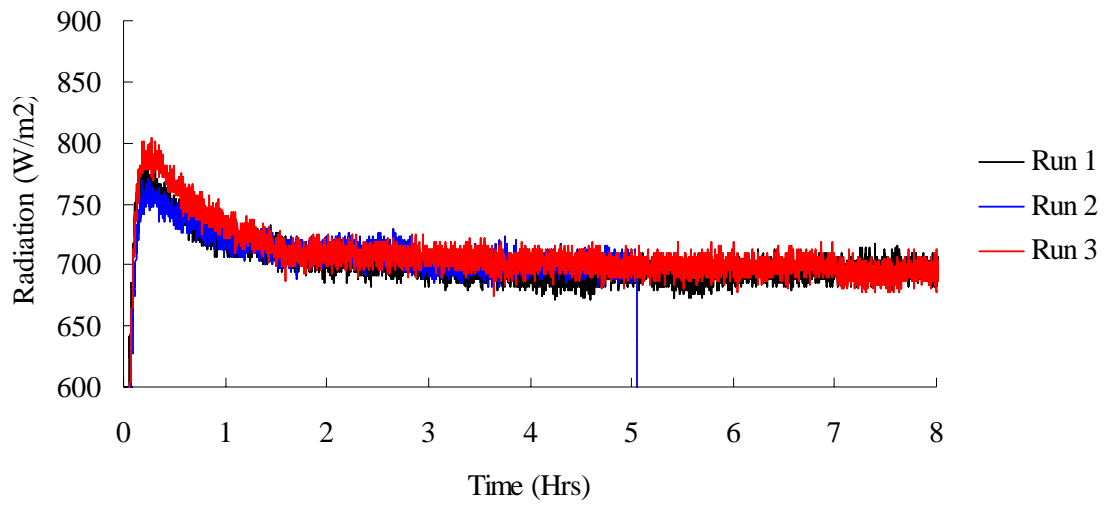
FIGURE A.18 – Measured Radiation (Insulated / 120% Fill).
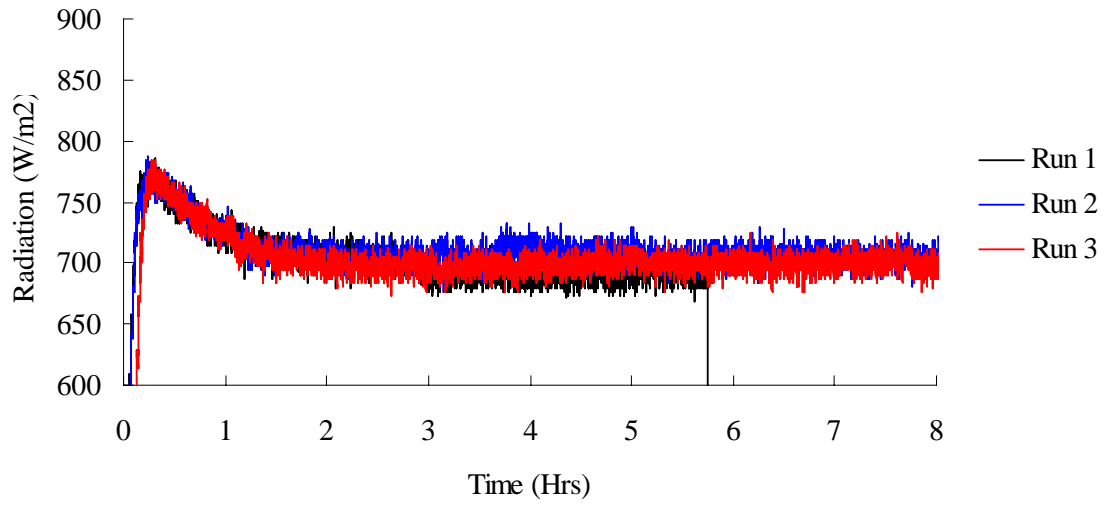
FIGURE A.19 – Measured Radiation (Un-insulated / 140% Fill).
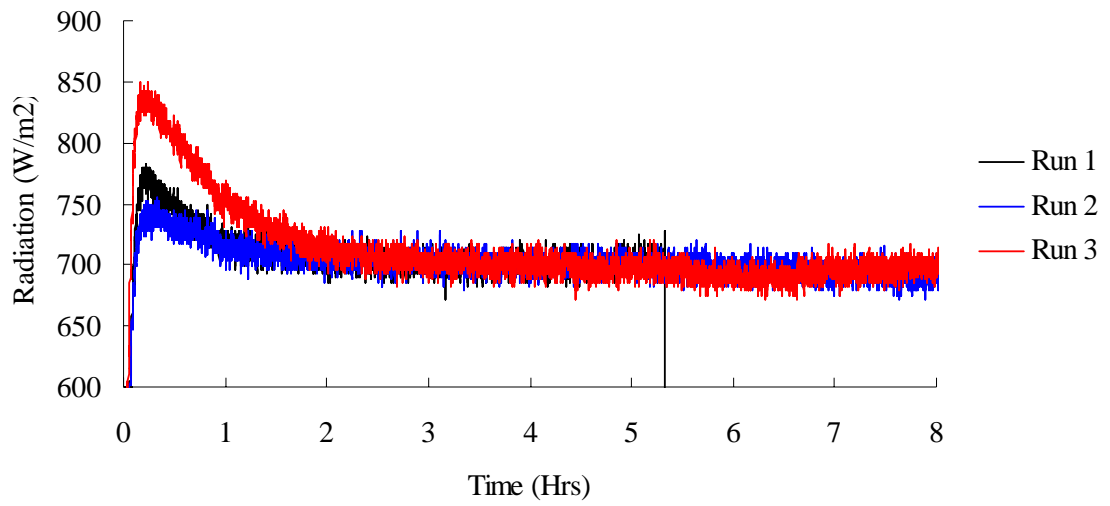
FIGURE A.20 – Measured Radiation (Insulated / 140% Fill).

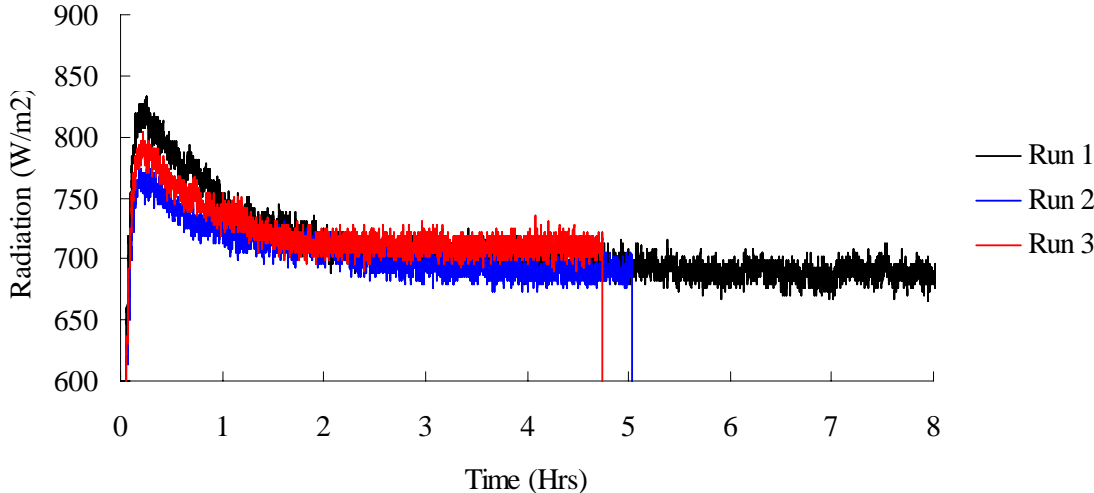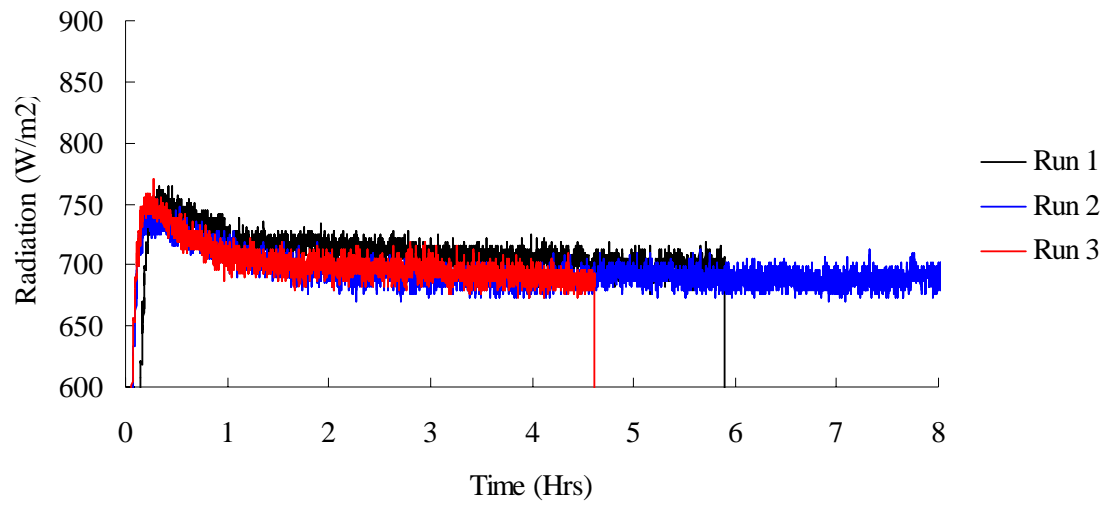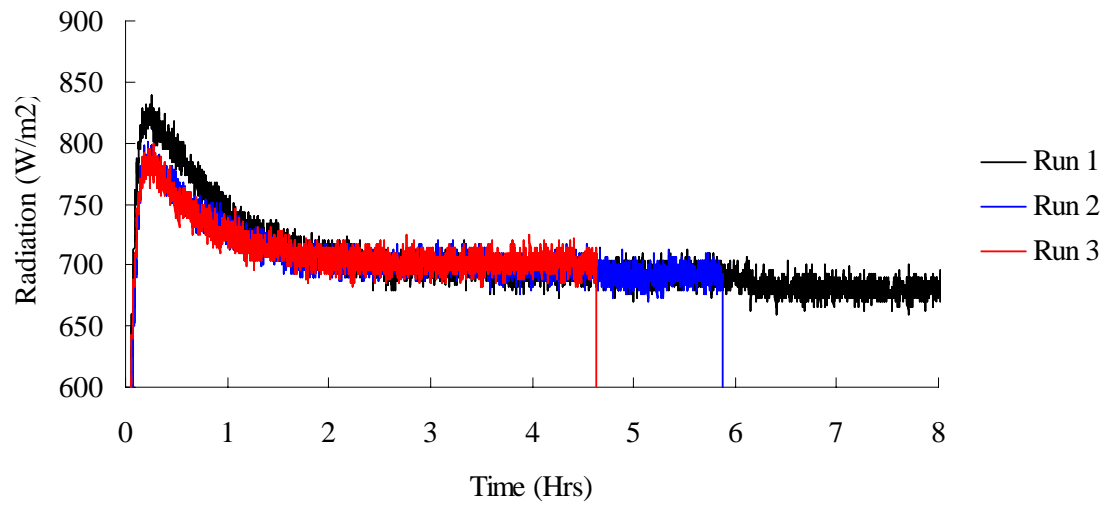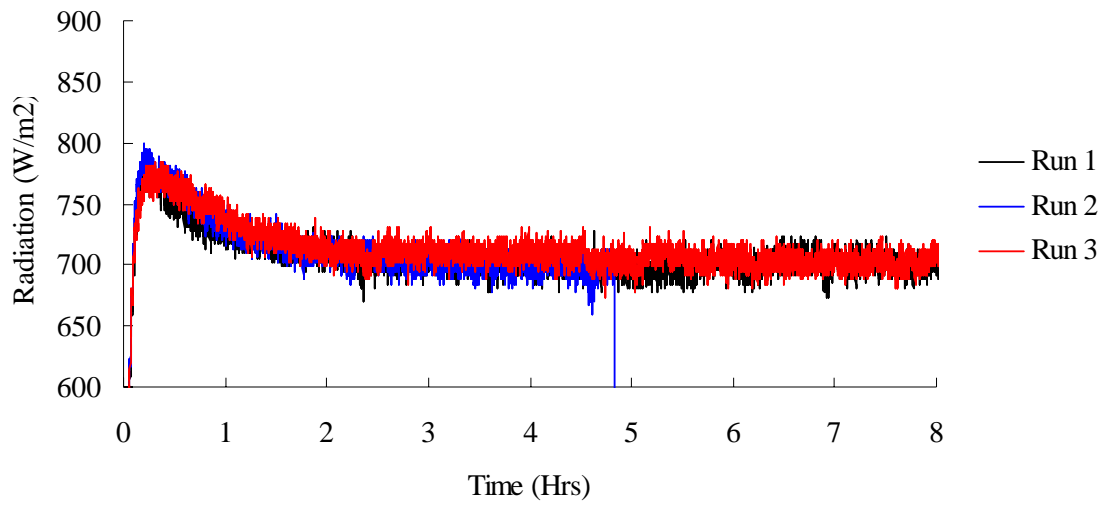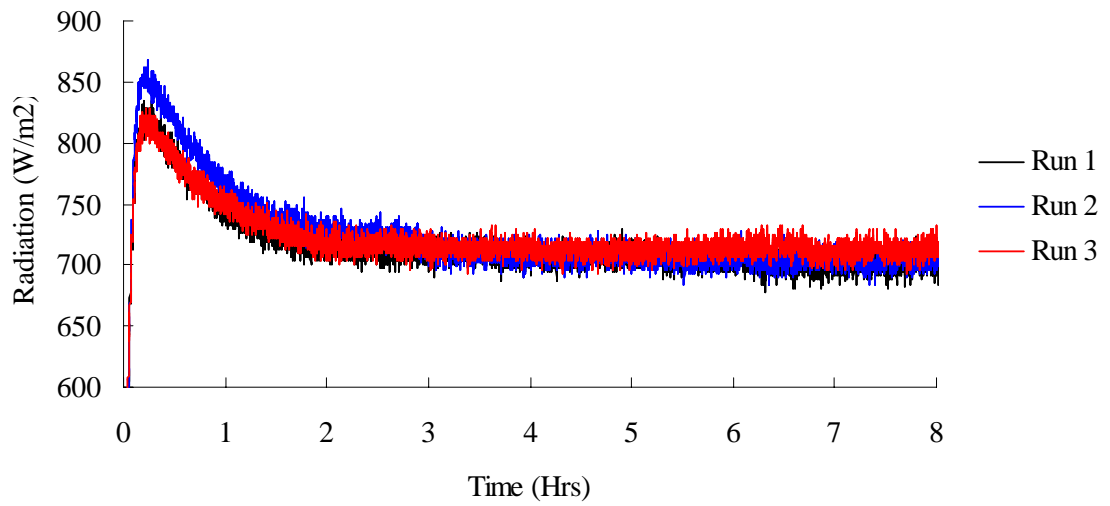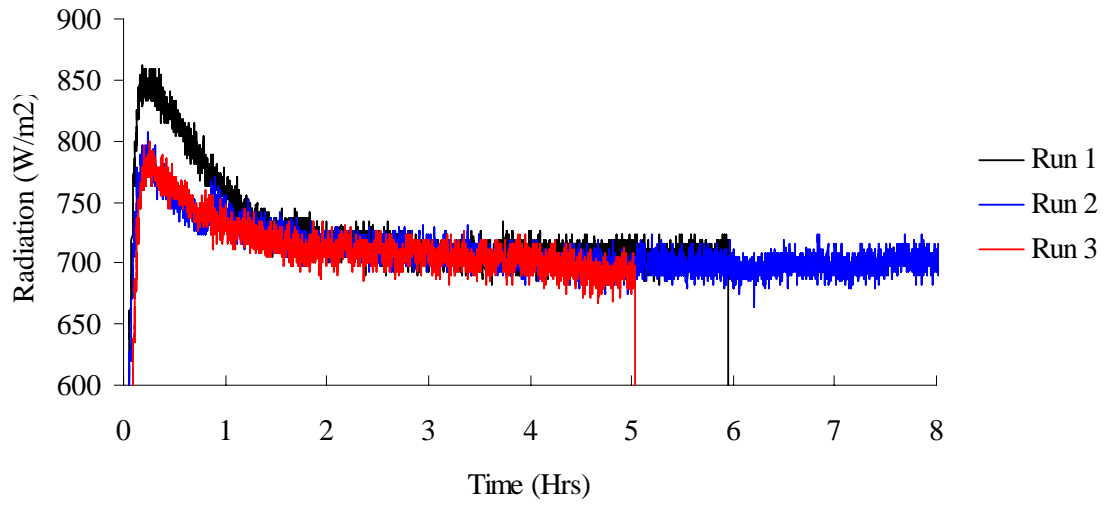*FIGURE A.21 – Measured Radiation (Un-insulated / 120% Fill / Finned).*

ROOM UA LOAD CALCULATIONS

TABLE XXXII

UA CALCULATION FOR 7.53m^2 (81ft^2)

Building Element	Gross Area m^2, Number Of	Net Area m^2	R Value m^{2}K/W	UA W/K
Roof	16.723	16.723	6.688	*2.500*
Floor	7.525	7.525	3.52	*2.138*
North Wall	6.689	6.689	3.52	1.900
N.W. Windows	0	0.929	0.352	0.000
N.W. Doors	0	1.301	0.1672	0.000
Subtotal				*1.900*
South Wall	6.689	5.760	3.52	1.636
S.W. Windows	1	0.929	0.352	2.639
S.W. Doors	0	1.301	0.1672	0.000
Subtotal				*4.276*
East Wall	6.689	6.689	3.52	1.900
E.W. Windows	0	0.929	0.352	0.000
E.W. Doors	0	1.301	0.1672	0.000
Subtotal				*1.900*
West Wall	6.689	4.459	3.52	1.267
W.W. Windows	1	0.929	0.352	2.639
W.W. Doors	1	1.301	0.1672	7.779
Subtotal				*11.685*
ACH				0.500
ADR				0.880
Infiltration				*0.145*
UA Building Total				**24.254**
UA/A				10.00
Collector Area (m^2)				2.43
House Area (m^2)				7.53
Percent of South Wall				**36.26%**

TABLE XXXIII

UA CALCULATION FOR 179.86 m^2 (1936 ft^2)

Building Element	Gross Area m^2, Number Of	Net Area m^2	R Value m^{2}K/W	UA W/K
Roof	81.755	81.755	6.688	*12.224*
Floor	179.860	179.860	3.52	*51.097*
North Wall	32.702	31.773	3.52	9.026
N.W. Windows	1	0.929	0.352	2.639
N.W. Doors	0	1.301	0.1672	0.000
Subtotal				*11.666*
South Wall	32.702	29.543	3.52	8.393
S.W. Windows	2	0.929	0.352	5.279
S.W. Doors	1	1.301	0.1672	7.779
Subtotal				*21.450*
East Wall	32.702	32.702	3.52	9.290
E.W. Windows	0	0.929	0.352	0.000
E.W. Doors	0	1.301	0.1672	0.000
Subtotal				*9.290*
West Wall	32.702	30.472	3.52	8.657
W.W. Windows	1	0.929	0.352	2.639
W.W. Doors	1	1.301	0.1672	7.779
Subtotal				*19.075*
ACH				0.500
ADR				0.880
Infiltration				*3.473*
UA Building Total				**121.329**
UA/A				10.00
Collector Area (m^2)				12.13
House Area (m^2)				179.86
Percent of South Wall				**37.10%**

APPENDIX IX

FUTURE FUEL COST

TABLE XXXIV

Present Worth Of Future Fuel Cost

Year	Fuel Cost	PW of Fuel Cost	Current PW Total
1	842.64	822.09	822.09
2	876.35	834.12	1,656.21
3	911.40	846.33	2,502.54
4	947.86	858.71	3,361.26
5	985.77	871.28	4,232.54
6	1,025.21	884.03	5,116.57
7	1,066.21	896.97	6,013.54
8	1,108.86	910.09	6,923.63
9	1,153.22	923.41	7,847.05
10	1,199.35	936.93	8,783.97
11	1,247.32	950.64	9,734.61
12	1,297.21	964.55	10,699.16
13	1,349.10	978.66	11,677.82
14	1,403.06	992.99	12,670.81
15	1,459.19	1,007.52	13,678.33
16	1,517.55	1,022.26	14,700.59
17	1,578.26	1,037.22	15,737.81
18	1,641.39	1,052.40	16,790.21
19	1,707.04	1,067.80	17,858.02
20	1,775.32	1,083.43	18,941.44
21	1,846.34	1,099.28	20,040.73
22	1,920.19	1,115.37	21,156.10
23	1,997.00	1,131.69	22,287.79
24	2,076.88	1,148.25	23,436.05
25	2,159.95	1,165.06	24,601.10
26	2,246.35	1,182.11	25,783.21
27	2,336.20	1,199.41	26,982.62
28	2,429.65	1,216.96	28,199.58
29	2,526.84	1,234.77	29,434.35
30	2,627.91	1,252.84	30,687.18

APPENDIX X

LIFE CYCLE COSTING

TABLE XXXV

LIFE CYCLE COSTING INITIAL INPUTS

Reduction of Fuel Purchase	42.67%	
Cost of Collector and Equipment	$9,127.30	
Length of Mortgage	30	Years
Mortgage Interest Rate	5.75%	
Down Payment	1,825	
Inflation Rate	4.00%	
Cost of Fuel	0.1	$/kWh
Amount of Fuel In First Year	8426.44	kWh
Discount Rate	2.50%	
Fuel Cost Inflation	4.00%	
Resale Value	30.00%	
Tax Inflation Rate	4.00%	
Effective Income Tax Rate	28.00%	
First Year Maint. Insu. Etc.	$50	
Extra Property Tax	$0	
Mortgage Payment	$511.32	

TABLE XXXVI

LIFE CYCLE COST ANALYSIS

Year	Fuel Savings	Extra Mortgage Payment	Extra Insurance, Maintenance, Energy	Extra Property Tax	Interest In Year	Principal Payment	Principal Balance	Income Tax Savings	Solar Savings	PW of Solar Savings
0							7,301.84		-1,825.46	-1,825.46
1	359.56	-511.32	-50.00	0.00	419.86	91.46	7,210.38	117.56	-84.20	-82.15
2	373.94	-511.32	-52.00	0.00	414.60	96.72	7,113.65	116.09	-73.29	-69.76
3	388.90	-511.32	-54.08	0.00	409.04	102.28	7,011.37	114.53	-61.97	-57.55
4	404.45	-511.32	-56.24	0.00	403.15	108.17	6,903.20	112.88	-50.23	-45.50
5	420.63	-511.32	-58.49	0.00	396.93	114.39	6,788.82	111.14	-38.04	-33.62
6	437.46	-511.32	-60.83	0.00	390.36	120.96	6,667.85	109.30	-25.40	-21.90
7	454.95	-511.32	-63.27	0.00	383.40	127.92	6,539.93	107.35	-12.28	-10.33
8	473.15	-511.32	-65.80	0.00	376.05	135.27	6,404.66	105.29	1.33	1.09
9	492.08	-511.32	-68.43	0.00	368.27	143.05	6,261.61	103.12	15.44	12.37
10	511.76	-511.32	-71.17	0.00	360.04	151.28	6,110.33	100.81	30.09	23.50
11	532.23	-511.32	-74.01	0.00	351.34	159.98	5,950.35	98.38	45.28	34.51
12	553.52	-511.32	-76.97	0.00	342.15	169.17	5,781.18	95.80	61.03	45.38
13	575.66	-511.32	-80.05	0.00	332.42	178.90	5,602.28	93.08	77.37	56.12
14	598.69	-511.32	-83.25	0.00	322.13	189.19	5,413.09	90.20	94.31	66.75
15	622.63	-511.32	-86.58	0.00	311.25	200.07	5,213.02	87.15	111.88	77.25
16	647.54	-511.32	-90.05	0.00	299.75	211.57	5,001.45	83.93	130.10	87.64
17	673.44	-511.32	-93.65	0.00	287.58	223.74	4,777.71	80.52	149.00	97.92
18	700.38	-511.32	-97.40	0.00	274.72	236.60	4,541.11	76.92	168.59	108.09
19	728.39	-511.32	-101.29	0.00	261.11	250.21	4,290.91	73.11	188.90	118.16
20	757.53	-511.32	-105.34	0.00	246.73	264.59	4,026.31	69.08	209.95	128.13
21	787.83	-511.32	-109.56	0.00	231.51	279.81	3,746.51	64.82	231.78	138.00
22	819.35	-511.32	-113.94	0.00	215.42	295.90	3,450.61	60.32	254.41	147.78
23	852.12	-511.32	-118.50	0.00	198.41	312.91	3,137.70	55.55	277.86	157.46
24	886.20	-511.32	-123.24	0.00	180.42	330.90	2,806.80	50.52	302.16	167.06
25	921.65	-511.32	-128.17	0.00	161.39	349.93	2,456.87	45.19	327.36	176.57
26	958.52	-511.32	-133.29	0.00	141.27	370.05	2,086.82	39.56	353.46	186.00
27	996.86	-511.32	-138.62	0.00	119.99	391.33	1,695.49	33.60	380.51	195.36
28	1,036.73	-511.32	-144.17	0.00	97.49	413.83	1,281.66	27.30	408.54	204.63
29	1,078.20	-511.32	-149.94	0.00	73.70	437.62	844.04	20.63	437.58	213.83
30	1,121.33	-511.32	-155.93	0.00	48.53	462.79	381.25	13.59	467.67	222.96
30									2,738.19	1,305.41
Total of Solar Savings									5,291.89	1,825.67
Payback Period										22.21

174

VITA

Michael Albanese is a graduate student at the University of Louisville. Michael received his Bachelor of Science degree in mechanical engineering in 2005.